Damian Giziński

Liquid-phase chemoselective flow hydrogenation over resin supported catalysts for synthesis of industrially relevant chemicals

Institute of Physical Chemistry
Polish Academy of Sciences

PhD THESIS

Liquid-phase chemoselective flow hydrogenation over resin supported catalysts for synthesis of industrially relevant chemicals

Damian Giziński, MSc

Supervisor:

Jacinto Sá, PhD, DSc, Assoc. Prof. IPC PAS

Doctoral dissertation prepared within International Doctoral Studies
of the Institute of Physical Chemistry, Polish Academy of Sciences
Kasprzaka 44/52, 01-224 Warsaw

January 2019
Warsaw

Niniejszą pracę dedykuję moim wspaniałym rodzicom

Acknowledgements

Firstly, I would like to thank my supervisor, prof. Jacinto Sá, for giving me the opportunity to work in his group, for his patient guidance and advice he has provided throughout my time as his student.

I would also like to express my sincere thanks to prof. Anna Śrębowata for support and encouragement, which I have received from her since the beginning of my work at Institute of Physical Chemistry PAS.

I am thankful to all members of Modern Heterogeneous Catalysis group, who created friendly and helpful atmosphere during my work.

Special thanks to my colleagues and friends made throughout my time in IPC PAS, especially Ilona Goszewska, Ewelina Kuna and Emil Kowalewski.

Finally, I would like to thank my significant others, my dear parents and, of course, Kuba for being extremely supportive during this time. *Dziękuję!*

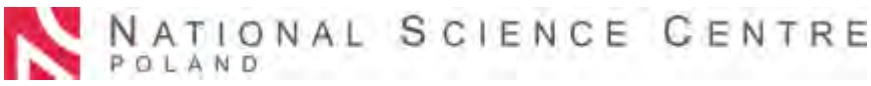

This work was realized with financial support of National Science Centre of Poland within OPUS8 project 2014/15/B/ST5/02094

Abstract

The aim of presented work was to design and develop an integrated and comprehensive catalytic continuous-flow system applicable in chemoselective hydrogenation of polyunsaturated aldehydes; hence, in process of high relevance for chemical industry. In this transformation, α,β-unsaturated aldehydes are subjected to competitive C=O vs C=C saturation within the same molecule. Depending on which unsaturated bond is selectively hydrogenated over a catalyst, the reaction may yield various intermediates used in pharma and cosmetics.

Demonstrated methodology includes set of consecutive protocols thoroughly described in subsequent chapters of the dissertation. Each of those chapters is dedicated to constituent step, such as catalyst design and preparation, catalytic flow reactions and *in-situ* catalyst modification. Therefore, the work collates extensive strategy for optimization of catalyst performance in liquid-phase flow processing.

Catalyst was designed to meet demanding continuous flow conditions, as well as, to display high selectivity in above-mentioned reaction. As a result, novel Ni based catalyst was prepared by combining metal nanoparticles and functionalized polymeric resin support. The material was found highly selective towards alkenyl bond saturation and showed better product specificity than adequate Pd material. All catalytic reactions and reaction conditions optimizations were conducted in continuous-flow micro-reactor suitable for hydrogenation processes.

Application of continuous flow, as an alternative to conventional batch operating, introduces significant improvements in studies on catalytic system, leading to high process intensification. In this light, compact and intensified method for structure sensitivity investigation in flow micro-reactor was proposed. In this approach, resin supported catalyst can be modified in sequence with catalytic reaction, hence, it is possible to estimate the optimal catalyst morphology for a given process in short time with low expenditures.

To conclude, the dissertation presents unified strategy for intensified catalyst investigation in liquid-phase flow conditions. By following this methodology, new and efficient catalytic system was demonstrated for highly selective production of value-added chemicals relevant to pharma and cosmetics.

Streszczenie

Celem badań było opracowanie zintegrowanego, kompleksowego układu katalitycznego w warunkach przepływowych do zastosowań w chemoselektywnym uwodornieniu aldehydów polinienasyconych, a więc w procesie o dużym znaczeniu przemysłowym. W tej reakcji aldehydy α,β-nienasycone ulegają saturacji poprzez konkurencyjne reakcje uwodornienia wiązania C=C oraz wiązania C=O w obrębie tej samej molekuły. W zależności od tego, które z w/w wiązań zostanie selektywnie uwodornione z użyciem katalizatora, wynikiem reakcji mogą być produkty o zróżnicowanych właściwościach i zastosowaniach w przemyśle kosmetycznym i farmaceutycznym.

Zademonstrowana metodologia została podzielona na zbiór procesów pośrednich, opisanych w kolejnych sekcjach rozprawy. Każda z sekcji obejmuję protokół oraz wyniki badań nad takimi procesami jak: zaprojektowanie oraz synteza katalizatora, przepływowe reakcje katalityczne czy modyfikacja katalizatora w przepływie. Tak więc, niniejsza praca zawiera szczegółową strategię optymalizacji układów katalitycznych w warunkach przepływowych.

Podstawowym katalizatorem użytym w pracy był katalizator niklowy otrzymany w wyniku połączenia nanocząstek metalu z żywicą polimerową zawierającą aminowe grupy funkcyjne. Materiał ten wykazał wysoką selektywność do uwodornienia wiązania C=C we wszystkich badanych reakcjach.

Zarówno reakcje katalityczne jak i optymalizacja warunków reakcji zostały przeprowadzone w reaktorze mikro-przepływowym dedykowanym reakcjom uwodornienia. Zastosowanie warunków przepływowych, jako alternatywy dla tradycyjnie stosowanych układów stacjonarnych, wprowadza szereg zalet i udogodnień w badaniach nad optymalizacją procesów katalitycznych, w konsekwencji prowadząc do wysokiej intensyfikacji tych procesów. Jak w przypadku zademonstrowanej w pracy metody zoptymalizowania morfologii katalizatora w sekwencji z rekcją chemiczną w tym samym mikro-reaktorze.

Podsumowując, praca zawiera złożoną strategię optymalizacji i intensyfikacji procesów katalitycznych w warunkach przepływowych, która została zastosowana do opracowania efektywnego i wysoce selektywnego układu katalitycznego w produkcji związków o dużym znaczeniu przemysłowym.

CONTENTS

1. INTRODUCTION

Flow heterogeneous catalysis, in the sense of process where solid catalyst is exposed to continuous flow of liquid phase, attracts great attention of both academia and industry. Coupling flow catalysis with micro-reactor technology can be highly advantageous due to savings in resources consumption, safety benefits and overall process efficiency. Therefore, flow catalysis, is a 'green' and sustainable platform for new developments in chemical industry. Flow dynamic processing overcomes restraints limiting stationary batch systems. In this light, application of continuous flow opens the door to innovative and unconventional approaches in catalysis.

Herein, it is demonstrated how to take advantage of flow conditions for studies of catalyst performance in industrially relevant process. Thus, presented work focuses on the comprehensive protocols including: catalyst design and preparation, reaction conditions optimization, *in-situ* morphology modification and stability tests elaborated in flow conditions. All operations over catalyst were conducted in a single compact flow micro-reactor, remarkably expediting and simplifying process optimization.

The best way to exhibit the improvements of any chemical method is to implement this method to the process of industrial meaning. In this case, flow catalysis has been applied in catalytic chemoselective hydrogenation of α,β – unsaturated aldehydes. The biggest challenge in this reaction is to direct the process towards semi-saturated products by competitive saturation of carbonyl versus conjugated alkenyl bond within the same molecule.[1] Therefore, the process can be directed towards various value-added intermediates used for drugs and fragrances production. The flow hydrogenation process was investigated with three representatives of α,β – unsaturated aldehydes: prenal, cinnamaldehyde and citral. Studied compounds feature various functional groups, such as presence of benzene ring or additional, isolated carbonyl bond. Those dissimilarities are crucial to investigate versatility of the method.

Structural diversity results in miscellaneous properties of studied aldehydes and corresponding products of their hydrogenation. Depending on which of unsaturated bond undergoes hydrogenation, the reaction yields compounds, which indicate different properties, such as odor and flavor. For instance, isovaleraldehyde, product of selective C=C hydrogenation in prenal, is responsible for malty character of beer[2], whereas, prenol (selective C=O hydrogenation) has fruity green lavender odor.

Irrespective of bond configuration, all partially saturated products obtained from hydrogenation of prenal, cinnamaldehyde and citral find application in fragrance industry. However, smell is not the only feature, which differentiates products of competitive partial hydrogenations. Hydrocinnamaldehyde and cinnamyl alcohol, as products of corresponding selective C=C and C=O hydrogenation in cinnamaldehyde, are important intermediates in drug production. Hydrocinnamaldehyde can be used to produce pharmaceuticals for HIV treatment[3] and cinnamyl alcohol to synthesize chloromycetin antibiotics[4].

Due to presence of additional isolated alkenyl bond, citral selective hydrogenation can result in accordingly higher number of products. Thus, each partial hydrogenation forms compound with different properties and applications. For instance, nerol, product of selective C=O hydrogenation, indicates rosy odor, hence, is widely used in perfumes production. On the other hand, citronellal (saturation of C=C in α position) is a main component of citronella oil, which adds fresh lemon notes to various cosmetics. Further hydrogenation of citronellal may yield dihydrocitronellal (both αC=C and isolated C=C reduced) known as FEMA2390, flavoring agent added to e.g. alcoholic and non-alcoholic beverages, sweets and bakery products to enhance their fruity taste.[5] From the point of view of pharmaceutical applications, citronellal indicates antifungal and mosquito repelling properties[6], whereas, citronellol (αC=C and C=O saturation) attracts mite[7].

Taking into consideration that such subtle changes in chemical structure significantly moderate chemical properties of presented molecules, it is important to develop highly selective catalytic system for their production. In this matter, presented work shows set of continuous flow protocols for exceedingly intensified, effective and convenient methodology, which can be applied to steer the selectivity in catalytic surface reactions.

2. LITERATURE BACKGROUND

2.1. BOND CONTROL IN α,β – UNSATURATED ALDEHYDES HYDROGENATION

Strict control over formation of a specific bond is a clue for increasing overall efficiency of industrial processes. High product-specificity of chemical production eliminates or significantly decreases formation of side products and consequently enhances energy performance and atom efficiency of industrially relevant processes.

Control of bond formation has been widely studied on α,β-unsaturated aldehydes (Scheme 1) hydrogenation. The fact that each compound included in this group possesses at least two different unsaturated bonds, makes α,β-unsaturated aldehydes suitable for bond control studies.

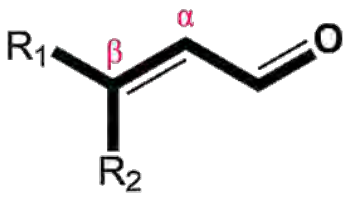

Scheme 1. Conjugated alkenyl and carbonyl bonds in α,β-unsaturated aldehydes.

Both carbonyl and conjugated alkenyl bonds can be hydrogenated in various order yielding different partially saturated compounds. Products of these competitive hydrogenations find wide application in many branches of chemical processing. The key is to steer the reaction towards semi-saturated product by reduction of only one of those bonds. To attain that, the reaction is conducted over a catalyst. Mainly, heterogeneous catalysts are employed in the selective reduction of unsaturated aldehydes. Furthermore, catalysts based on group VIII transition metals dominate when it comes to this type of chemical transformation due to their high activity towards reduction of various unsaturated bonds. Singh and Vannice[8] showed that the d-character of metal influences its catalytic performance. It has been shown that plotting initial turn-over frequencies (TOF) in citral hydrogenation with percentage of d-character of metals results in formation of a volcano-shape dependence (Fig. 1). This result indicates that there is an optimal and balanced d-electrons contribution at which the highest catalyst activity can be achieved.

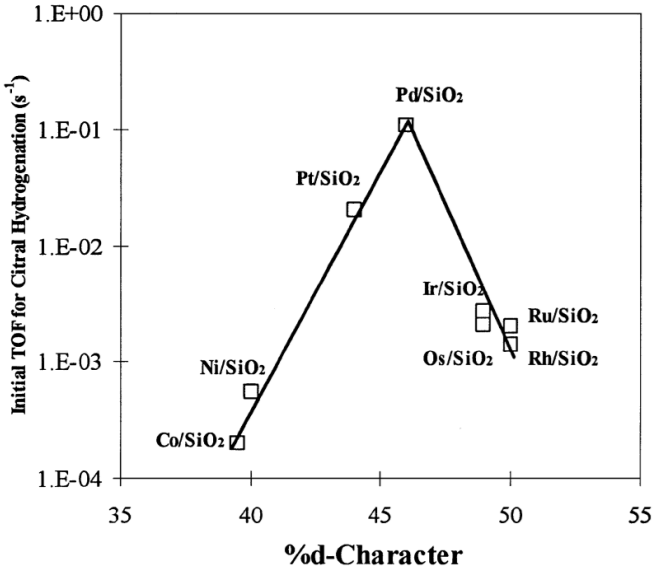

Figure 1. The influence of d-character of group VIII metals on catalytic performance in citral hydrogenation. Reproduced from[8] with permission.

In another study,[9] theoretical calculations revealed a direct correlation between d-band width of transition metals and their selectivity in competitive alkenyl vs carbonyl bond hydrogenation. It was shown that metals with higher d-band radial expansion possess higher selectivity towards carbonyl bond reduction. Greater d-bands cause stronger repulsive interactions with four electrons of the C=C bond lowering its adsorption probability. These theoretically derived conclusions found their experimental confirmation. For instance, in hydrogenation of crotonoaldehyde[10] and cinnamaldehyde[11] over group VIII metals on carbon supports. The reactions catalyzed by metals with wide d-bands (Os, Ir) led to formation of unsaturated alcohol by C=O reduction. On the other hand, application of metals with narrower d-bands (Pd, Ni) decreases selectivity towards carbonyl bond hydrogenation.

Besides the nature of a specific d-block metal, many different aspects need to be taken into account when it comes to bond control in surface reactions. All those factors and considerations are described in subsequent parts of this chapter.

2.1.1. NOBLE METAL CATALYSTS

Evaluation of numerous studies on α,β-unsaturated aldehydes hydrogenation clearly displays a great preference of catalysts based on noble metals, especially palladium and platinum. Nonetheless, high activity can affect selectivity of noble metals making them less product-specific. It means that parallel reactions can simultaneously occur on surface of highly active metal phase. To improve product-specificity, catalysts are modified in different ways, such as: by introduction of another less active metal, modulation of metal – support interactions or optimizing the entire catalytic systems.

In the case of platinum catalyst which is most frequently used in α,β - unsaturated carbonyls hydrogenation, mainly mixture of semi-saturated products is obtained. To direct the reaction towards one specific product, electronic structure of Pt catalysts is tuned by various additives. It has been demonstrated that thiol modifiers deposited on a Pt/Al_2O_3 surface can change its selectivity in cinnamaldehyde[12] and prenal[13] hydrogenation. During the modification self-assembled monolayers were created on Pt surface changing the electronic properties of the catalyst. Additionally relatively long-chained alkenethiol molecules caused noncovalent interactions with approaching aldehydes. Combination of those factors promoted carbonyl bond reduction leading to increase in unsaturated alcohol formation. Kahsar et al.[6] showed that coating Pt/Al_2O_3 catalyst with 3-phenyl-1-propanethiol monolayer increased selectivity to C=O hydrogenation from 25 to 90%. This significant enhancement was obtained at the expense of activity. By addition of surface modifiers, active sites that host competitive parallel reactions are blocked.[14,15]. Consequently it resulted in lower accessibility of Pt surface and decreased catalyst activity.

Rautio et al.[16] presented improvement of Pt catalyst selectivity to carbonyl reduction by Sn doping. In this case TiO_2 supported Pt was enriched with various loadings of tin and tested in citral hydrogenation. Selectivities to C=O hydrogenation were higher at higher tin loadings but activity dropped dramatically. The 100% conversion of monometallic 2 wt.% Pt catalyst was reduced to 10% when tin and platinum were in equal proportions (2 wt.% Sn – 2 wt.% Pt). Theoretical calculations showed that tin presented on the catalyst surface impacts the adsorption of polyunsaturated carbonyls.[17] Due to their wide radial expansion, Sn atoms cause steric repulsions with adsorbing carbonyl molecules, which tunes catalyst selectivity. By those repulsions specific adsorption mode is enforced favoring C=O hydrogenation. Bidaoui et al.[18]

modified Pt catalyst with zinc in order to improve its selectivity. A similar trend to the Sn modification was observed when Pt/SBA-15 (mesoporous silica) material was doped with various amount of Zn. Higher addition of Zn promoter led to increase in unsaturated alcohol formation (up to 75%). Note that the Zn promoter deposited on platinum underwent oxidation. Zinc in oxidized form can fix the oxygen atoms from carbonyl group leading to its activation. Different metals from IIB-IVB groups, such as Ga or In[19], indicate similar impact on competitive adsorption between C=O and conjugated C=C bond. In all cases, these dopants enhanced platinum catalyst selectivity to carbonyl hydrogenation sacrificing its activity.

This trend was not observed when surface of Pt catalyst was modified with group VIII transition metals, especially iron. As study shows, α,β – unsaturated aldehydes hydrogenation over Pt-Fe catalysts may result in high selectivity while preserving or even improving activity. Qu et al.[20] demonstrated how addition of small quantities of Fe altered Pt catalyst performance in citral hydrogenation. When the parent catalyst, 5% Pt supported on multiwalled carbon nanotubes was enriched with 0.25% of Fe, selectivity to unsaturated alcohols rose from 33.7 to 90.7%. Moreover, conversion values for both materials were the same (~ 67%).

In another study[21] the use of Fe modification led to significant improvement in both activity and selectivity. Zeolite supported Pt catalyst displayed doubled activity (77% of conversion) and advanced alcohol production by 10% when iron contributed 0.25% of the catalyst. The presence of Fe species can play a twofold role in competitive C=O and C=C hydrogenation. Firstly, it can tune platinum electronegativity and increase electron density on its surface decreasing probability of alkenyl bond activation.[22] Moreover, it could facilitate polarization of carbonyl group for nucleophilic attack by hydrogen atoms.[23] Secondly, FeO_x species may interact with C=O bond as Lewis acidic sites favoring its hydrogenation.[24]

Modification of electronic properties of metal active phase can be also achieved by application of electron-donating supports. Materials which are able to transfer electrons to metal surface change the charge density of Pt surface. Stronger repulsions of conjugated C=C bond results in higher probability of carbonyl function activation. Richards et al.[25] compared two Pt catalysts supported on activated carbon (AC) and graphite (G) to study an influence of electronic effect. Synthesis of Pt/G material involved graphite pretreatment with NaOCl solution leading to carbonyl groups formation on its surface. Platinum was introduced by ion exchange with $[Pt(NH_3)_4]^{2+}$

and then reduced under H_2 atmosphere. It was found that this catalyst indicated higher selectivity towards unsaturated alcohol than similar activated carbon supported material. Results showed lattice expansion of Pt for Pt/G catalyst, which was interpreted as a consequence of electron transfer from graphite to antibonding orbitals of Pt clusters.[26]

Steffan et al.[27] expanded this comparison to commonly used supports in heterogeneous catalysis. Beside activated carbon and graphite, they employed silica and alumina as Pt catalyst supports. It was shown that graphite due to its electron transfer properties indicates the highest ability to promote carbonyl hydrogenation. The trend was as follows: Pt/AC < Pt/Al_2O_3 <Pt/SiO_2 < Pt/G. Moreover, citral hydrogenation with graphite supported catalyst showed significant increase in selectivity towards unsaturated alcohol in comparison to conventional supports.

Wei et al.[28] demonstrated electron enrichment of Pt surface by acidity alteration with CeO_2 – ZrO_2 composite. In their approach, zirconium was incorporated into ceria lattice structure, resulting in an enhancement of overall acidity of the material. Application of this composite as a Pt catalyst support led to formation of electron-rich platinum species and surface defects, which together with acidic sites promoted carbonyl bond activation. As shown Pt/ZrO_2-CeO_2 catalyst displayed very high activity (95% of conversion; TOF = 10423 h^{-1}) and selectivity to unsaturated alcohol (94%).

Malathi and Viswanath[29] established a correlation between titania reduced species (TiO_{2-x}) and selectivity of citral hydrogenation over Pt/TiO_2 catalyst. In their report, the selectivity improvement was assigned to electron transfer from Pt to the support. Reduced titania species were found to coordinate C=O group and facilitate its hydrogenation. Different study[30] proved that titania supported platinum catalyst showed enhancement in activity and selectivity towards C=O reduction when compared with Pt/SiO_2. Thus, strong metal-support interactions make TiO_2 an interesting material for α,β – unsaturated aldehydes hydrogenation.

On that basis, new catalyst supporting composite was synthesized by combination of titania and carbon xerogel using sol-gel method.[31] Moreover, porosity of the carbon xerogel could be determined by introduction of various amount of titania. The series of Pt catalyst supported on composite with different TiO_2 content was tested in citral hydrogenation. It was found that addition of titania also change product distribution in the reaction. When pure carbon xerogel was used as a support, the C=C hydrogenation

was a main reaction. After composition modification, the selectivity was shifted towards unsaturated alcohol. Authors interpreted this selectivity change as a result of synergetic effects between both phases of the composite, responsible for Pt-support interactions.

Catalysts based on another noble metal, palladium, were also extensively investigated in competitive carbonyl and alkenyl bond hydrogenation. Mainly, Pd/support catalysts exhibit higher affinity to C=C activation forming products of conjugated carbonyl bond saturation in α,β – unsaturated aldehydes hydrogenation. Numerous reports showed that palladium catalysts indicate very high selectivity to alkenyl bond reduction in low temperature and pressure. In Steffan et al. report,[32] hydrogenation of citral over Pt/Al_2O_3 material at 30°C and 0.5 MPa resulted in 95% of selectivity to citronellal (product of conjugated alkenyl bond saturation) with 73% of conversion. That tendency has been confirmed with Pd supported on different materials, like: $Pd/CaCO_3$ ($S_{C=C}$ = 95%, X = 94%)[33], Pd/zeolite ($S_{C=C}$ = 80%, X = 99%) or $Pd/C/TiO_2$ ($S_{C=C}$ = 90%, X = 99%)[34]. Wang et al.[35] applied magnetic porous material Fe_7Co_3/C as a support for Pd active phase in hydrogenation of citral. The catalyst was able to convert 84% of the unsaturated aldehyde with 93% of selectivity to citronellal. Additionally, it was shown that due to magnetic properties, catalyst could be easily separated from the reaction media with a magnet.

Similarly to platinum, palladium catalysts have been also subjected to surface modifications in terms of selectivity change. To increase unsaturated alcohol formation by C=O reduction, various additives have been used. Generally, surface modification shifts selectivity of Pd towards carbonyl bond activation but not very spectacularly. Kahsar et al.[36] coated Pd/Al_2O_3 surface with different thiol monolayers. The behavior of such modified catalyst differed from thiol-coated Pt materials. In Pd catalysts, presence of thiol monolayer slightly increased C=O hydrogenation only under low pressure (6 bar). When higher pressure (40 bar) was applied, the catalyst showed better selectivity to C=C bond hydrogenation then naked Pd/Al_2O_3. Moreover, in contrary to Pt catalysts, there was no difference in selectivity change between thiols with various organic tails. This might be a consequence of different adsorption geometries that occur on Pt and Pd surfaces. Therefore, mechanisms explaining interactions between thiol decorated metal surface and reactants are divergent.

Regarding metallic dopants, Fe and Zn were also used to steer selectivity of palladium

catalysts. Similarly to platinum materials, the presence of those transition metals additives on Pd surface promoted C=O hydrogenation in expanse of activity but with lower efficiency. For example[37], $FeCl_2$ addition to the Pd/natural zeolite catalyst shifted its selectivity towards carbonyl bond saturation. The highest value (40%) was obtained with atomic ratio of $Fe^{2+}/Pd = 1$.

The unique catalytic properties were observed for PdZn/ZnO material.[38] PdZn catalyst containing 30 wt.% of Pd exhibited unusual behavior during cinnamaldehyde hydrogenation. Initial stage of the reaction with low conversion yielded mainly C=C saturation product. However, selectivity started to change in favor of C=O reduction when conversion was rising. It was found that hydrocinnamaldehyde (formed in initial stage) was adsorbed via carbonyl groups on PdZn surface without undergoing hydrogenation. Therefore, catalysts poisoning enforced specific adsorption geometry of cinnamaldehyde molecules promoting aldehyde group hydrogenation (Fig. 2).

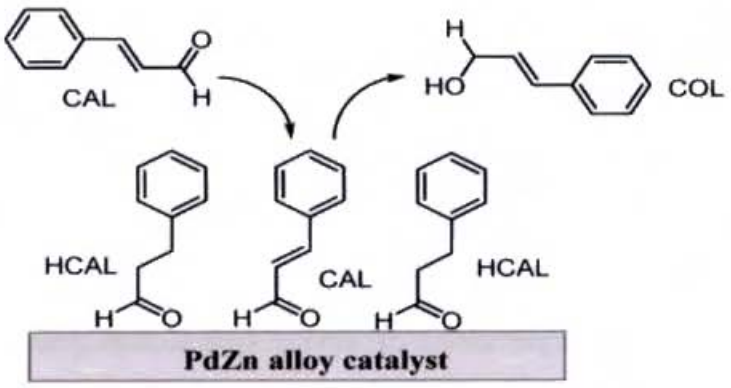

Figure 2. Cinnamaldehyde adsorption on PdZn surface crowded by hydrocinnamaldehyde molecules. Reproduced from[38] with permission.

Bimetallic catalysts, such as PdAu also indicate possibility to tune selectivity in α,β – unsaturated aldehydes hydrogenation. Szumełda et al.[39] presented catalytic performance of carbon supported Pd doped with gold at various Au/Pd ratios in cinnamaldehyde hydrogenation. Addition of Au to Pd catalyst induced selectivity change to C=O saturation with tendency: the higher Au contribution the higher the selectivity to carbonyl reduction.

Pd on MCM-41 silica material enriched with small amout of Ag (0.3%) was found to support C=C activation improving Pd properties in cinnamaldehyde hydrogenation.[40] Authors concluded that presence of silver inhibits nanoparticles growth providing

well-dispersed metal active phase. Additionally, Ag influences electronic structure of Pd surface, which results in selectivity shift. Silver-doped Pd catalyst significantly improved performance in comparison to monometallic Pd material. Conversion increased from ~ 60% to > 99.9% and selectivity towards alkenyl bond reduction from 85 to 99%.

Supporting material can also have a significant impact on palladium selectivity in competitive hydrogenations. Nagpure et al.[41] studied the effect of nitrogen incorporation in mesoporous carbon used as a support for Pd catalyst. For that purpose, they compared two catalysts supported by either pure mesoporous carbon and material doped with N. It was observed that presence of nitrogen remarkably enhanced catalytic performance of palladium catalyst. Catalyst supported on N-doped carbon indicated conversion improvement from 66% to 100% in cinnamaldehyde hydrogenation. Moreover, catalyst enriched with N was more selective towards C=C reduction with 93% of selectivity in comparison to 44% for mesoporous carbon supported one. Activity increase after nitrogen incorporation resulted from better Pd dispersion on the support surface, hence, higher population of metal active sites that host hydrogenation. Selectivity improvement might have been caused by higher electron density on Pd surface after N doping. Electron transfer form N enriched support to the metal modulated electronic properties of Pd and consequently promoted C=C reduction.

Considering Pd catalysts, presence of acidic functional groups has a significant impact on metal-support interactions and further on catalytic performance of the catalysts.[42] Pd valence consists primarily of 4d orbitals which are partially hybridized with 5s orbitals. These states can interact with the lone electron pair of carbonyl bond from surface modifiers (anhydrides or carboxylic acids),[43] resulting in strong metal - support interactions that facilitate dissociative H_2 adsorption on Pd. Consequently, metal surface is abundant with reactive hydrogen species crucial in hydrogenation reactions.

Besides dissociative adsorption, the presence of oxygen functional groups conduces H species spillover on Pd surface increasing H atoms accessibility.[44] It has been demonstrated that Pd supported on carbon materials with oxygen functional groups displayed enhanced catalytic activity in butadiene hydrogenation. In this instance, increase in activity (100% of conversion) was accompanied by drop in selectivity to butane yielding completely saturated product.[45] This behavior clearly indicates that

oxidative properties of a support improve Pd – H interaction and overall catalyst activity in hydrogenation processes.

Divakar et al.[46] showed that the presence of a Lewis acid on catalyst surface may influence selectivity of Pd. Bentonite supported Pd particles were reduced by three different agents: ethanol, H_2, $NaBH_4$ and then subjected to citral hydrogenation. It was found that only catalysts reduced with $NaBH_4$ were able to activate C=O group leading to 35% of selectivity to unsaturated alcohol. They concluded that the traces of B on palladium surface were responsible for charge transfer to Pd species. Increased charge density on palladium surface caused stronger repulsive four-electron interactions with C=C bond facilitating C=O hydrogenation.

According to scientific reports on the subject, platinum and palladium are undoubtedly the most widely applied noble metals in chemoselective hydrogenation of α,β – unsaturated aldehydes. However, methodologies involving other noble metals, such as Au and Ir, have been also reported. Khanderi et al.[47] demonstrated citral hydrogenation over Au catalyst supported on carbon nanotubes. As shown, gold indicated higher probability to promote C=O activation than Pd or Pt especially with lower conversions. Additionally, doping the catalyst with ZnO favored carbonyl reduction yielding unsaturated alcohol with 50% selectivity and 20% conversion.

More spectacular result was obtained over Au/hydrotalcite catalyst.[48] In this case, citral hydrogenation resulted in formation of unsaturated alcohol with 98% selectivity with higher conversion. This tendency is confirmed with various Au – supported catalysts.[49,50,51]

Pristine gold nanoparticles were also found active in hydrogenation reactions.[52] Butt et al.[53] demonstrated a protocol for α,β – aldehydes hydrogenation with unsupported mesoporous Au nanoparticles. With formic acid as internal hydrogen source the reaction yielded unsaturated alcohol as the only product. In addition, naked Au nanoparticles were able to reach conversion at the level of ~ 97%. Proposed mechanism of the hydrogenation over mesoporous Au NP is presented in Fig. 3.

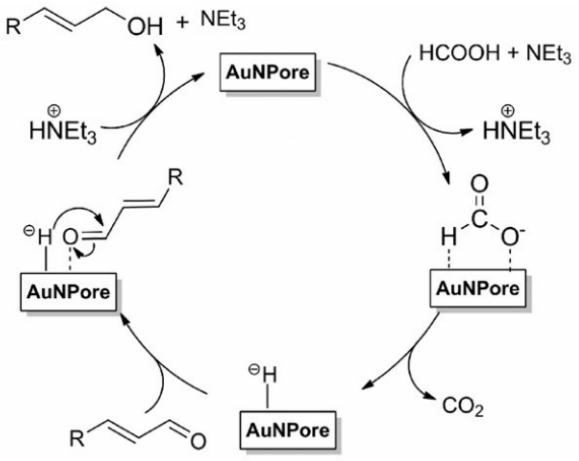

Figure 3. Mechanism of selective hydrogenation over naked gold nanoparticles. Reproduced from[53] with permission.

Similarly to gold, supported iridium catalysts were also able to promote carbonyl hydrogenation in competitive C=C vs C=O reduction. It was reported that Ir supported on TiO_2 or SiO_2 containing TiO_2 was employed in citral hydrogenation.[54,55] Irrespective of supporting material composition all tested catalysts displayed high selectivity to C=O reduction. It was observed that titania plays a crucial role in activation of carbonyl bond. Strong metal – support interactions (SMSI) resulted from an electron transfer from Ir to TiO_2 lead to increase of charge density on metal surface. The presence of TiO_{2-x} species enabled polarization of C=O bond and consequently its hydrogenation.

More recent studies on catalytic performance of Ir catalysts in hydrogenation reactions involved various modifications of the metal phase. To increase activity and selectivity, iridium can be enriched with small amounts of different oxides such as: NiO_x[56], ReO_x[57], CrO_x[58] or FeO_x[58]. In general, those catalysts show better catalytic performance and higher probability to promote C=O bond then monometallic Ir analogue in selective reduction of crotonaldehyde. Such improvement can be interpret as a result of creating new active sites $Ir^{\delta+}$ - MeO_x on the catalyst surface, which have higher affinity to C=O bond reduction. Therefore, the mechanism is similar to Ir/TiO_2 and relies on electron transfer between Ir and oxides additives.

2.1.2. LOW-COST TRANSITION METAL CATALYSTS

Non-noble metals have been also extensively applied to steer product-specificity of α,β – unsaturated aldehydes reduction. Better cost-efficiency and activity in hydrogenation reactions make non-noble metals attractive catalysts for industrially relevant chemical processes. Literature survey concerning this topic shows that nickel supported catalyst is one of the most thoroughly investigated material in competitive alkenyl and carbonyl bonds hydrogenation. Application of Ni based catalysts leads mainly to formation of saturated aldehyde as a main product. Mäki-Arvela et al.[59] demonstrated citral hydrogenation catalyzed by Ni/Al_2O_3 at wide range of temperatures and pressures. Product distribution clearly indicated hydrogenation of conjugated C=C bond as a dominant reaction. Besides main product (citronellal), the reaction yielded citronellol (conjugated C=C and C=O reduction) and completely saturated compound (dihydrocitronellol). It was found that unsaturated alcohol was formed in traces.

In another report from Mäki-Arvela et al.[60], the authors compared Ni catalysts supported on silica and alumina prepared via various methods. All prepared catalysts contained relatively high metal content 4.7 – 16.7 wt.% which resulted in good activity in citral hydrogenation. High metal dispersion affected product-specificity in the reaction, leading to the formation of products related to the hydrogenation of both carbonyl and conjugated alkenyl bonds. Nevertheless, the authors managed to reach selectivity to citronellol as high as 70 – 85% in all cases. Additionally high metal content facilitated addition of two ethyl groups to citronellal yielding diethyl acetal as undesired side product.

Neelakandeswari et al.[61] tested nickel aluminosilicate nanocomposite in chemoselective carbonyl hydrogenation. In this case, used support combined properties of silica and alumina in composite material synthesized by sol-gel method. The authors examined catalytic performance with different heterocyclic carbonyl compounds using isopropanol as hydrogen source. They showed that Ni based catalyst displayed very high activity towards alcohols formation. However, it should be mentioned that in this case the α-position is occupied by phenyl ring which introduces additional structural aspects when compared to aliphatic alkenyl bond in α,β – unsaturated aldehydes.

The influence of preparation method was also investigated with titania supported Ni.[62]

A series of catalysts was prepared via four different techniques. The authors found that the preparation methods influenced essentially metal nanoparticles size and surface composition. Analysis of cinnamaldehyde hydrogenation revealed that catalysts with smaller particles showed higher activity and a slightly higher selectivity towards C=O reduction. However in all cases the reaction yielded all possible products. Low product – specificity could be connected with high metal content (15 - 16 wt.%). Selectivity to carbonyl bond reduction on Ni surface could be increased by promoting metal – support interactions. Titania has a tendency to be an electron acceptor, which led to formation of oxidized Ni species. The Ni^{2+} species affected adsorption of aldehyde molecules by steric hindrance, favoring adsorption via C=O groups and consequently facilitating their reduction (Fig. 4).

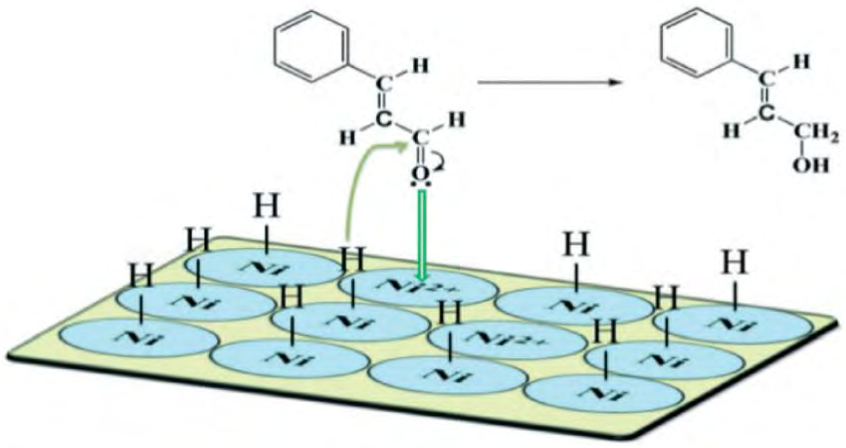

Figure 4. Cinnamaldehyde hydrogenation on Ni oxidized species. Reproduced from[62] with permission.

Such approach yielded an unprecedentedly high selectivity towards unsaturated alcohol (61% for catalyst reduced with d-glucose) when compared with similar catalysts reported in literature[63]. As shown in this report[63], titania supported Ni with 11 wt.% of metal transformed cinnamaldehyde into saturated aldehyde with 98% of selectivity with no traces of unsaturated alcohol. Selectivity of the catalyst did not change even after doping with noble metal Ir. Another examples clearly indicated that Ni catalysts preferably hydrogenate C=C bond irrespective of supported material: 5%Ni/SBA-15[64], 10%Ni/CNF/AC[65], $10\%Ni_{12}P_5/SiO_2$[66].

Generally, carbon supported catalysts display different products distribution when compared to metals supported on SiO_2 and Al_2O_3. In citral hydrogenation, application

of Ni/C type catalysts leads to hydrogenation of only conjugated alkenyl bond (both C=C and C=O with SiO_2 or Al_2O_3) yielding high selectivity towards citronellal. For instance, carbon nanotubes supported Ni catalyst[67] and Ni/graphite[68] displayed 87% and 93% selectivity to C=C reduction, respectively. Moreover, it was noticed that the temperature of catalyst reduction and the type of a reducing agent had impact on selectivity of those catalysts. Mahata et al.[69] used Raney-type NiC catalyst for crotonoaldehyde hydrogenation. They found that irrespective of reaction time and solvent, reaction yielded C=C hydrogenation product with ~ 99% of selectivity.

To tune Ni selectivity in citral hydrogenation Yang et al.[70] doped Ni/C catalyst with ZnO. Interactions between zinc oxide and nickel influenced both electronic and geometric properties of metallic active sites and consequently catalytic performance of the material. They showed that higher content of ZnO modifier decreases Ni activity especially in short-term reaction. The relation between ZnO content and selectivity followed a volcano shape plot indicating Ni – (10.6 wt.%)ZnO/C as most selective catalyst to both C=O and conjugated C=C hydrogenation product (citronellol). In addition, citronellol formation was decreasing during the reaction over Ni/C catalyst down to 0% after 7 h, whereas, Ni – (10.6 wt.%)ZnO/C showed opposite trend yielding citronellol with 92% selectivity after the same period of time.

A similar effect was obtained by Bhogeswararao et al.[71] with nickel catalyst supported on CeO_2 and ZrO_2. The authors found that selectivity of Ni supported on various combinations of cerium and zirconium oxides changed after addition of NaOH to reaction medium. Alkali-free cinnamaldehyde hydrogenation over Ni catalysts yielded C=C reduction product with 90 – 100% of selectivity after 8 h on stream. When NaOH was added, the selectivity shifted towards completely saturated compound (65 – 90%). The authors concluded that presence of OH^- electronically influenced metal properties, whereas, Na^+ ions might facilitate C=O bond polarization promoting its hydrogenation.

Selectivity in citral hydrogenation could also be steered by using metal borides materials. Liaw et al.[72] used Ni and Co borides as catalysts in competitive citral hydrogenation reaction, in the following formulations NiB, CoB and CoNiB. Amorphous NiB material yielded almost exclusively conjugated C=C hydrogenation. The CoNiB material containing equal quantities of Ni and Co displayed similar behavior forming citronellal with 71% after 2 h. The authors found that binding energy

of alloying B state was higher on the CoNiB catalyst. This result led to conclusion that Co and Ni in CoNiB had a higher electronic density then monometallic materials. Therefore, combined CoNiB catalyst was the most active in this collation. On the other hand, CoB catalyst showed very high affinity to carbonyl bond yielding unsaturated alcohol with 75% of selectivity after 2 h.

Subsequent study[73] provided more insight into catalytic behavior of Ni and Co borides. As previously, with Ni_7B_3 material the C=C bond was preferably hydrogenated, whereas, Co_2B led to carbonyl bond saturation as a dominant reaction. They showed that reaction temperature impacts selectivity of this catalytic system. The CoNiB catalyst displayed lower selectivity towards citronellal (conjugated C=C reduction) favoring citronellol formation (both conjugated bonds saturation). Rudolf et al.[74] demonstrated that binary NiAl and CoAl materials are active and highly selective in cinnamaldehyde hydrogenation. The materials were prepared from takovite-like layered double hydroxide (LDH), calcinated and then reduced. NiAl material showed a very high affinity to conjugated C=C hydrogenation yielding hydrocinnamaldehyde with 95% at complete conversion of α,β – unsaturated aldehyde. The nickel containing material was remarkably more active than CoAl. It was observed that CoAl activity could be increased by catalyst reduction at higher temperature (700°C). However, cobalt binary material displayed high probability to activate C=O bond forming cinnamyl alcohol with 70% of selectivity at 50% conversion of cinnamaldehyde.

Recently, it was reported that aluminum itself can by highly active and selective in α,β – unsaturated aldehydes reduction. Xu et al.[75] showed methodology for core/shell nanospheres of metallic Al coated with amorphous Al_2O_3 synthesis and their catalytic performance in cinnamaldehyde and furfural hydrogenation. Such catalyst indicated very high activity in abovementioned reaction (99%) leading to formation of unsaturated alcohols with equally high selectivity (99%). The excellent catalytic properties of the material were assigned to synergetic effect between highly electrically conductive Al core and unsaturated sites of ultrathin (3.2 ± 0.5 nm) Al_2O_3 coating. The mechanism of the molecules activation on Al/Al_2O_3 surface is presented in Fig. 5.

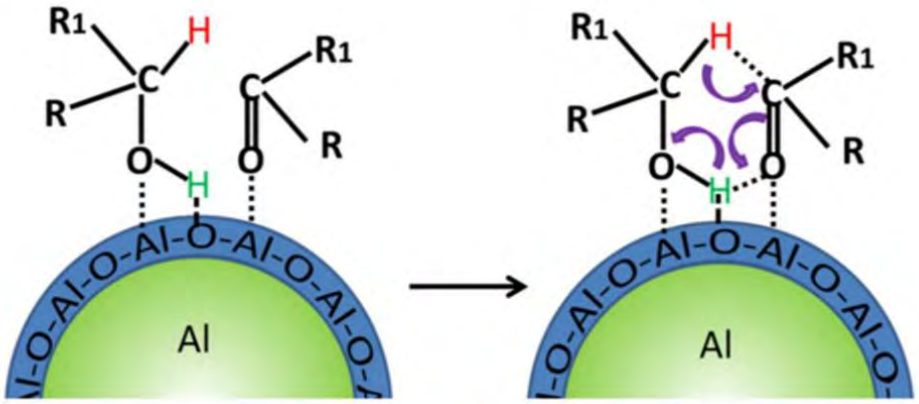

Figure 5. Mechanism of C=O bond activation on Al/Al_2O_3 nanospheres. Reproduced from[75] with permission.

Shi et al.[76] proposed $CePO_4/Ni_2P$ nanocomposite prepared in a one-pot synthesis as active catalyst for the competitive C=C vs C=O hydrogenation. The solvothermal synthesis relied on co-bonding of Ni^{2+} and Ce^{3+} with HPO_4^{2-} ions. This material was found very active and selective towards alkenyl bond reduction with numerous compounds. It was concluded that $CePO_4$ is responsible for hydrogen activation which than attacks C=C bonds in molecules adsorbed on Ni_2P species.

Current studies on development of new and efficient catalyst for selective hydrogenation also include metal-organic frameworks (MOF) materials. Their properties such as very high porosity and surface area make MOFs suitable materials for catalytic applications.[77] Their customizable structures offer multiple possibilities for catalyst designing.[78] Zhang et al.[79] prepared MOFs-derived catalysts containing non-noble metals and utilized them in cinnamaldehyde hydrogenation. In their approach, Ni, Fe or Co supported on silicides were incorporated to porous carbon nanocrystals forming Me_2Si/C materials. Preparation process affected catalysts surface removing carbon accumulated on metal surface consequently enabling deposition of Si atoms. This atom exchange introduced electronic and geometric changes, which resulted in activity improvement of Me_2Si/C in comparison to adequate Me/C catalysts. Ni material yielded mainly C=C reduction product with conversion higher than 90% after fifth cycle. When Co_2Si/C was used, selectivity shifted towards C=O hydrogenation forming 60% of unsaturated alcohol.

Cobalt supported catalysts indicate high probability of carbonyl bond activation in

selective α,β – unsaturated aldehydes hydrogenation. It has been proven with Co catalysts on various carriers in citral hydrogenation.[80] In all cases, formation of unsaturated alcohol was dominant reaction, nonetheless, the catalysts showed rather poor activity. Lee et al.[81] reported that by strong metal-support interactions Co/TiO_2 catalyst can be stabilized in furfural aqueous – phase hydrogenation (Fig. 6). Thin TiO_x layer on Co nanoparticles preventing sintering and leaching of the active phase in aqueous medium. Therefore, the catalyst displayed very good performance in the reaction. Titania – coated Co catalyst was highly selective towards C=O reduction with yield to alcohol as high as 95%.

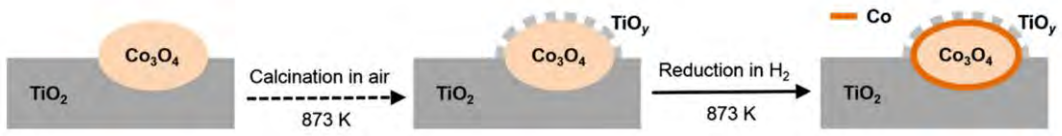

Figure 6. Preparation of titania-stabilized Co/Co_3O_4 catalyst for citral hydrogenation. Reproduced from elsewhere[81] with permission.

Audemar et al.[82] investigated influence of reaction conditions on catalytic behavior of SBA-15 supported Co catalyst. As reported, increase in temperature from 100°C to 150°C resulted in activity improvement (from 20% to 100% of conversion; 2h, 2 MPa) accompanied by selectivity loss from 90% to 76%. Notwithstanding, Co active phase deposited on SBA-15 demonstrated good catalytic properties in furfuryl alcohol production from furfural, as well as γ – valerolactone from levulinic acid. The report suggested that Co-based catalyst activity strongly depends on the reaction temperature. The trend is as follows: Co is low active at low temperature and low selective at higher temperature.

Carbonaceous materials have been also used as carriers for Co catalyst in furfural hydrogenation.[83] Recently Jiang et al.[84] applied nitrogen – doped carbon porous material (CPN) as a support for Co nanoparticles for α,β – unsaturated carbonyls hydrogenation. Besides temperature influence, the researchers investigated impact of various solvents. Among polar and non-polar substances, reaction carried out in alcohols (methyl alcohol, ethyl alcohol and isopropanol) resulted in best activities (99% of conversion). In terms of selectivity, reaction in isopropanol formed 99% of furfuryl alcohol which was the highest value obtained.

Regarding noble metal – free bimetallic catalysts, Ni – Me (Me = various transition metals) systems preponderate in the literature. For instance, addition of Co to carbon supported Ni catalyst shifted its selectivity in cinnamaldehyde reduction towards unsaturated alcohol.[85] The equal contribution of both metals (5 wt.%) led to balanced selectivity between C=O and conjugated C=C hydrogenation products.

Modification of highly active metal phase with less active dopant for selectivity improvement is a common operation in catalysis. In this light, moderately active transition metals are incorporated to Ni active sites to change their electronic properties and to promote more energy demanding carbonyl bond reduction. Prakash et al.[86] showed that Ni – Cu systems embedded on TiO_2 indicated slightly higher selectivity to C=O hydrogenation with cinnamaldehyde than monometallic Ni material while preserving good activity. Use of electron - accepting support facilitated C=O activation even over monometallic Ni active phase. However, the presence of dopants changed product distribution increasing selectivity to completely saturated product. Therefore it can be assumed that saturated aldehyde formed on Ni species underwent further hydrogenation triggered by second metal. Similar effect was observed with Ni – Cu catalyst supported on organo-functionalized graphene oxide.[87] Studies on optimization of Ni/Cu molar ratio revealed that material with equal loadings of both metals displayed the best catalytic performance in cinnamaldehyde reduction. Furthermore, it was noticed that higher temperature increased both conversion and formation of unwanted, completely saturated product.

Copper addition to Ni catalyst exhibited different catalytic behavior when citral was subjected to hydrogenation. In this case, the presence of copper enhanced Ni selectivity to C=C hydrogenation and suppressed side reactions increasing product – specificity in citral chemoselective saturation. For instance, selectivity to citronellal of Ni(4 wt.%) – Cu(1 wt.%)/KL – zeolite material was increased from 75% to >90% when Cu contributed 4 wt.% of the catalyst as well.[88] Nevertheless, the authors found that activity decreased with higher loading of copper and it was concluded that the presence of copper influences the nature of Ni species. The number of metallic Ni active sites deceased with increase of Cu loading. Generally, in NiCu systems more than 90% of copper and less than 90% of Ni is in metallic state. This tendency was proved with different supports irrespective of catalyst pretreatment.[89] Hence, copper modulates electronic structure of Ni surface due to Ni oxidation.

2.2. CONTINUOUS FLOW CATALYSIS

Development of chemical manufacturing constantly strives towards new and more efficient solutions for making chemical industry 'greener' and more sustainable. In this matter, process intensification seems to be the key to introduce significant improvements to chemicals production. Ramshaw defined process intensification as a strategy for minimization and optimization of chemical processing by significant reduction of all expenditures involved in the process.[90] This can be accomplished either by shrinking the equipment, reducing the size of individual apparatus parts or reducing number of unit operations.[91] Moreover, process intensification by such serious cuts should maintain comparable or even better efficiency of chemical transformations. In this matter, continuous flow catalysis with micro-reactors fits in the prospects of modern chemical manufacturing.

2.2.1. CONTINUOUS FLOW FOR PROCESS INTENSIFICATION

In spite of the remarkable advances on flow chemistry with micro-reactors in 1990s[92], this technology has not been widely developed. This restrained progress could have been caused by many patents that covered multiple aspects associated with micro-reactors operating.[93] However, more recently, micro-capillary devices have found wide-range application in chemically related areas. That might be a result of the fact that many of those patents have expired consequently pursuing development of flow chemistry.

The advantages of continuous processing vary from great catalytic performance, in terms of both activity and selectivity, through better energy efficiency to safety issues. In comparison to conventional batch reactors, continuous flow systems exhibit improved mass and heat transfer. Therefore, reaction conditions in flow are well defined, which is important in terms of process scalability for industrial implementation. Furthermore, continuous flow operating conducted in micro-reactors is usually completely or partially automatized, hence, it demands less manpower. From environmental point of view, flow chemistry minimizes generation of wastes due to high atom-efficiency.

In heterogeneous catalytic micro-reactors, a reactant containing liquid phase is flown through solid catalyst bed. Generally, catalyst consists of two main components: active

phase and high surface area, porous support. Therefore mass transfer in heterogeneously catalyzed flow reactions needs to be interpreted in two ways, namely: externally and internally. External mass transfer includes the diffusion of reactant and product molecules on catalyst surface, whereas, internal mass transfer defines diffusion of molecules in porous network of the support.

External mass transfer is defined as a difference between reactant concentrations in the liquid phase that flows through catalyst bed and in the interphase layer on catalyst particles surface multiplied by mass transfer coefficient:

$$N_a = k_g(C_a - C_{aS})$$

where N_a is the molar flowrate of reactant A [kmol/m^{2}s]; k_g is the mass transfer coefficient and C_a and C_{aS} are concentrations of a in liquid bulk and on particles surface, respectively.

Since the reaction rate – r_a depends on interphase concentration of A, under steady state conditions r_a can be limited by itself as reaction proceeds and A molecules are consumed or by the velocity in which A molecules are delivered to the catalyst surface. Thus, those two limitation factors have to be considered in kinetic studies:

$$r_a = C_a/(\frac{1}{k_g} + \frac{1}{k_r})$$

where r_a is the reaction rate and k_r is the intrinsic kinetic constant for first order reactions.

Internal mass transport introduces additional limitations associated with the nature of the supporting material. The diffusion of molecules inside porous network occurs differently in pores with narrow and relatively wide diameters. Therefore to calculate the diffusion coefficient, two limiting phenomena need to be taken into consideration. When the size of pores is significantly bigger than the molecules, it is more likely for molecules to collide with each other than with the pore walls. On the other hand, the molecule interactions with pore walls dominate when their sizes are comparable. Hence, by summing diffusion coefficients of those possible resistances, an effective diffusivity can be obtained:

$$\frac{1}{D_E} = \frac{1}{D_{MM}} + \frac{1}{D_{MW}}$$

where D_E is the effective diffusivity, D_{MM} diffusion coefficient that includes molecule to molecule collisions and D_{MW} molecule-walls collisions (Knudsen diffusion coefficient).[94] Mass transfer as a limitation of reaction rate strongly depends on surface area-to-volume ratio, A/V. When A/V is high, statically it takes a shorter time for reactant molecules to diffuse to the catalyst surface. In other words, high A/V ratio decreases diffusion resistances that can limit surface reactions rates. In this light, continuous operating in micro-reactors displays significant advantage over batch systems. Small internal volume of micro-reactors results in remarkably higher values of surface area-to-volume ratio when compared to batch mode.

Typical A/V value in micro-reactors is in a range of 10,000 – 50,000 m^{-1},[95] which ensures large interfacial area between liquid and solid phases in heterogeneous catalysis. High value of this parameter is also essential for improved heat transfer especially when process bases on exo- and endothermic reactions.

The interphase heat transfer is addressed similarly to convective mass transport, when heat is transferred to and from catalyst surface with flowing liquid.[96] Thus, the area-to-volume ratio has direct impact on temperature changes in interfacial catalytic reactions. Convective heat transfer in surface reaction, according to Newton's law of cooling, can be described by following equation:

$$(-\Delta H_{reaction})r_A = hS(T_S - T_\infty)$$

where h is the convection heat transfer coefficient (W/m^2K), S is the heat transfer surface area (m^2), T_S temperature of surface (K) and T_∞ temperature of the fluid sufficiently far from the surface (K). The h coefficient can be obtained using Nusselt (Nu) and Pranlt (Pr) numbers. Those dimensionless values refer to the ratio of heat transfers by convection and conduction (Nu) and ratio of viscous diffusion and thermal diffusion rates (Pr).[97] Nusselt and Pranlt numbers are given as:

$$Nu = \frac{hL_c}{\lambda} \qquad Pr = \frac{\mu c_p}{\lambda}$$

where L_c is the characteristic length, λ is the thermal conductivity, c_p is the heat capacity and μ is the dynamic viscosity. Furthermore, time for heat transfer related to characteristic channel diameter can be given as follows:

$$t_{heat} = \frac{\rho c_p}{h}\left(\frac{A}{V}\right) = \frac{\rho c_p}{\lambda}\frac{D^2}{Nu}$$

The $\lambda/\rho c_p$ is the thermal diffusivity (m^2/s) and D is channel diameter, usually 10 – 1000 μm for micro-rectors. Since the *Nu* number for laminar flow in cylindrical cubes is constant (3.66), it can be concluded that the narrower channels in micro-reactors leads to better heat transfer. Continuous flow micro-channel devices indicate orders of magnitude better heat transfer in comparison to conventional reactors.[98] This has significant impact on temperature control during catalytic reaction. Better heat control often provides improved product-specificity, enables avoiding the formation of hot spots and ensures short radial heat distribution in catalyst bed.

Similarly, small internal volume of micro-channels enables operating under well-defined pressure in flow condition. In addition, since pressure is a force applied to area ($p= F/A$), even high pressure conditions result in minor forces on capillary walls. Therefore, automated flow systems ensure safety during processes conducted under pressure as high as 400 bar[99], whereas, conventional systems require skill-demanding autoclaves.

In narrow capillaries of micro-reactors, fluids flow in parallel layers as a laminar pattern. The nature of fluid movement is strongly dependent on diameters of reactor channel and is defined by the dimensionless Reynolds number *Re*:

$$Re = u\rho L/\mu$$

where u is the flow velocity, ρ – liquid density and μ is the fluid viscosity. The characteristic length L is an equivalent of microchannel diameter D. A typical *Re* value for micro-reactors is in the range of 10 to 500, confirming fluid flow in parallel layers (laminar flow for $Re < 2200$). Considering that mass transfer between fluid layers occurs via lateral diffusion in a very short length, the mixing process can be very fast and intensive in micro-reactors.[100]

Regarding chemical reactions, mainly two coexisting phases flow through the capillaries. Depending on their flow velocity, different flow patterns can be formed.[101] For instance, when two phases coexist in two streams flowing side by side they form parallel flow pattern. In such case, surface tension is stronger than gravitational forces and their velocity determines flow regime rather than density or weight (Fig. 7a). Besides parallel flow, the most common two-phase flow regimes are: segmented (slug) flow, dispersed flow and annular (tube) flow.

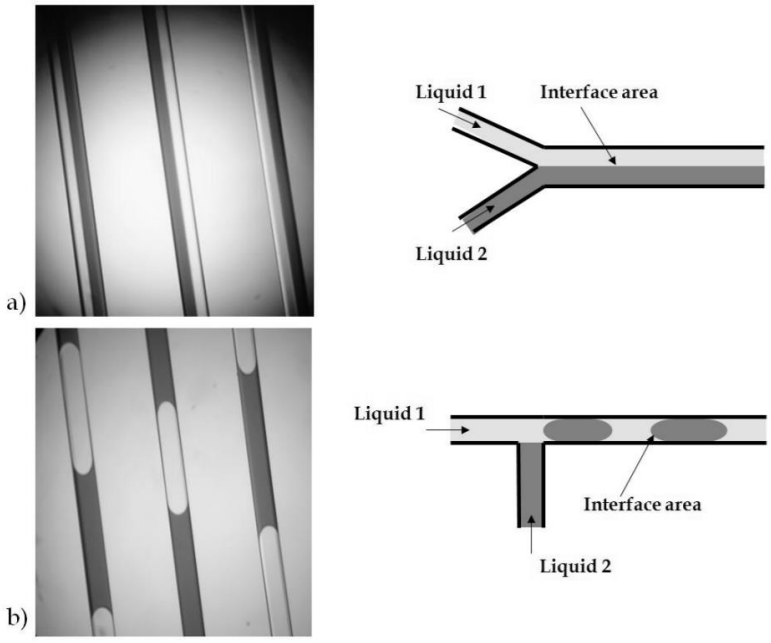

Figure 7. Two common examples of two-phase flows patterns, a) parallel flow and b) segmented (slug) flow.[102]

Segmented flow occurs when one phase is introduced to the second continuous phase through *e.g.* T junction (Fig. 7b) and forms slugs or bubbles. In dispersed flow pattern one phase percolates into the other continuous phase and an emulsion is formed. The last type of two phase flow pattern, annular flow, is preferred for heterogeneously catalyzed gas-liquid reactions. It occurs when linear velocity of both coexisting phases differs significantly. In that case, phase with much higher linear velocity (gas phase) flows in the center of capillary, whereas, second phase (liquid phase) forms a thin film separating the first phase from capillary walls. Thin liquid layer results in high interphase area for gas to dissolve and facilitates mass transfer to catalyst particles by short diffusion length.[103] To accurately describe the flow patterns in micro-reactors Computational Fluid Dynamics (CFD) method can be used. This computational approach allows to model flow regimes as well as the mass and heat transports in capillary channels. Hence, CFD method is applied in terms of system optimization which leads to enhanced performance of processes conducted in micro-reactors. The examples of CFD utilization have been reported in literature *e.g.* for catalytic H_2 conversion over Pt based catalyst[104] or for oxidation of volatile organic compounds[105].

2.2.2. HETEROGENEOUS CATALYSTS IN FLOW MICRO-REACTORS

In the majority of cases, heterogeneously catalyzed reactions involve three phases: liquid and gas reagents which interact with each other on surface of solid catalyst. It is a basis of the most important chemical transformations, such as hydrogenation or oxidation. To ensure high efficiency of those processes, large interfacial area needs to be provided. In this matter, low internal volume of micro-channel reactors needs to be well developed. Therefore the placement of solid catalyst in micro-channel systems should be designed to provide large and easily accessible active phase. In heterogeneous catalytic micro-reactors three types of catalyst are mainly used: wall coating, monolithic and packed bed as shown in Fig. 8.

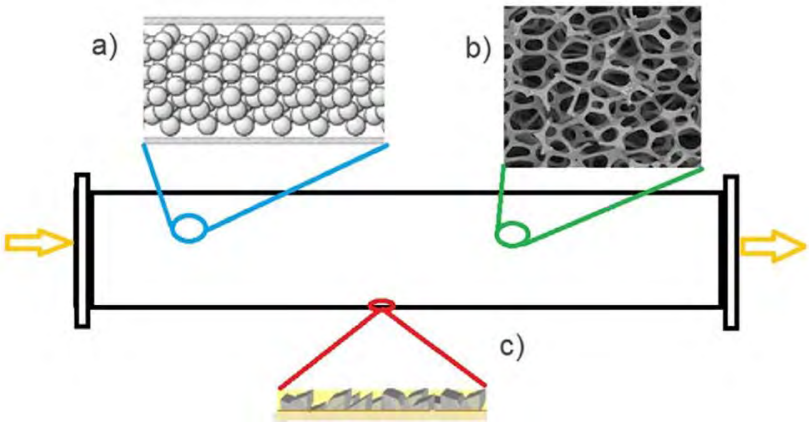

Figure 8. Three types of heterogeneous catalysts applied in micro-reactors: a) packed bed, b) monolith and c) wall coated.[106]

2.2.2.1. WALL-COATINGS

Capillaries internally coated with catalyst layer offer several benefits. First, this class of microchannel catalysts provides very large surface area which is crucial in the light of high performance of heterogeneously catalyzed reactions. Secondly, the presence of additional layer inside micro-channels decreases their interior diameter resulting in shorter diffusion length. Therefore, reaction rate diffusion limitations are reduced. In addition, catalyst anchored on capillary walls avoids excessive pressure drops, which can occur with packed bed or monoliths catalysts. Nevertheless, the setup of wall-coated catalyst is more complex since it requires direct deposition of catalyst inside very narrow channels. The immobilization process is usually performed by chemical methods.

Bogdan et al.[107] demonstrated a methodology for synthesis of 1,4 – disubstituted 1,2,3 – triazoles in micro-reactor with wall-coated catalyst. The authors showed microchannel reactor with sandwich-type coating where metal soil was located between two copper plates for better heat transfer. The reaction of 1,3 – dipolar cycloaddition of alky halides and sodium azide with acetylenes was tested with adequate catalyst containing soils of various materials deposited inside copper plates.

In another example, Wörz et al.[108] demonstrated wall-coated micro-reactor design for oxidation of long-chain alcohols to form corresponding aldehydes. The researchers presented similar two-plate heat exchanger separated with silver foil as an active metal. The reactor displayed orders of magnitude higher heat transfer coefficient than in conventional methodologies. The micro-channel system provided isothermal conditions leading to 96% of selectivity with 55% of conversion.

Shore et al.[109] showed the procedure of thin Pd layer formation on micro-capillary walls. For that, dimethyloformamid solution of palladium acetate was introduced into the system and heated up to 150°C for 30 min. The presence of a black film on capillary walls indicated formation of metallic Pd crystallites. The authors found that Pd coated micro-reactor was highly active in Suzuki-Miaura and Heck coupling reactions.

In the case of wall-coated catalysts, the pre-treatment of capillary surface is usually required to modify its properties. Thus, surface modification is performed to extend surface area and consequently create larger platform for active phase deposition. Hence, surface preparation increases number of active sites available during the reaction. Additionally, such modification of superficial properties may improve adhesion on micro-channel walls leading to more efficient immobilization of catalyst. It can be achieved by different methods such as: anodic oxidation, thermal oxidation or chemical oxidation.

The anodic oxidation or electochemical oxidation relies on formation of oxide films with highly adhering properties that facilitate subsequent immobilization of catalyst. Anodization enhances anti-corrosion properties of the wall-coating and improves their biocompatibility.[110]

Thermally oxidized films are formed in temperature range of 800 to 1200°C on metallic surfaces (Ti[111], 5% Al stainless steel[112]) with atmospheric air. Thermal oxidation is also implied to enhance adhesion properties, which ensure optimal conditions for subsequent catalyst deposition.

The most widely used method for surface modification involves chemical pre-

treatment. The versatility and diversity of chemical oxidizers serves wide array of methodologies suitable for various types of capillary channels. In addition, chemical modification can be used to introduce surface decorates that facilitate catalyst immobilization.[113] Many examples of chemical oxidation methods have been reported in the literature.

For instance, Rebrov et al.[114] as well as Zheng et al.[115] demonstrated simple methodologies for quartz capillary pre-treatment with NaOH or HCl. More complex multistep procedure was reported by Stefanescu et al.[116] In their approach acetone, acetic acid hydroxide, phosphoric acid and hydrogen peroxide were used. Worth-mention methodology for chemical oxidation is surface enhancement with piranha etch (sulfuric acid and hydrogen peroxide mixture) used for stainless steel reactors. However, for this type of capillaries procedures involving sulfuric and nitric acids are the most broadly applied.[117]

2.2.2.2. MONOLITHS

Monolithic catalysts are continuous, highly porous structures which act as supports for catalytically active phases. Monoliths are directly incorporated into reactor channels by polymerization of both inorganic or organic compounds. Those porous networks generated inside capillaries are then subjected to activation process, which introduces catalytically active component. This class of micro-channel catalysts attracted huge interest and was widely applied in organic flow synthesis. On the other hand, due to the very irregular structures, kinetic studies of monolithic catalysts are marginally advanced.

Inorganic monoliths applied in continuous flow micro-reactors are mainly silica based. Their preparation process relies on spinodal separation of alkoxysilanes-containing mixture into silica-rich phase and solvent phase. Phase separation is initiated by introduction of additives, such as surfactants. The porosity of created silica matrix can be modified after polymerization. Normally, spinodal decomposition leads to formation of microporous structure, however, to enlarge pore size to mesoscale, silica network can be subjected to ammonia treatment.[118]

Alotaibi et al.[119] incorporated silica monolith matrix into borosilicate tube as a support for gold nanoparticles. The authors performed two different activation methods: Au nanoparticles incorporation in-situ during polymerization and metal immobilization

after monolith functionalization. Catalysts were then tested in cyclohexene oxidation. As reported, catalyst with metal nanoparticles anchored onto thiol-functionalized matrix displayed better catalytic performance in above-motioned reaction.
Koreniuk et al.[120] used titania-silica monolithic catalyst to oxidize 2,3,6-trimethylphenol with hydrogen peroxide. They found that application of catalytic flow system resulted in significant improvement in reaction outcomes when compared to batch mode. Conversion of 85% was reached after 12 min for monolith catalyst, whereas, reaction carried out in batch yielded 75% of conversion after 1h.

Organic monoliths are created in various reaction types, among which free radical polymerization is the most commonly applied.[121] However, ring opening metathesis polymerization, polyaddition or polycondensation are also frequently implemented to form organic monoliths. Their porosity can vary form micro- (<2 nm) to macro-pores (>50 nm). That feature defines crucial properties of polymeric structures in the light of their targeted application. Microporous monoliths are suitable for retention and separation of analytes[122], whereas, macro-porosity is desirable when good flow-through efficiency is required. Generally there are three strategies that enable controlling the porosity in relatively predictable way:

a) by modulation of polymerization temperature;
b) by changing the cross-linking agent;
c) by using different type or amount of porogen.[123]

Macro-porous structures facilitate mass transport by convection, hence, reactions are not limited by diffusion exclusively.[124] Therefore, large flow-through pores of organic monoliths are especially preferable in flow catalytic reactions.
There are three main types of organic-polymer monoliths used in heterogeneous catalysis: organometallic materials, metal nanoparticles immobilized into polymer structure and biocatalysts. The division is based on the nature of active phase and the way of its incorporation on monoliths.
In the first type (organometallic catalysts) active metal is embedded into polymeric matrix resulting in formation of continuous phase material, like in Buchmeiser et al.[125] report. The authors demonstrated methodology for preparation of Cu containing monolith by free radial polymerization of ethylene methacrylate and trimethylopropane triacrylate in the presence of porogenic solvents. The catalyst was

then used for hydrosilylation and hydrocyanation reactions. Similarly, in another example, Bolton et al.[126] synthesized Pd containing monolith for Suzuki-Miyaura reactions.

Palladium-based materials are also a major group of monolithic catalysts with an active phase immobilized as metal nanoparticles. In this case polymeric structure of monolith needs to be functionalized to provide linkers for metal particles. For instance, Bandari et al.[127] decorated acrylate-based polymeric matrix with Pd nanoparticles. In their approach palladium was immobilized onto porous structure via epoxy sites and then reduced forming 4 nm nanoparticles. The material was used as a catalyst for Suzuki coupling reaction.

2.2.2.3. PACKED BED CATALYSTS

Packed bed catalysts are the most commonly used systems for heterogeneous catalytic reactions in flow. This concept offers multiple advantages in catalyst investigation prior to its industrial scale implementation. Packed bed format is easily scalable, hence, rapid reaction screening, optimization of reaction conditions or kinetic studies in laboratory scale provide essential data valid for processes in larger extend. In addition, packed bed catalysts can be easily assembled in micro-reactors enabling high catalyst loading. In contrary, application of packed bed system may introduce fluid dynamics perturbations. Therefore, poor mass and heat transfer as well as pressure drop can occur in those reactors. Pressure disturbance depends on the bed size and the nature and form of catalyst packed inside bed. Pressure drop can be computed by the Ergun equation:

$$\frac{\Delta p}{L} = 150\frac{\mu u_S(1-\varepsilon)^2}{{D_p}^2\varepsilon^3} + 1.75\frac{\rho_f u_S^2(1-\varepsilon)}{D_p\varepsilon^3}$$

where L is the packed bed length, D_p is the catalyst particle diameter and ε is the porosity of the catalyst, μ is the dynamic velocity of the fluid and u_S is the spherical velocity.

In this configuration, metal or metal oxide active phase is mainly supported on porous materials formed in particles with particular diameter to minimize flow maldistributions. The optimal diameter of catalyst particles depends on the reactor construction which may place regulations for preventing clogging or particles leaching

from catalyst bed. In such systems, catalyst supported on various oxides, carbonaceous materials or polymeric beads were used in flow micro-reactors.

Durndell et al.[128] employed granulated 2%Pd/SiO_2 catalyst with particle size of 0.1 – 0.5 mm as a packed bed system in flow cinnamaldehyde hydrogenation. The catalyst was inserted into cartridge with diameter of 10 mm with a GEM II coil-in-coil gas pre-saturator. Micro-reactor system equipped with that catalyst displayed good catalytic performance in the reaction. Moreover, the authors demonstrated that the reaction depended on residence time (time which molecules spend in catalyst bed).

Liu et al.[129] demonstrated slightly different approach of using palladium based packed bed catalyst in continuous flow oxidation reaction. They used single channel reactor, which was firstly packed with glass beads with diameter of 0.75 mm. Glass filling formed thin layer which retained the aqueous slurry of finely grinded Pd/Al_2O_3 catalyst. System was used to oxidize isopropylbenzaldehyde.

In another report, Dendic et al.[130] immobilized Candida antarctica lipase B onto acrylate resin beads with diameter of 425 – 710 μm and packed the material into a 4.3 mm wide tube. The reactor was applied for transesterification of ethyl butyrate with 1-butanol in continuous flow. The reaction led to 99.9% of conversion with 4 min of residence time for the catalyst bed. This was a significant improvement in comparison to batch system, in which the reaction resulted in 87% of conversion after 30 min.

2.2.3. APPLICATION OF CONTINUOUS FLOW CATALYSTS

There are numerous advantages offered by flow heterogeneous catalysis, which promote application of this new technique in chemical synthesis. Since continuous flow processes show improved performance on so many levels, serving environmental, efficiency and safety benefits, it can be expected that flow catalysis will play a prominent role in future chemical development. Currently industrial-scale organic synthesis is still dominated by batch processing. However, among recent studies on the subject there is a growing tendency towards synthesis in flow conditions. As it will be shown in this chapter, flow catalysis can be applied in the most important chemical transformations on the research level. In the light of industrial implementation, academia-scale processes conducted in flow mode indicate advantage over batch systems due to the better scalability. Scaling-up catalytic flow system while preserving

constant residence time can be achieved either by increasing reactor diameter at constant flow rate or by increasing reactor length and flow velocity. Nevertheless, in both cases, changes of mass and heat transfer may occur since those phenomena depend on surface area-to-volume ratio. To avoid heat and mass maldistributions, numbering up was proposed as an alternative for industrial implementation of flow reactions. The strategy of using multiple parallel flow reactors in chemical production enables keeping exact the same conditions as during small-scale testing.

2.2.3.1. RECENT DEVELOPMENTS OF FLOW HETEROGENEOUS CATALYSIS

Over the past years, micro-reactor technology has been applied in a plethora of catalytic reactions which are crucial for chemical industry. Therefore, flow processing has been used for e.g. hydrogenation, oxidation, bond-forming, coupling, enzymatic or photocatalyzed reactions.

Barbaro et al.[131] demonstrated effective approach for hydrogenation of double and triple carbon-carbon bonds in a flow system. For that, the authors prepared Pd based catalyst by ion-exchange technique where the Pd^{2+} ions were immobilized onto Li^{+} containing polymeric resin. After immobilization, catalyst was reduced in hydrogen flow. As they reported, polymer supported Pd catalyst can be employed to produce leaf alcohol fragrance in flow conditions with ~ 400 h^{-1} TOF achieved for that system.

In subsequent study,[132] the authors improved leaf alcohol fragrance production in flow conditions. They anchored Pd nanoparticles onto borate macroporous monolith and used it as a catalyst for partial hydrogenation of substituted alkenes. The reaction outcomes indicated excellent catalytic performance of the material in the light of both selectivity, activity and stability under mild conditions. As reported, continuous flow approach displayed improvement in comparison to industrial production of leaf alcohol conducted in batch conditions.

Kobayashi et al.[133] also applied supported Pd nanoparticles as a catalyst for flow hydrogenation reaction. Using $Pd(OAc)_2$, poly(dimethyl)silane (DMPSi) and alumina, the researches prepared PdDMPSi catalyst for alkenes and alkynes reduction in grams and kilograms scale. They showed that continuous flow hydrogenation over PdDMPSi displayed better activity than conventional Pd/C catalyst. This efficient methodology

was used for vegetable oil and squalenes transformation. In addition, the authors adapted continuous flow strategy for nitro compounds transformation: hydrogenation of nitriles[134] and both aromatic[135] and aliphatic[136] nitro compounds.

Another application of metal/support catalyst in flow hydrogenation was reported by Gericke et al.[137] The researchers studied Ru based catalyst in glucose hydrogenation carried out in continuous flow. They immobilized Ru nanoparticles on two different supporting materials: hyperbranched polystyrene (HPS) and nitrogen-doped carbon nanotubes. The catalysts were investigated in terms of their activity in glucose hydrogenation – industrially relevant process. Presented approach resulted good efficiency which was comparable to industrial process over Raney Ni catalyst. As the authors concluded, the use of RuHPS catalyst together with flow conditions increases environmental compatibility of the process.

Immobilization of metal nanoparticles onto polystyrene support was also demonstrated by Osako et al.[138]. The researchers dispersed Pt nanoparticles on amphiphilic polystyrene PEG resin and employed the material to catalyzed olefin and nitrobenzenes hydrogenation. The reaction was conducted in continuous flow micro-reactor. As reported, after 30 seconds both olefins and nitrobenzenes were hydrogenated to corresponding products with conversion up to 99%. Long term experiment in flow conditions indicated no significant drop of activity after 63 – 70 h.

Worth mentioning system for continuous flow hydrogenation was demonstrated by Hudson et al.[139] In their approach flow hydrogenation in ethanol or water was catalyzed by Fe nanoparticles stabilized with amphiphilic polymer. Protected iron nanoparticles displayed very interesting properties in terms of chemoselectivity with wide array of unsaturated compounds. The authors were able to reduce alkenes, alkynes, aromatic imines and aromatic aldehydes with excellent yield and selectivity. Moreover, hydrogenation of different functionalities than above-mentioned was not observed over Fe based material. Beside high efficiency in flow chemeselective hydrogenation, protecting layer of polymer also ensured very good stability of the catalyst.

Continuous flow micro-reactors have been also applied in asymmetric hydrogenation processes. Mainly two types of chiral catalysts were used as packed bed systems in flow reactions, namely: immobilized molecular catalysts and surface-modified catalysts. The molecular catalysts in asymmetric hydrogenation are usually Rh containing materials immobilized on supports with anionic linker.[140] For instance,

such catalysts are used in hydrogenation of dimethyl itaconate with supercritical CO_2 as a mobile phase.[141] The chirally modified catalysts were also utilized in the process conducted under continuous flow conditions. It was reported that Pd and Pt catalysts enriched with cinchona-alkaloid as a chiral agent can successfully catalyze enantioselective hydrogenation of unsaturated carboxylic acids or activated carbonyl compounds.[142]

Continuous flow oxidation and oxidative transformation reaction have been also widely reported. In this case, the safety benefits of flow catalysis in micro-reactors are especially important. Oxidants such as oxygen or hydrogen peroxide may cause an explosion threat when used for organic synthesis. Oxidation carried out in flow micro-reactor minimize that risk due to precise temperature control and low internal volume which reduces potential explosion area.

Derikvand et al.[143] showed hydroquinones oxidation with 30% aq. H_2O_2 for benzoquinone production in continuous flow. The process was catalyzed by Ag_2O packed in tubular reactor under environment-friendly conditions. The reaction yielded excellent conversion and selectivity to desired product. Moreover, the catalyst could be recovered by simple filtration and reused for at least several times showing similar catalytic performance. Application of flow processing significantly facilitated catalyst recovery, since reaction and regeneration could be conducted alternately.

Aerobic oxidation of primary and secondary alcohols has been also performed in a flow mode. Zetova et al.[144] employed commercially available alumina supported Ru catalyst to produce aldehydes and ketones by oxidation of various alcohols. They used packed bed system with the residence time of the cartridge with catalyst up to 3 min depending on flow rate. Since the reaction was performed in flow system, the researchers recirculated reactants flow through catalyst bed until complete conversion. The results of flow oxidation over Ru/Al_2O_3 showed good yields for benzylic and allylic alcohols and moderate yield when primary aliphatic alcohols were transformed into their corresponding aldehydes.

In another example of employing flow conditions for oxidation process, Pascanu et al.[145] demonstrated catalytic performance of double-supported Pd catalyst in 1-phenylethanol oxidation. The authors impregnated Pd into NH_2-containing metal-organic framework structure and formed catalyst particles coated with silica. The flow mode reaction was conducted under relatively mild condition, whereas, usually

oxidation is performed at high temperature and pressure. The catalyst was exposed for constant operation for 7 days at 110°C. The material showed no deactivation and leaching during the experiment.

Selective oxidation of sulfides with hydrogen peroxide in packed bed flow system was reported by Doherty et al.[146]. They used polymer supported ionic liquid phase catalyst and obtained good efficiency in sulfoxides formation. As authors reported, sulfoxidation of thioanisole was performed for 8 h with stable catalytic performance under constant flow. Those results indicated remarkably improved stability in comparison to commercially available ionic liquid phase catalysts, which undergo rapid deactivation due to the leaching.

The impact of flow micro-reactors technology on safety improvement was demonstrated by Basavaraju et al.[147] Their approach for the oxidative C=C cleavage catalyzed by hazardous osmium tetroxide allows handling the toxicity and volatility of the catalyst during the process. The authors applied micro-reactor system with wall-coating catalyst. The polymer support was grown on inner wall of reactor in nanobrush structure which acted as a matrix for OsO_4 catalyst. The immobilization of OsO_4 was achieved by coordination with tertiary N atoms in repeating pyridine unit. The catalyst indicated excellent performance in the dihydroxylation and the oxidative cleavage reactions transforming given olefins in corresponding diols and ketones.

Besides hydrogenation and oxidation, flow micro-reactor technology has been spread among all the most important organic transformations. Recent reports on heterogeneously catalyzed organic synthesis point flow processing as a powerful tool that brings significant advances in multiple aspects of synthetic organic chemistry.

Elizarov et al.[148] presented an highly efficient continuous flow methodology for acid-catalyzed Hosomi-Sakurai allyladdition reaction. The Bi(III) salts containing montmorillonite catalyst was used for nucleophilic addition of allyl trimethylsilanes to aromatic aldehydes. The Lewis acid catalyst was found to promote protected alcohols formation with very good yields (71 – 96%).

Recently, flow catalysis was implemented for an important organic process – asymmetric nitroaldol synthesis known as Henry reaction.[149] Nanoyama and coworkers employed NdNa bimetallic catalyst supported on multiwalled carbon nanotubes to asymmetric addition reaction. The catalyst was prepared by simple mixing of chiral ligand with both metals salts and carbonaceous support. The flow

system was operated for ca. 400 h maintaining stable catalytic performance with 81% of conversion and excellent stereoselectivity. Reaction yielded a key intermediate for production of AZD7594 drug that can find application in asthma and chronic obstructive pulmonary disease therapy.

In another application of flow organic synthesis over heterogeneous catalyst Seghers et al.[150] demonstrated significant improvements of Diels-Alder synthesis of heterocyclic compounds. In industry, batch application of Diels-Alder reaction is limited due to the safety and purity issues that affect atom-efficiency of the process. In this matter, the authors proposed a methodology for Diels-Alder reaction of cyclopentadiene with various dienophiles in flow system. The reaction was catalyzed by H-Beta zeolite. As reported, the process carried out under flow conditions resulted in 3.5 times higher catalytic productivity and 14 times higher Diels-Alder adducts production then batch system. The 95% conversion with high endoselectivity was reached during 7 h on stream with no significant symptoms of deactivation leading to throughput of 0.87 g/h.

Futura et al.[151] reported flow Fischer esterification with commercially available sulfonic acid – functionalized silica as heterogeneous catalyst. The catalyst was packed in tubular stainless steel flow reactor and utilized in reaction of various long chain carboxylic acids with alcohols conducted at 110°C with residence time of 3 min. This flow system yielded corresponding esters with good to excellent efficiency. The esterification of lauric acid with methanol resulted in stable conversion (99%) for > 6.5 h, indicating good robustness of the catalyst.

Additionally, versatility of flow operating has been implemented to attend highly efficient photo-assisted catalytic reactions. In many cases photocatalysis is applied to conduct reactions that require processing under harsh conditions or include hazardous intermediates. Therefore, in this case, flow micro-reactor technology may be especially beneficial leading to new advances in photo-induced catalytic processes. Continuous flow systems containing photocatalyst usually consist of transparent capillaries with diameter smaller than 1 mm to ensure efficient irradiation of the reactor. Currently, due to simplified operating the homogeneous photocatalsts dominate in flow applications. Nevertheless, current developments in the field include reactions catalyzed by heterogeneous photo-active materials such as TiO_2.[152] For instance, recent study of Rehm et al.[153] showed application of micro-structured falling

film reactor (FFMR) with immobilized TiO_2 in photochemical arylation of heteroarenes. The researchers demonstrated successful C-C bond formation with several compounds such as: furan or pyridine with yields up to 99% with blue light source.

2.2.3.2. MULTI-STEP PROCESSING

Flow micro-reactor technology can be successfully implemented to perform multi-step synthesis. In comparison to batch systems, sequential reactions in flow are achieved without losing valuable intermediate products that can be isolated during ongoing process. Flow multi-step operating entails two methodologies which require different reactor design. In the first case, subsequential stages of the process occur in catalyst bed by dosing different reactants, modifiers or regeneration agents. In the other option, flow system contains several segments such as multiple catalyst beds, heaters or membranes.[154] In this case, reactants flowing through consecutive reactor parts undergo various transformations.

Fan et al.[155] demonstrated a structured compact reactor for a multi-step synthesis of 1,2-diphenylethane. Two-stage process involved a Heck C-C coupling reaction of toluene and styrene forming unsaturated diphenylethene which was then hydrogenated in the second step yielding desired product. The reactor consisted of two separate segments with dual catalyst beds dedicated to Heck coupling and hydrogenation (Fig. 9). Both intermediate reactions were catalyzed by 5% Pd supported on microsperical carbon.

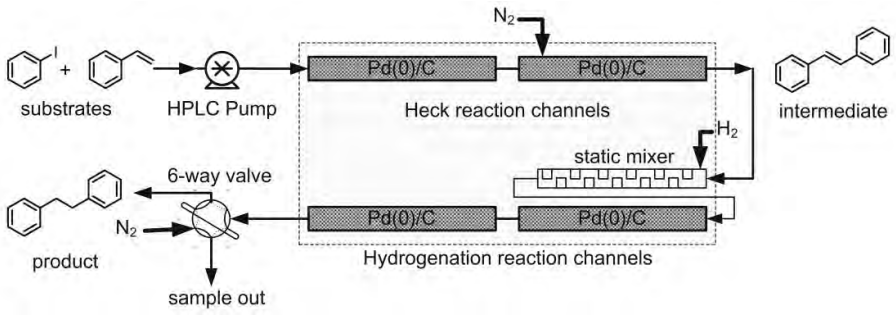

Figure 9. A scheme of flow reactor for dual-step coupling/hydrogenation protocol with packed-bed Pd/C catalyst. Reproduced from[155] with permission.

The presented one-steam approach for coupling/hydrogenation reactions in flow was found to be significantly more efficient that adequate batch transformations. The reported flow system reduced reaction time from couple of hours (batch) to 7 min and

enabled operating at lower pressure and temperature. In addition, the authors found that Pd leached in Heck coupling section could be recovered in the following hydrogenation step, hence, the catalytic activity of the system could be maintained by reversing the flow.

More recently, Wu et al.[156] reported a design of multi-step flow system for synthesis of cyclic carbonates from various olefins and CO_2 (Fig. 10).

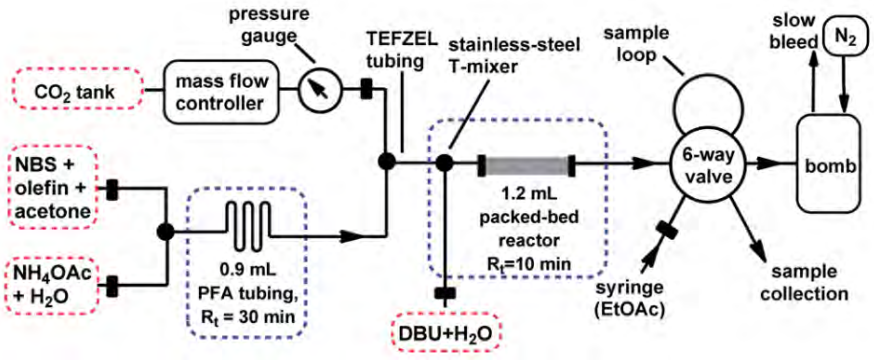

Figure 10. Multi-segmented flow reactor for cyclic carbonates synthesis through multiple sequential reactions. Reproduced from[156] with permission.

Conventionally, cyclic carbonates production from bromohydroxylation of olefins with NBS (*N*-bromosuccinimide) and DBU (1,8-diazabicyclo[5.4.0]undec-7-ene) generates unwanted byproducts such as, epoxides or 1,2-dibromoalkanes decreasing yield of the process. The application of flow system enabled direct introduction of different reagents at specific reaction stage preventing their former mixing. As the authors reported, multi-step flow synthesis pathway resulted in remarkable suppression of undesired products formation compared to batch system. Moreover, multicomponent production of cyclic carbonates could be obtained for wider scope of olefins with excellent yields.

3. AIM OF THE STUDIES

The aim of this work is to develop a versatile and thorough strategy for continuous flow chemoselective hydrogenation of α,β – unsaturated aldehydes in liquid phase, i.e., chemoselectivity studies of competitive C=C vs C=O saturation. To attain that, the course of the research was divided into consecutive stages, which can be represented as set of intermediate objectives:

1) Design and synthesis development of metal-resin catalysts intended for flow catalysis applications. The procedure performed in two separate steps: metal nanoparticles preparation and their subsequent grafting on functionalized polymeric resin.

2) Preparation of resin supported catalyst based on low-cost transition metals for highly selective hydrogenations used in production of industrially relevant intermediates.

3) Application of flow processing in optimization studies. Investigating the influence of reaction temperature and pressure on catalyst performance in terms of both activity and selectivity.

4) Development of protocol for catalyst morphology modulation in flow conditions. Intensification of structure-sensitivity studies.

5) Elaboration of comprehensive catalytic flow system for chemoselective hydrogenation of various α,β – unsaturated aldehydes, which can be used for production of value-added compounds.

4. EXPERIMENTAL SECTION

4.1. RESIN SUPPORTED CATALYST - DESIGN AND SYNTHESIS

Novel polymeric resin supported catalysts were designed and synthesized to meet demanding flow conditions. For that, functionalized resin was selected and subsequently used as catalyst support, namely the commercially available material labeled as Tentagel-S-NH_2 (*Rapp Polymere GmbH*). The resin consists of polyethylene glycol (PEG) based polymer terminated with primary amine group, i.e., -NH_2 (Fig. 11). The resin is in beads form with a diameter of 130 μm and a capacity of 0.2 – 0.35 Nmmol·g^{-1}.[157] The specific morphology of such material enables unclogged flow operations, and the presence and the nature of terminal groups is ideal for grafting of metallic nanoparticles.

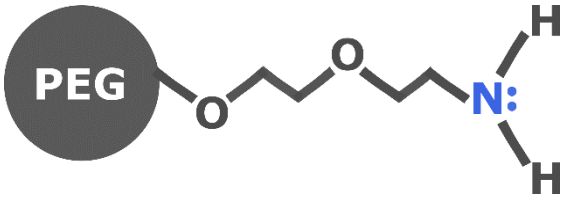

Figure 11. Tentagel-S-NH_2 ($TSNH_2$) polymeric resin

Nickel catalyst - $NiTSNH_2$

Catalyst synthesis procedure was performed in one pot and involved two steps. In the first one, metal nanoparticles were formed in a simple chemical reduction method. In a typical nanoparticles synthesis, nickel (III) acetylacetonate was dissolved in ethanol in a presence of capping agent – trioctylphosphine oxide (TOPO). The laboratory setup consisted of two-neck round bottom flask fastened above magnetic stirrer and connected to argon line, which ensured anaerobic conditions (Fig. 12). Sodium borohydride ($NaBH_4$, reducing agent) was dissolved in ethanol and injected dropwise into the mixture under constant stirring (1000 rpm) with 1:2 $Ni(acac)_2$: $NaBH_4$ molar ratio. After that, there was an immediate color change from green to black indicative of nickel nanoparticles formation. To control their growth, the concentration of TOPO exceeded the [Ni^{2+}] by 10 times. The used excess of the stabilizer halted agglomeration and enabled formation of Ni nanoparticles smaller than 10 nm. The presence of 8-C

chains in a single molecule makes TOPO a commonly used capping ligand, which creates coating layer on nanoparticles surface. The presence of this layer results in strong steric repulsions between nanoparticles indisposing their further growth after reaching a given size.

The second step relates to nickel nanoparticles immobilization onto polymeric matrix. For that, polymeric resin was added to the nanoparticles containing solution and stirred for 36 hours (1000 rpm). Immobilization was performed at room temperature under argon atmosphere. Ni nanoparticles grafting was achieved via self-assembly, leading to a covalent bond formation with $–NH_2$. The exact nature of the bond will be discussed in the result section. Afterwards, the material was filtrated, washed with ethanol and dried for 3 hours at 100°C. This grafting process enables both nanoparticles stabilization and extraction from solution without complicated workflow. The use of PEG based resin with amino linkers yields for well exposed and easily accessible metallic phase crucial for catalysis.

The division of the synthesis procedure into two separate steps allows for higher control of metal nanoparticles morphology (shape and size) prior to grafting by e.g. manipulating capping agent concentration.

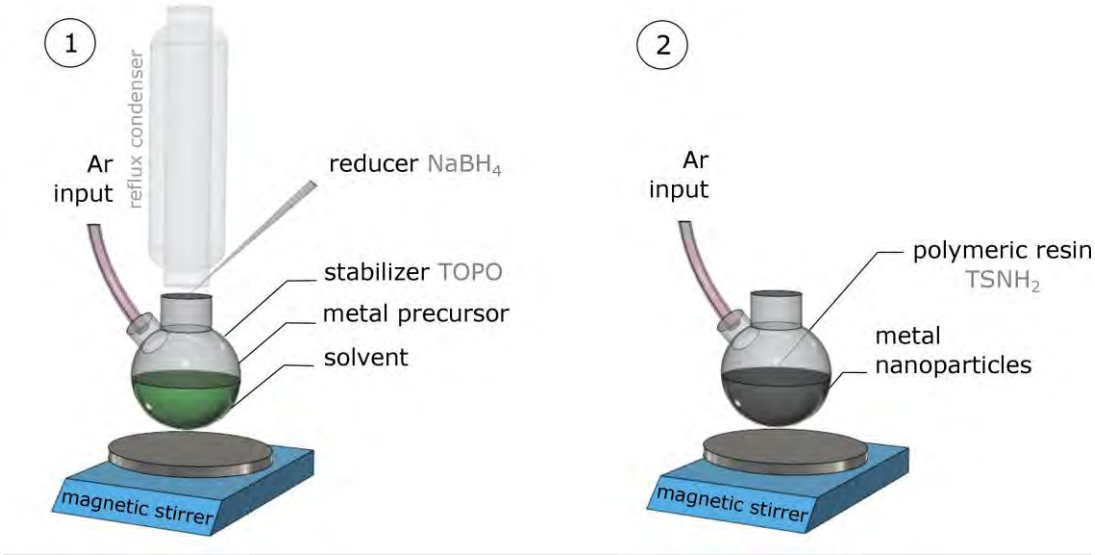

Figure 12. Two-step catalyst synthesis: 1. Preparation of metal nanoparticles; 2. Grafting onto polymeric support

Palladium catalyst - $PdTSNH_2$

Palladium based catalyst was successfully synthesized with the same experimental procedure. Considering that noble metals, such palladium or platinum are commonly used in hydrogenation processes, similar resin supported Pd catalyst can act as a reference material. Correspondingly, palladium (II) acetylacetonate was used as nanoparticles precursor. Nevertheless, its poor solubility in ethanol induced additional treatment prior to reduction. In this case, $Pd(acac)_2$/EtOH solution was heated up to boiling temperature (78.3°C) of ethanol under reflux condenser. Afterwards, palladium ions were reduced, which was indicated by color change from yellow orange to black. Moreover, during the immobilization phase, polymeric support was able to capture all nanoparticles from the solution.

4.2. CATALYST MODIFICATION

Parent $NiTSNH_2$ catalyst was modified to examine the relation between material morphology and its catalytic performance. The modification procedure relied on accretion of Ni nanoparticles anchored onto polymeric matrix. To attain this, 150 mg of $NiTSNH_2$ material was packed into cartridge and mounted in continuous flow micro-reactor (described below). The catalyst was pretreated in H_2 and ethanol flow for 30 min at 100°C and 80 bar of pressure to purify the metal surface. This treatment was conducted to ensure that nickel is present in reduced state prior to catalyst modification, since nickel oxidation would indispose metal deposition and consequent nanoparticles accretion. After pretreatment, parent catalyst was flown with solution of $Ni(acac)_2$ in ethanol (1.5 $\mu molNi^{2+} \cdot min^{-1}$) for predetermined times with hydrogen at 80 bar and 100°C. After given times, the resultant materials were washed with ethanol.

By following this procedure, three modified catalysts were prepared by changing the time of saturation with nickel ions. Catalysts subjected to modification for 15, 60 and 105 min were labeled as mod15-$NiTSNH_2$, mod60-$NiTSNH_2$ and mod105-$NiTSNH_2$, respectively (Tab. 1). This innovative method was carried out in a sequence with catalytic reaction, which will be thoroughly described in the subsequent section of the work.

Table 1. Resin supported catalysts

Catalyst	Metal precursor/Modifier	Support	Description
$NiTSNH_2$	$Ni(acac)_2$	Tentagel-S-NH_2	parent catalyst
$PdTSNH_2$	$Pd(acac)_2$		reference catalyst
$mod15NiTSNH_2$	$Ni(acac)_2$	Tentagel-S-NH_2	15 min of modification
$mod60NiTSNH_2$			60 min of modification
$mod105NiTSNH_2$			105 min of modification

4.3. CATALYTIC REACTIONS IN CONTINUOUS FLOW

4.3.1. CONTINUOUS-FLOW MICRO-REACTOR

The hydrogenation reactions were carried out in a commercial micro-reactor H-Cube Pro ™ that enables operating under continuous flow-conditions. The device consists of two main sub-assemblies presented in Fig. 13. The yellow part is a hydrogen generation system and the grey one is assigned to the hydrogenation part. Hydrogen is generated via electrolysis of water and supplied to the reaction line in-situ during the experiment. Special separator unit ensures that hydrogen is dried prior to reaching reaction line.

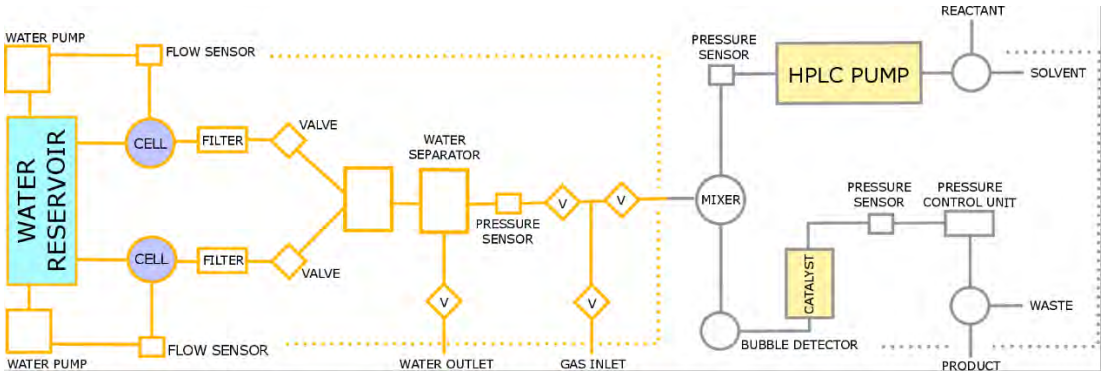

Figure 13. Design of H-Cube Pro ™ system.

The second part, which enables continuous-flow operating, is located on the front panel of the reactor (Fig. 14). The constant flow of a reactant/solvent is caused by an external HPLC pump connected to the instrument. H-Cube Pro ™ reactor operates within the range of flow rate from 0.3 to 3 ml per minute. After mixing with hydrogen, reaction solution is flown through cartridge filled with a catalyst. The cartridge (CatCart®) is a stainless steel columnar container in length of 70 mm sealed with both

sides enabling uninhibited flow through the catalyst bed. To prevent blockage in the reactor lines the granularity of the material in the cartridge should be higher than 50 μm. Beads of polymeric resin used for catalyst synthesis are 130 μm in diameter, which complies with this requirement. Cartridge with a catalyst is placed in a heating chamber that allows to reach pressure as high as 100 bar and the temperature up to 150°C.

Figure 14. H-Cube Pro™ continuous-flow micro-reactor.

4.3.2. REACTION PARAMETERS OPTIMIZATION

A manageable device interface delivers multiple features, which simplify and facilitate performance of hydrogenation processes. The reactor enables regulation of reaction parameters such as temperature, hydrogen pressure and flow rate. It is also possible to set a given reaction time as well as duration of pre- and post-washing periods. Additionally, those parameters can be adjusted or regulated during ongoing operation. It means that previously set parameters are maintained while reaction is paused. Process optimization was conducted for every hydrogenation reaction included in this study with all resin-supported catalysts. In a typical conduct, 150 mg of catalyst was inserted to cartridge and pretreated for 30 min in continuous flow. Pretreatment was intended to prepare a catalyst in terms of maximization of its catalytic performance.

For that, the material was flown with solvent and hydrogen under 80 bar pressure and at 100°C. This operation serves a dual purpose. Firstly, considering the fact that polymeric materials tend to swell polar solvents, during pretreatment phase, catalyst is saturated with solvent. Consequently, material expands its structure lowering diffusion limitation and preventing potential blockage. Secondly, hydrogen treatment reduces metal phase that could have been superficially oxidized while exposed to atmospheric air.

Afterwards, catalyst was subjected to screening reactions to estimate optimal temperature and pressure values for the process. Screening consists in carrying out short reactions at given conditions. The typical protocol includes investigation of four pressure values: 10, 20, 40 and 60 bar and five temperature values: 25, 45, 65, 85 and 100°C under each pressure. It was found that 60 bar and 100°C is sufficient for complete conversion of tested α,β-unsaturated carbonyls (citral, cinnamaldehyde and prenal). Only in the case of citronellal hydrogenation, screening reactions were carried out at higher temperature (110, 120 and 130°C) and pressure (80, 90 and 100 bar).

The reactor automatically switches to reaction mode after reaching set parameters. Therefore, with regard to time needed for reactant to reach a catalyst bed, samples were collected 8 min (flow rate: 0.5 $ml \cdot min^{-1}$) when the process was initiated after each parameter change. Subsequently, samples of products of the reactions conducted at given conditions were analyzed with gas chromatography on SCION 465-GC (Bruker) instrument. The chromatograph is equipped with flame-ionization detector (FID) suitable for analysis of hydrocarbons under study. Reaction products were separated in a non-polar capillary (30m x 0.25μm) column with 5% phenyl polysilphenylene-siloxane filler. This equipment provides suitable conditions for obtaining well-separated peaks of analyzed hydrocarbons at isothermal conditions.

4.3.3. LONG-TERM STABILITY TESTS

Optimization tests allowed establishing temperature and pressure parameters under which selectivity to desired products were the highest and those conditions were selected for long-term experiments. In stability tests catalyst under consideration was subjected to 5 h reaction at isothermal and isobaric conditions. The reactant solution with 0.05 M concentration was flown through the reactor with constant rate 0.5

$ml \cdot min^{-1}$. First sample of product solution was collected after 15 min, which ensured stabilization of the system. Further reaction progress was monitored by sampling 2 ml of product solution every 30 min. As previously, product evolution was determined by gas chromatography.

4.4. MATERIAL CHARACTERIZATION

Powder X-ray diffraction (PXRD)

Powder X-ray diffraction measurements were performed at PANalytical Empyrean diffraction platform powered at 40 kV × 40 mA with Bragg-Brentano arrangement (Fig. 15). The diffractometer is equipped with a vertical goniometer in theta-2theta geometry. The Ni filtered Cu K_α radiation was used as a X-ray source. Data were collected in the range of 2θ = 5 – 95 °, with a step size of 0.008 ° and counting time 60 s per step.

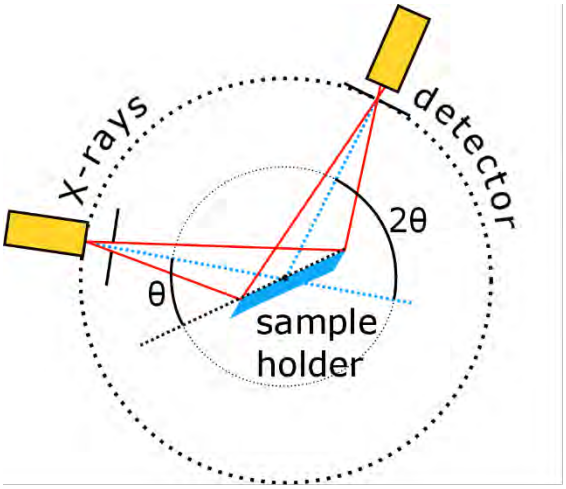

Figure 15. Bragg-Brentano geometry in X-ray diffractometer.

Beside structural analysis, powder XRD was used to determine the average Ni nanoparticles size in accordance to Scherrer equation[158]:

$$D = \frac{k\lambda}{\beta cos\theta};$$

where D is the average crystallite size (nm), λ is the wavelength of the Cu K_α X-ray radiation (λ = 0.154056 nm), k is a dimensionless shape factor (usually 0.94), β is the full width at half maximum (FWHM) peak intensity at 2θ (rad) and θ is the diffraction angle.

X-ray photoelectron spectroscopy (XPS)

Photoelectron spectroscopy was used to examine the chemical composition of the catalysts. The XPS measurements were conducted using Microlab 350 Thermo Electron spectrometer with high energy resolution spherical sector analyzer (SSA) to identify the chemical state of surface species. The high-resolution spectra were excited

using Al K_α ($h\nu$ = 1486.6 eV) radiation source and recorded using 40 eV pass energy with the step 0.1 eV. A Shirley background subtraction was made to obtain the XPS signal intensity. The peaks were fitted using an asymmetric Gaussian/Lorentzian mixed function. The binding energies measured were corrected in reference to the energy of C 1s peak at 284.5 eV. Advantage-based data system software (Version 5.97) was used for data processing.

X-ray absorption spectroscopy (XAS)

X-ray absorption spectroscopy measurements were done with crystal X-ray spectrometer of the von Hamos geometry (Fig. 16). The measurements were performed at ambient conditions in the in-air laboratory setup.

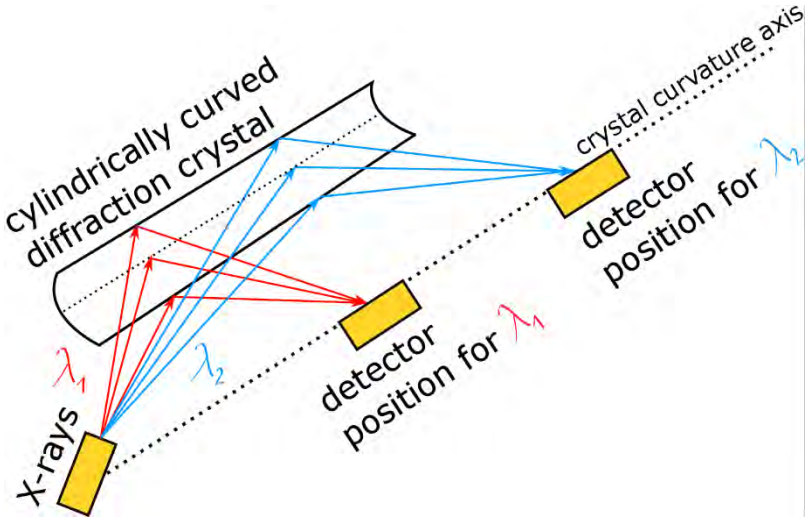

Figure 16. Illustration of the von Hámos geometry.

As a X-ray source, XOS X-Beam Superflux PF X-ray tube was used. The source is equipped with a focusing optics and operates at the voltage of 40 kV and the current of 0.9 mA. The polychromatic incident X-ray beam of about 3º divergence penetrated the sample placed in the beam focal point through a spot with the nominal size of 100 µm. The transmitted radiation was diffracted by a cylindrically bent Si(440) crystal of 25 cm-radius of curvature at the Bragg angle of 65.2º and registered by an Andor Newton CCD camera with front-illuminated 1024×256 matrix of 26 µm-sized pixels. The pressure in the camera's interior was decreased to 10^{-7} mbar and the sensor was cooled down to - 40 ºC with the thermoelectric cooler built in the device. The camera's entrance was sealed with 250 µm-thick Be window.

Transmission electron microscopy (TEM)

Prior the transmission electron microscopy analysis catalysts samples required proper preparation. Firstly, the sample was grinded in an agate mortar to a fine powder. The resulting powder was poured with 99.8% ethanol to form a slurry. The sample was inserted into the ultrasonic homogenizer for 20 s. Then, the slurry containing the catalyst was pipetted and supported on a 200 mesh copper grid covered with lacey formvar and stabilized with carbon (Ted Pella Company) and left on the filter paper until the ethanol has evaporated. Subsequently, the sample deposited on the grid was inserted to holder and moved to electron microscope. The electron microscope Titan G2 60-300 kV FEI Company, equipped with: field emission gun (FEG), monochromator, three condenser lenses system, the objective lens system, image correction (Cs-corrector), HAADF detector and EDS spectrometer (Energy Dispersive X -Ray Spectroscopy) EDAX Company with detector Si(Li) was used to display the prepared catalysts. Microscopic studies of the catalyst was carried out at an accelerating voltage of the electron beam equal to 300 kV. The size and shape of the nickel particles in the sample were determined by using the TEM imaging and a masking method of FFT available in the Gatan DigitalMicrograph software package.

Thermogravimetric analysis (TGA)

The thermal analyses of the polymeric resin as well as Ni catalyst were carried out using TG/SDTA 851e METTLER-TOLEDO thermobalance. The experiments were performed in nitrogen atmosphere at heating rate of 5°C·min-1 in the temperature range of 25 - 1000°C, using Al2O3 crucible. The thermoanalytical curves were obtained using STARe System METTLER-TOLEDO software.

Furrier-Transform Infrared Spectroscopy (FT-IR)

Infrared spectra of the samples were recorded on a Nicolet 380 FT-IR type spectrophotometer in the spectral range of 4000 - 500 cm-1 using the ATR-diffusive reflection method.

5. RESULTS AND DISSCUSION

5.1. SELECTIVE HYDROGENATION WITH PARENT Ni-CATALYST

5.1.1. BEFORE CATALYST PREPARATION

In regards to application of polymeric resin as catalyst support, several factors need to be taken into account prior to catalyst preparation. Synthetic resin materials display features that introduce certain restrictions to their treatment. The most important are: swelling due to solvent adsorption and their thermal stability.

Concerning the swelling, polymeric resin Tentagel-S-NH_2 ($TSNH_2$) used as metal nanoparticles carrier was subjected to microscopic investigation. Therefore, polar and non-polar solvents (ethanol, hexane and water) were added to $TSNH_2$ beads and examine in terms of their capacity of swelling the resin. Changes in beads diameter were monitored with microscopic camera and results are presented in Fig. 17.

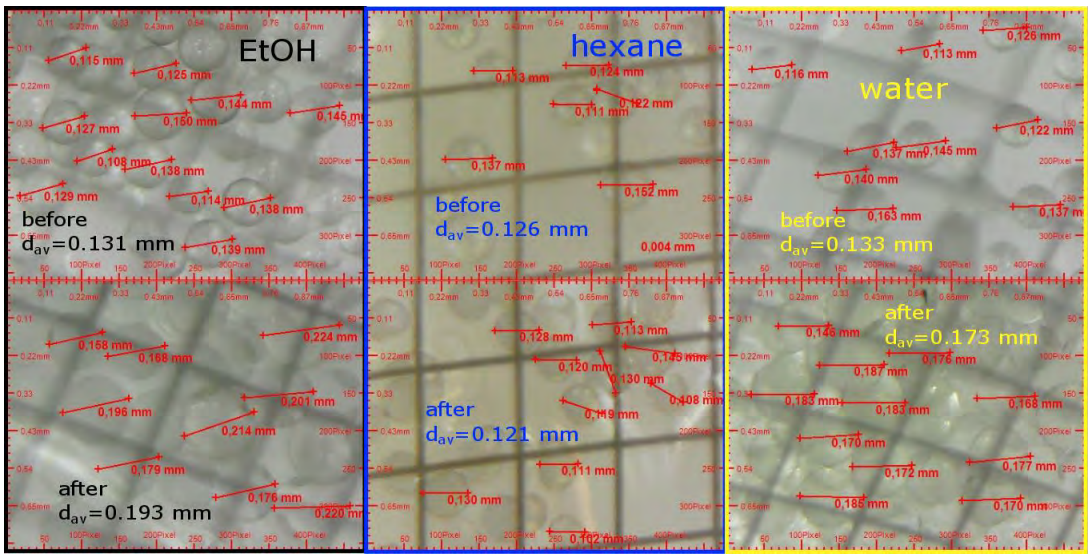

Figure 17. The capability of various solvents to swell Tentagel-S-NH_2 resin.

As anticipated from literature reports[159], swelling under polar solvents is more prominent. Similarly, in this case, ethanol indicated the best swelling properties. As shown, the average diameter of $TSNH_2$ beads in EtOH sample increased from 131 μm to 193 μm, which stands for 47% diameter elongation, i.e. the resin particles were 3.2 times bigger in volume after ethanol sorption.

The great ability of swelling is crucial and highly desired during either catalyst

synthesis and catalytic reactions, especially for quick flow processes.[160] On that basis, ethanol was selected as a solvent for both catalyst preparation and subsequent hydrogenation reactions. Catalyst synthesis conducted in ethanol ensured $TSNH_2$ structure relaxation providing optimal accessibility of $-NH_2$ functional groups during Ni nanoparticles grafting. Similarly, when metal/resin catalyst is applied to catalytic reaction, good swelling properties of solvent increase the accessibility of metal active sites anchored onto three-dimensional resin matrix.

In the next step, $TSNH_2$ material was investigated in terms of its surface and porosity properties. Results of N_2 physisorption are shown in Fig. 18.

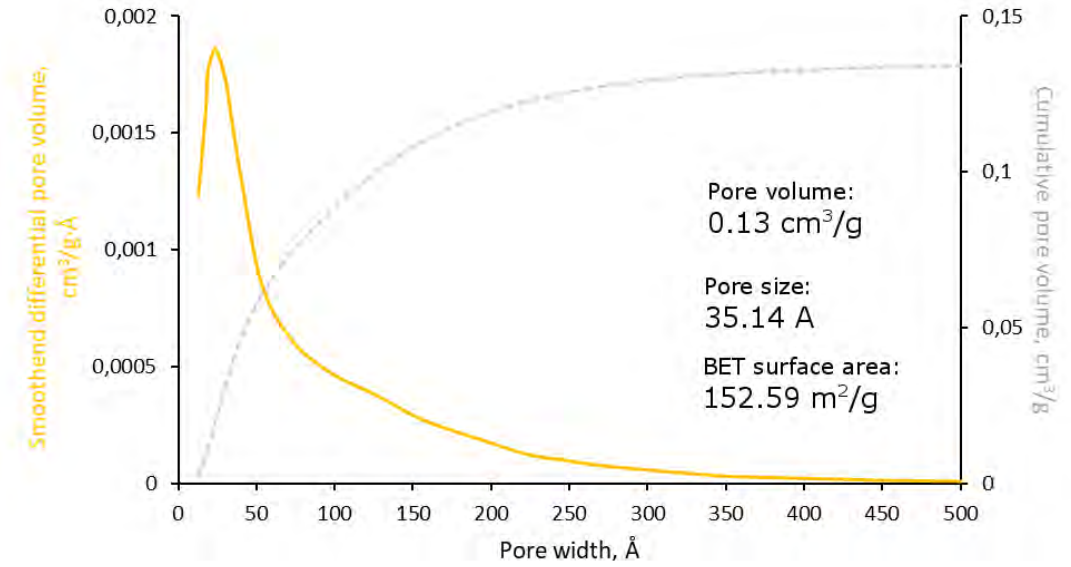

Figure 18. Horvath-Kawazoe plots of differential and cumulative pore volumes for cylinder pore geometry (Saito-Foley) in Tentagel-S-NH_2 resin.

The average pore size for $TSNH_2$ resin was calculated to be 35.14 Å (3.5 nm), hence, the material indicates mesoporosity with small mesopores (mesopores 2 – 50 nm). However, swelling properties of EtOH-$TSNH_2$ system lead to pore dilatation during operations in ethanol conditions. Therefore, narrow mesoporous structure is expanded, which results in better flow-through polymeric network. Additionally, good-swelling properties significantly suppress voids in the packing volume, expected since a cylindrical cartridge is filled with spherical shape beads. In result, resin supported catalyst is tightly packed in tubular reactor where the free spaces between spherical beads are utilized in favor of larger flow-through internal catalyst structure.

As aforementioned, thermal stability of the polymeric resin is another important feature. In this matter, thermogravimetric analysis (TGA) was performed to establish temperature up to which $TSNH_2$ resin can be treated without decomposing (important for preparation of active phase). The results are shown in Fig. 19.

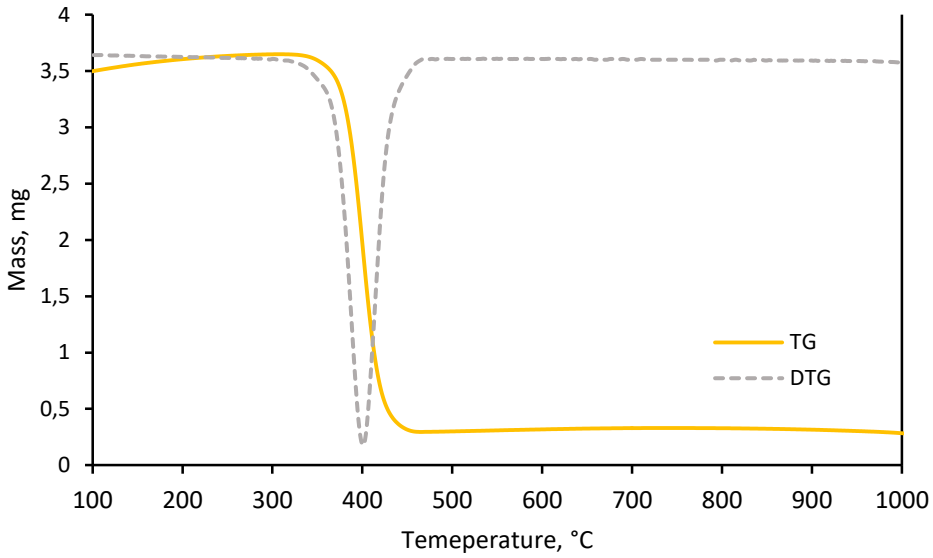

Figure 19. Thermogravimetric analysis of Tentagel-S-NH_2 resin.

As presented, thermal decomposition of $TSNH_2$ resin began beyond temperature of 300°C and led to complete decay when temperature reached 450°C. Relatively low thermal stability of the supporting material imposes constrictions on synthesis procedure and subsequent characterization of resin supported catalysts. Thus, temperature-programmed techniques could be applied at limited temperature range. Usually high temperature conditions are required to provide comprehensive and reliable data about metal active phase. Components generated during resin decomposition could change properties of metal phase and consequently distort measurement results.

5.1.2. Ni$TSNH_2$ CATALYST SPECIFICATION

To provide more detailed information on metal phase, the catalyst was subjected to further investigation. Firstly, the material was analyzed with high-resolution transmission electron microscopy (HR-TEM), which allowed obtaining insight into actual appearance and distribution of Ni nanoparticles anchored onto resin support. HR-TEM analysis (Fig. 20) revealed agglomerated form of nickel either on the surface

and inside pores. The agglomeration of nickel nanoparticles as well as presence of polymeric resin support considerably impeded thorough investigation of the sample. Consequently, above-mentioned features of the material constricted recognition of single particle and assessment of its actual shape.

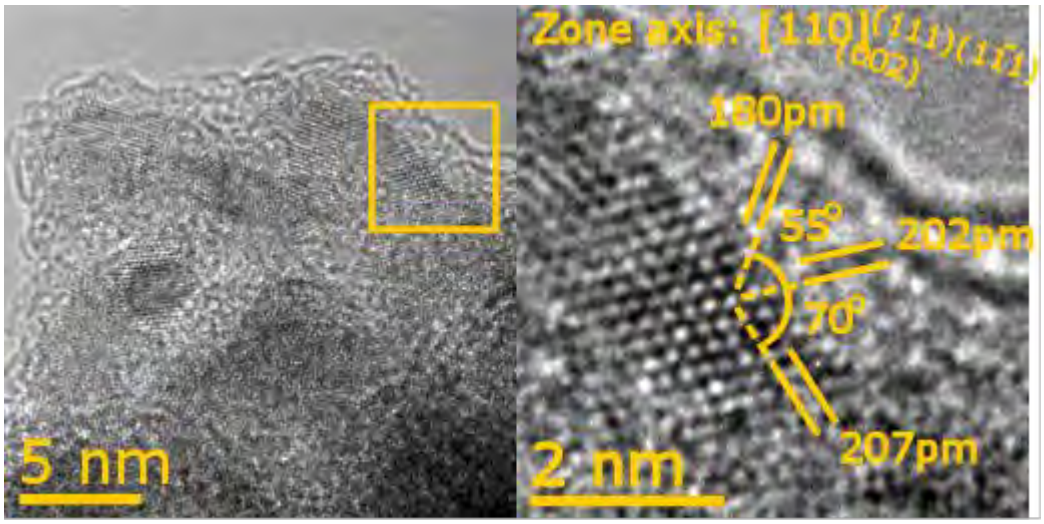

Figure 20. HR-TEM analysis of Ni nanoparticles immobilized on $TSNH_2$ resin.

Despite the impediments resulting from the nature of the support, it was found that the majority of Ni nanoparticles were smaller than 10 nm and the average particle size was established to be 3-4 nm. Crystallites with diameter wider than 20 nm were rarely spotted and their influence on average particle size was insignificant.

In the next step, to investigate metal-support interactions, the catalyst was subjected to Furrier-transform infrared spectroscopy (FT-IR). Catalyst design included application of polymeric support terminated with amino groups, which are able to bond metal nanoparticles. It was demonstrated in the literature[161] that ligands with reactive groups such as amine or thiols could act as a linker between polymer and metal nanoparticles. Therefore, as Dabbawala et al. showed in their work[162], covalent metal-amine interactions can be studied by monitoring the vibrations assigned to linking reactive group in FT-IR spectra.

In this regard, either polymeric resin and Ni catalyst were studied with FT-IR technique. Obtained spectra were compared in terms of changes in bands corresponded to characteristic vibrations of hydrogen atoms in primary amine. As presented in Fig. 21, the intensities of bands assigned to N-H bending (δ_{sym}N-H; 1550-1700 cm^{-1}) and N-H stretching (νN-H; 3200-3800 cm^{-1}) were significantly lower after grafting of Ni

nanoparticles. Presented results suggested suppression of N-H vibrations caused by approaching metal nanoparticles, indicating direct covalent interactions between amine from the resin support and Ni nanoparticles.

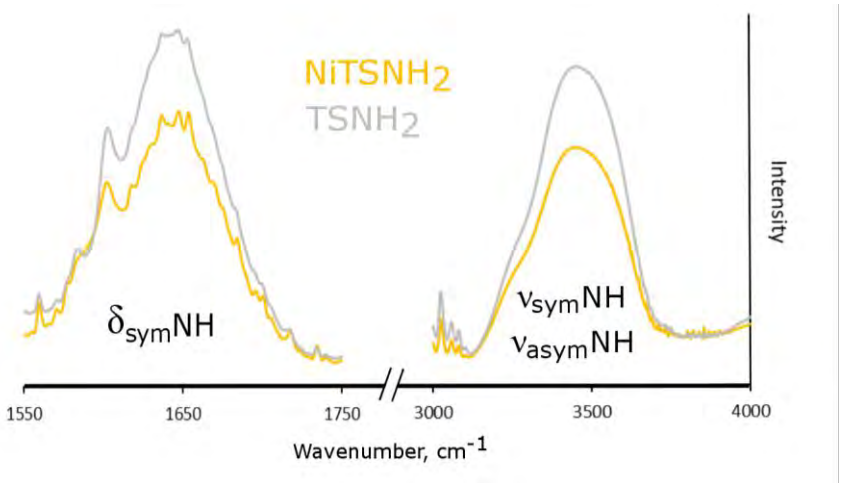

Figure 21. FT-IR bands of N-H vibrations in primary amine for $TSNH_2$ resin and catalyst after Ni nanoparticles grafting.

Therefore, according to these results, it can be concluded that Ni nanoparticles are immobilized onto $TSNH_2$ resin via $–NH_2$ terminal groups. Covalent Ni-NH_2 interaction ensure that nickel phase is well exposed and easily accessible, which is of great importance in continuous flow surface reactions.

To attain information about electronic structure of nickel phase, the $NiTSNH_2$ catalyst was tested with X-ray photoelectron spectroscopy (XPS). Surface distribution of Ni species of the grafted nanoparticles is presented in Fig. 22.

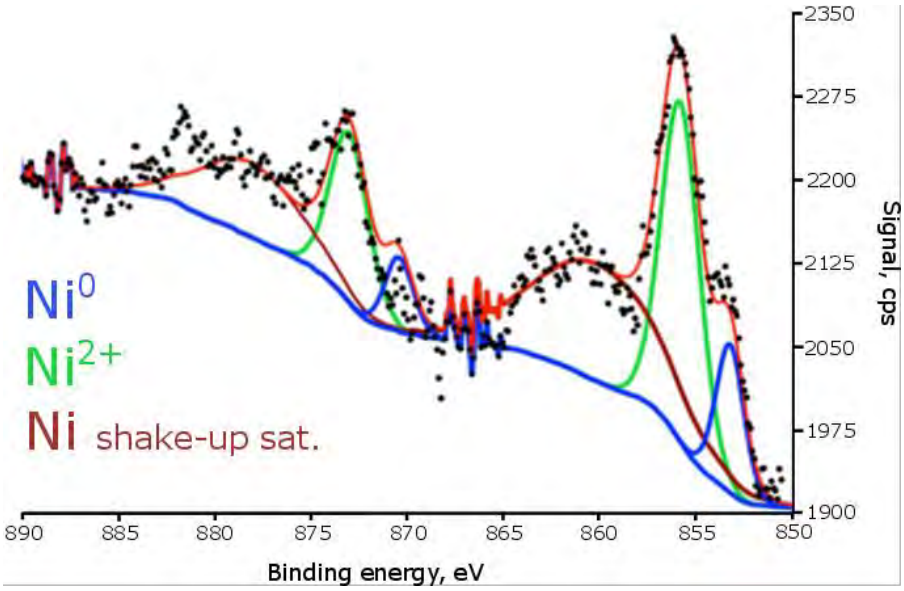

Figure 22. XPS profile of the nickel catalyst. Narrow scan of Ni *2p* region.

Superficial investigation of Ni oxidation states showed that oxidizes Ni dominates in the sample. This dominant signal of Ni $2p_{3/2}$ (856.1 eV) corresponds to $Ni(OH)_2$ which could be formed when catalyst was exposed to ambient conditions. FT-IR and TEM analysis revealed that small Ni nanoparticles are well-exposed on resin surface. Therefore, the oxygen from air can easily oxidize nickel phase. However, the superficial oxidation process can be reversed when catalyst is subjected to H_2 atmosphere, *e.g.* prior to hydrogenation reaction or catalyst modification in H-Cube Pro ™ reactor. It will be demonstrated in subsequent section on catalyst modification.

In addition, signals from both Ni^{2+} (856.1 eV) and Ni^0 (852.9 eV) were slightly shifted towards higher binding energy when compared to literature data[163,164]. Binding energy shifts originate from the fact that sample under investigation contained nanoparticles in small size.[165] Thus, this result is in line with previous findings on Ni nanoparticles size. The peak at highest binding energy (860.4 eV) is assigned to metallic Ni shake-up satellite.

Finally, the $NiTSNH_2$ material was investigated in terms of resin stability. In continuous flow operating it is especially important to maintain specific form and size of catalyst particles packed in flow-through cartridge. Thus, too small catalyst particles may cause flow clogging when leached to micro-channels of the reactor. According to producer's specification, for safe and stable processing in H-Cube Pro ™ micro-reactor, catalyst granularity should not be lower than 50 µm. In this light, the catalyst supported on 130 µm resin beads was tested due to possible particles fragmentation

during synthesis procedure. Therefore, the catalyst was subjected to scanning electron microscopy analysis to evaluate its granularity after chemical, mechanical (stirring) and thermal (drying) treatment. SEM images are presented below (Fig. 23)

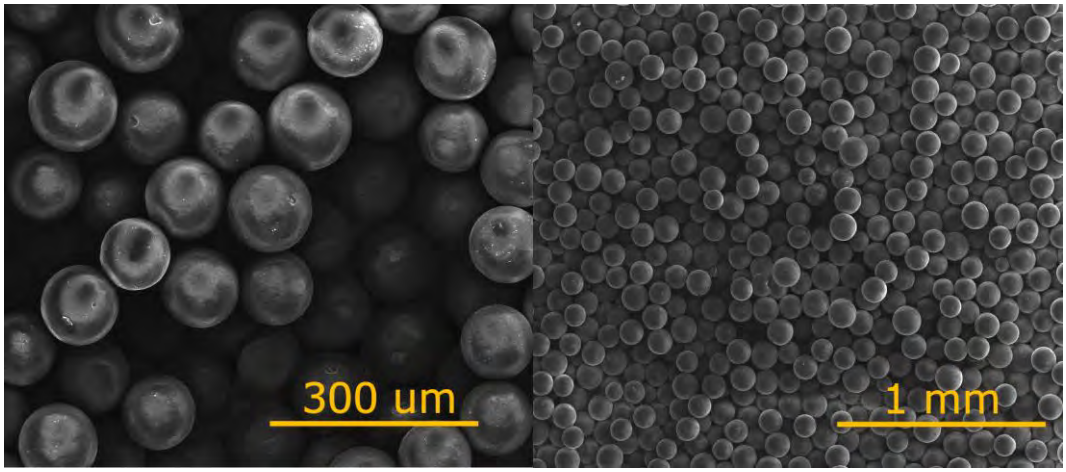

Figure 23. Scanning electron microscopy investigation of $TSNH_2$ resin beads after catalyst synthesis.

SEM investigation revealed that polymeric support preserved its initial form, hence, resin was not affected in subsequent synthesis steps. All beads captured on SEM images were neither crushed nor deformed indicating external stability of the support during catalyst preparation. To inspect whether internal structure of the resin was damaged or changed, X-ray diffraction technique was employed. Therefore, XRD profiles of both postsynthetic material and pure $TSNH_2$ resin were measured for compering (Fig. 24).

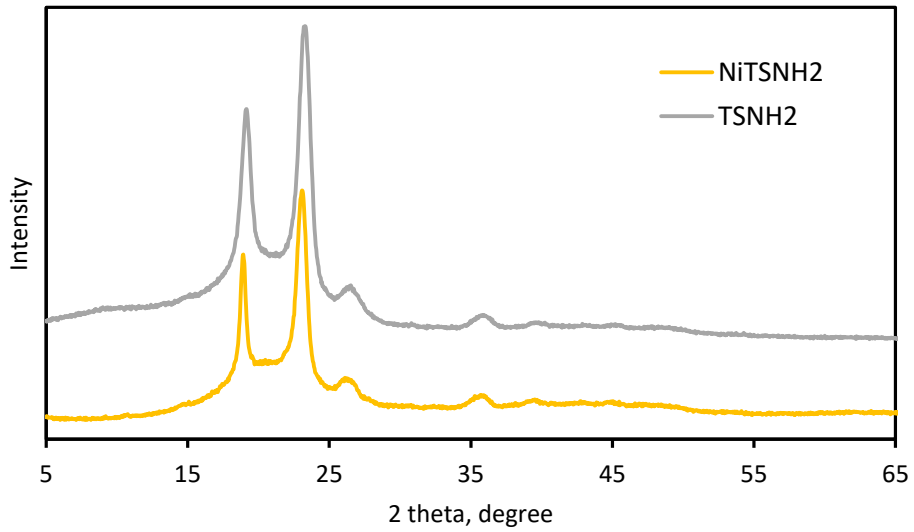

Figure 24. Powder X-ray diffraction profiles of $TSNH_2$ resin and material after synthesis.

As shown, diffractograms of both samples were identical, which confirmed stability of $TSNH_2$ support. Additionally, XRD measurement of $NiTSNH_2$ showed no reflects from nickel. This observation suggested very small nickel nanoparticles below the limit of quantification. Moreover, atomic adsorption spectrometry (AAS) measurement showed that Ni contributed 0.7 wt.% to the catalyst sample. Therefore, the large majority of Ni nanoparticles smaller than 5 nm in relatively low concentration might have affected recognition of Ni phase in XRD investigation.

5.1.3. PRENAL HYDROGENATION

In the first stage of catalytic tests, $NiTSNH_2$ was applied in prenal hydrogenation. Prenal, containing only methyl group in β position, is one of the simplest α,β-unsaturated aldehydes with high relevance for industry. Possible hydrogenation pathways of prenal are presented in Scheme 2. Depending on which unsaturated bond is hydrogenated, the reaction yields isovaleraldehyde or prenol by reduction of alkenyl or carbonyl bond, respectively. Further hydrogenation leads to formation of fully saturated compound – isoamyl alcohol.

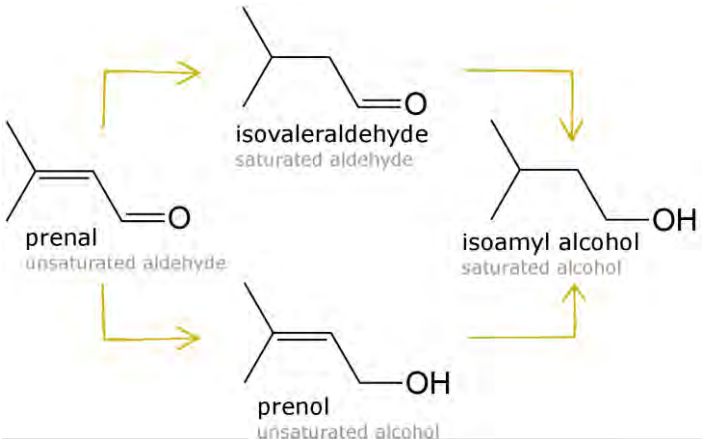

Scheme 2. Possible reaction pathways in hydrogenation of prenal.

Firstly, the catalyst was subjected to screening through reaction conditions, which enabled delineation of temperature and pressure profile of the process (Fig. 25).

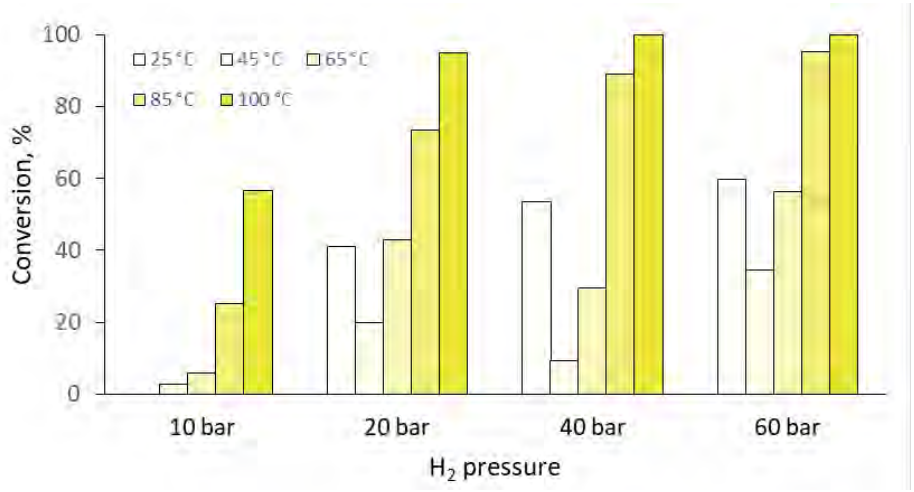

Figure 25. Temperature and pressure profile of prenal hydrogenation.

As shown, endothermic character of the hydrogenation was only disturbed at 25°C with pressure ≥ 20 bar. Therefore prenal conversion was rising with temperature and pressure increase leading to complete prenal transformation at temperature of 100°C and p ≥ 40 bar.

The reaction over $NiTSNH_2$ yielded mainly saturated aldehyde (isovaleraldehyde), the C=C bond saturation product. Besides C=C hydrogenation compound also completely saturated product was obtained with remarkably lower selectivity. Additionally, GC analysis indicated presence of compounds detected in significantly longer retention time. This observation suggested that completely saturated product underwent further transformation with solvent molecules leading to formation of acetals.

To eliminate competitive processes and optimize the reaction towards C=C saturation, prenal hydrogenation conditions were selected to maximize formation of isovaleraldehyde. Figure 26 shows dependence of hydrogenation conditions on C=C product concentration in prenal hydrogenation.

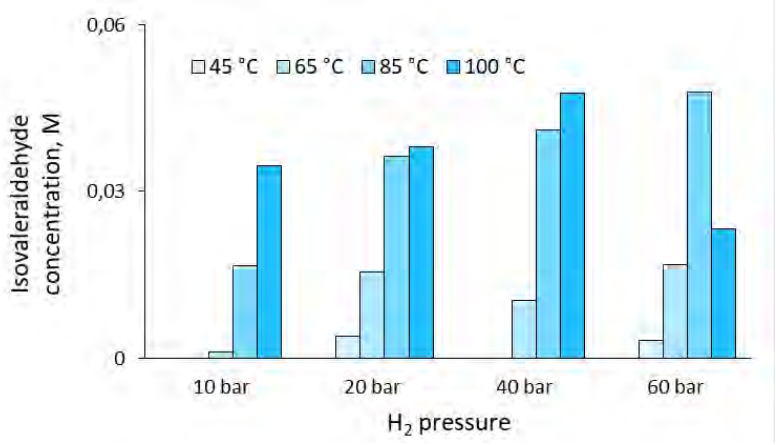

Figure 26. Isovaleraldehyde production under various conditions.

The highest amount of desired product was obtained at 85°C and 60 bar, hence, those conditions were chosen for stability test (Fig. 27). In long-term reaction the catalyst showed very high and stable selectivity towards C=C hydrogenation (95% after 5 h on stream) and moderately stable activity.

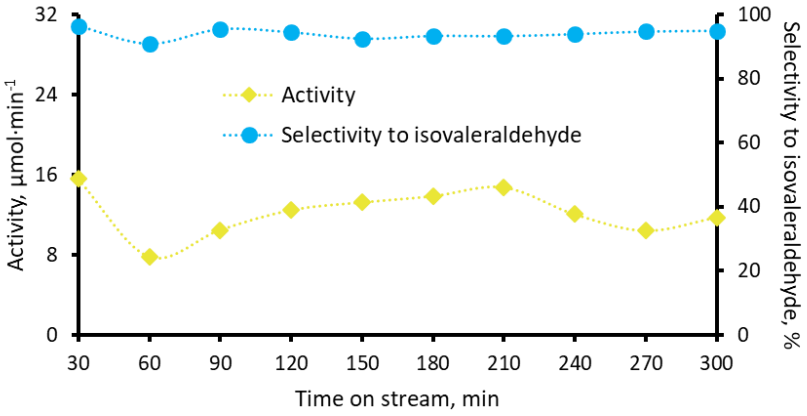

Figure 27. Long-term stability test of $NiTSNH_2$ in prenal hydrogenation at 85°C and 60 bar.

Considering that optimization tests displayed high activity at 85°C, 60 bar it can be concluded that catalyst lost its activity in the initial phase of the reaction (0-60 min on stream). After that time activity plot stabilized indicating activity of ~ 12 µmol·min^{-1} (~ 40% prenal conversion) after 5 h on stream.

5.1.4. CINNAMALDEHYDE HYDROGENATION

The second α,β-unsaturated aldehyde investigated in this study, cinnamaldehyde, contains phenyl group in β position. The presence of benzene ring may introduce additional steric repulsion with catalyst surface consequently affecting adsorption mode of the molecule. Therefore, taking into consideration wide industrial application of partially saturated products of cinnamaldehyde hydrogenation, this compound was selected to study versatility of $NiTSNH_2$ catalyst. Similarly to prenal, cinnamylaldehyde hydrogenation leads to two semi-saturated products converted into fully hydrogenated compound in further transformation (Scheme 3).

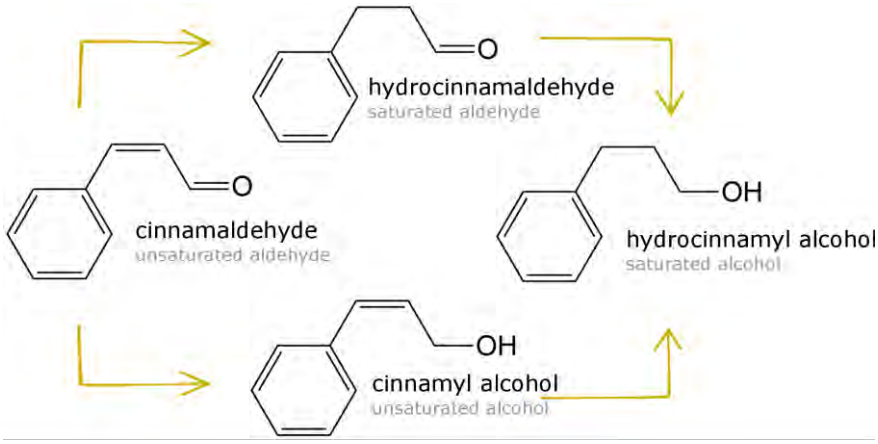

Scheme 3. Possible reaction pathways of cinnamaldehyde hydrogenation.

In optimization test of cinnamaldehyde hydrogenation, studied catalyst displayed similar trend as in the case of prenal but with higher conversion values (Fig. 28). Thus, similarly to previous example, relatively high conversion at 25°C dropped when temperature was increased up to 45°C and was rising with further temperature and pressure increase.

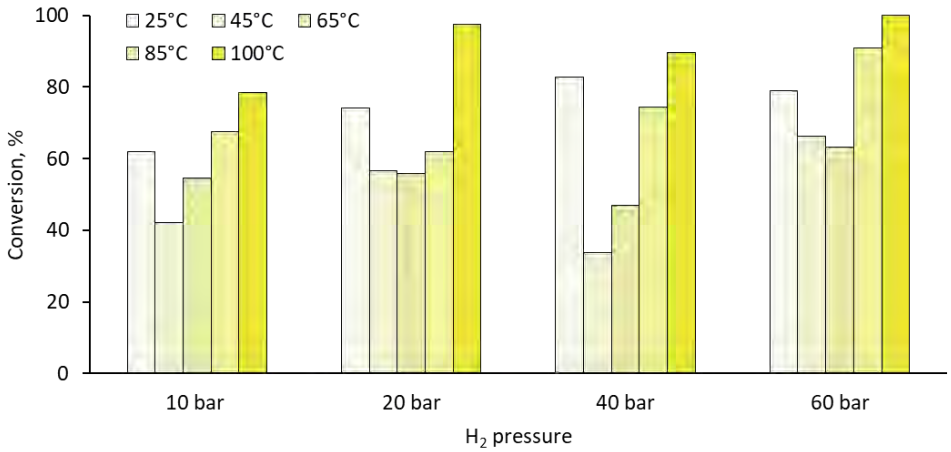

Figure 28. Temperature and pressure profile of cinnamaldehyde hydrogenation.

In terms of product distribution, $NiTSNH_2$ catalyst displayed high selectivity towards conjugated alkenyl bond hydrogenation yielding hydrocinnamaldehyde (HCA) as a main product. Secondary product of complete saturation was detected with significantly lower selectivity. As shown in Fig. 29, production of desired C=C reduction product in this catalytic system was the most effective when temperature was higher than 65°C. The biggest amount of HCA was formed when reaction was conducted at 100°C and 40 bar.

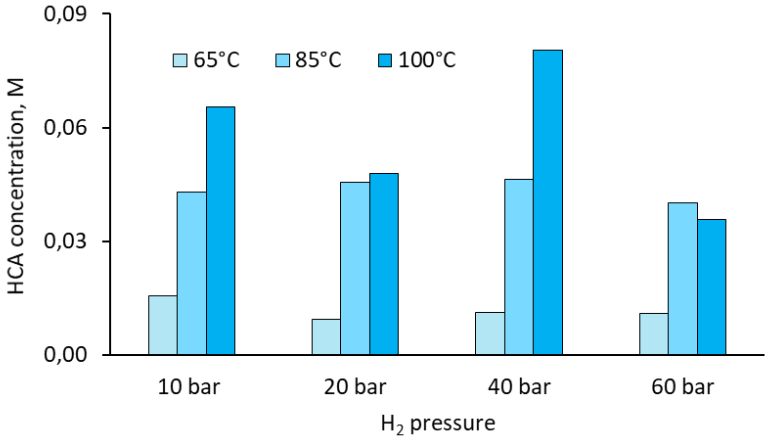

Figure 29. Hydrocinnamaldehyde production under various conditions.

After selecting the most optimal conditions, the catalyst was subjected to long-term reaction. Results presented in Fig. 30 show that very high and stable selectivity to C=C hydrogenation product (92%) was maintained during the whole experiment. Likewise, the catalyst indicated great activity in cinnamaldehyde hydrogenation. Presented catalytic system led to 91% of conversion after 5 h, which allowed transforming 22.5

μmol of cinnamaldehyde per minute. Nevertheless, after 150 min activity plot slightly drops indicating catalyst deactivation.

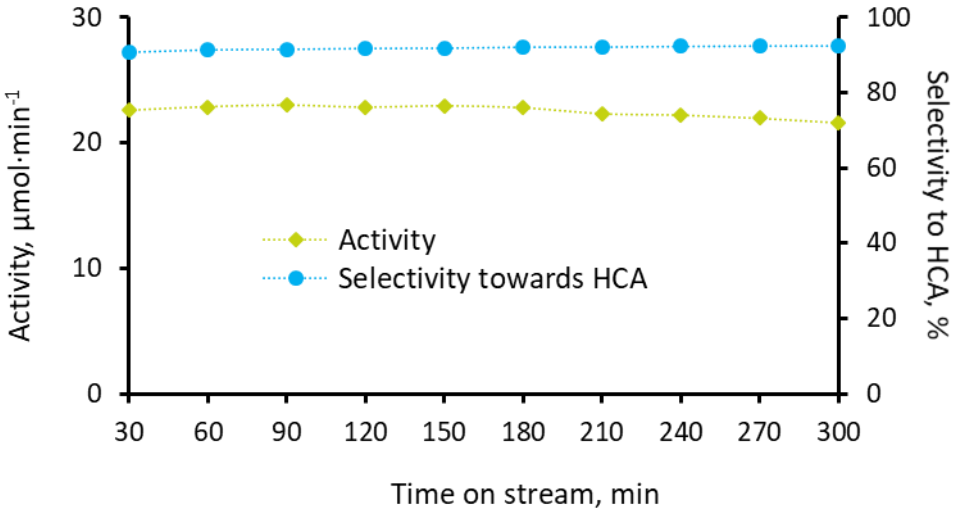

Figure 30. Long-term stability test of $NiTSNH_2$ in cinnamaldehyde hydrogenation at 100°C and 40 bar.

5.1.5. CITRAL HYDROGENATION

Both previous examples confirmed high selectivity of $NiTSNH_2$ to conjugated C=C hydrogenation in α,β-unsaturated aldehydes. It was also proved that alkenyl bond saturation was favored irrespective of functional group bonded to C atom in β position. However, to affirm that $NiTSNH_2$ catalyst is universally applicable for chemoselective conjugated alkenyl bond saturation, the material was tested with citral – compound with more extended structure. Citral, besides carbonyl and conjugated alkenyl bond, possesses second, isolated alkenyl bond which introduces competitive reaction of C=C hydrogenation. The presence of three unsaturated bonds results in respectively higher number of partially saturated intermediates. Therefore, in citral hydrogenation there are more possible reaction pathways (Scheme 4) including competitive reduction of the same unsaturated bonds but in different positions.

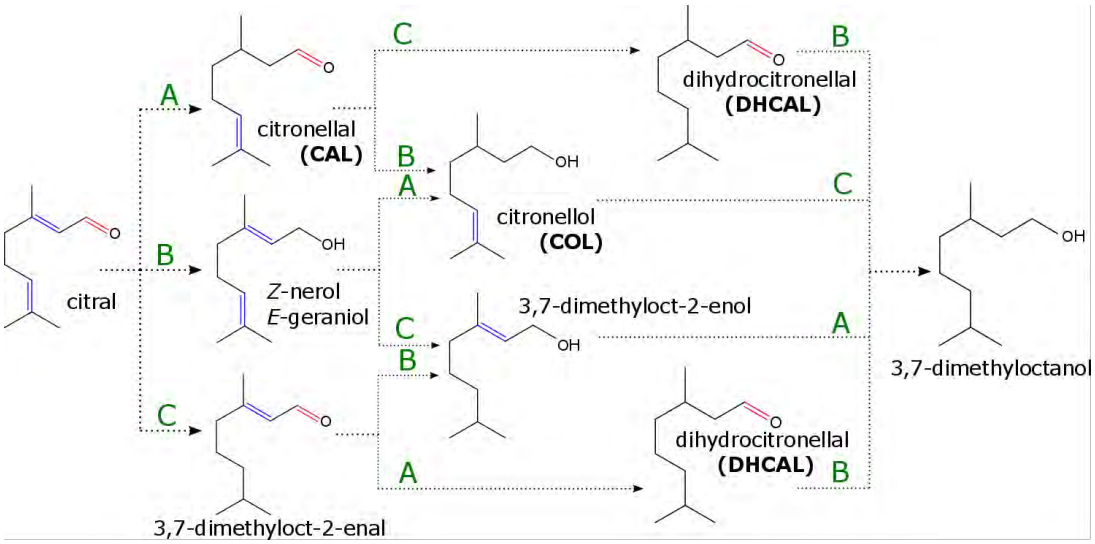

Scheme 4. Possible reaction pathways in citral hydrogenation. A – conjugated alkenyl bond hydrogenation; B – carbonyl bond hydrogenation; C – isolated alkenyl bond hydrogenation

Screening through reaction conditions (T, p) showed endothermic character of flow citral hydrogenation over $NiTSNH_2$ catalyst (Fig. 31). Thus, the best performance in terms of citral conversion was achieved at 100°C and 60 bar. With those reaction parameters ~ 99% of the substrate flown through catalyst bed was converted.

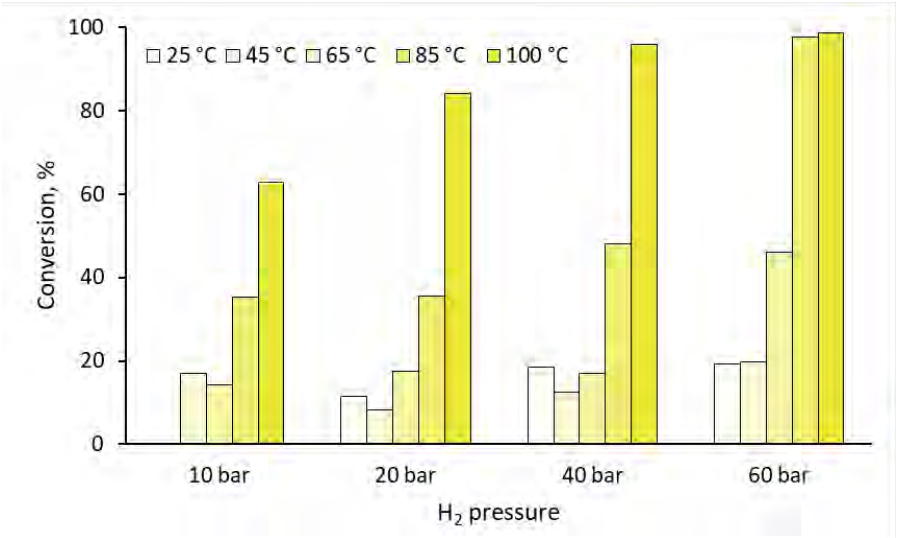

Figure 31. Temperature and pressure profile of citral hydrogenation.

However, citronellal (only conjugated C=C bond saturation) hydrogenation at various T and p values indicated 85°C and 60 bar as the most optimal conditions (Fig. 32). Basing on this result, the catalyst was subjected to stability test at selected conditions and experiment outcomes are presented in Fig. 33.

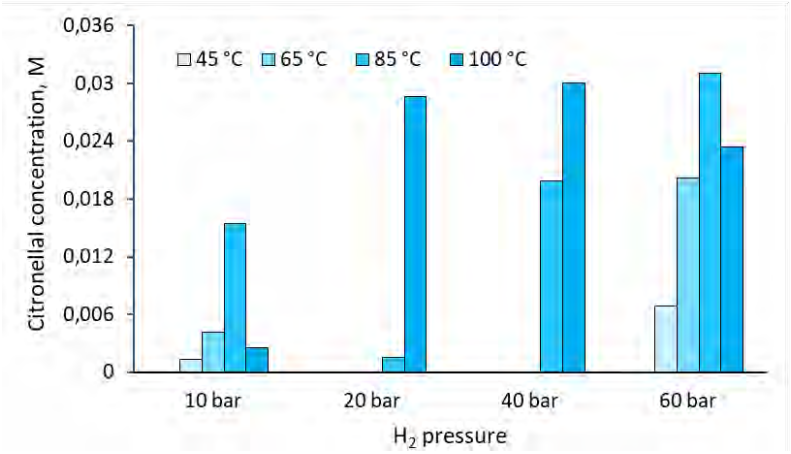

Figure 32. Citronellal production in various reaction conditions.

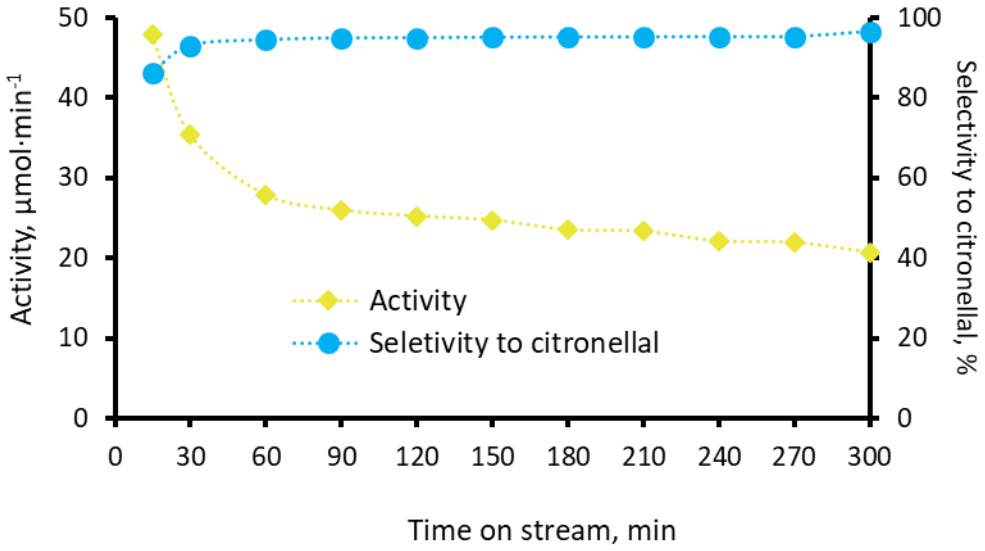

Figure 33. Long-term stability test of $NiTSNH_2$ in citral hydrogenation at 85°C and 60 bar.

As shown, the catalyst maintained high selectivity during the experiment yielding 96% of citronellal after 5 h on stream. In the case of activity, the catalyst performance dropped in an initial phase of the process and stabilized in time. Eventually, after 5 h, the catalyst displayed activity of 20.7 $\mu mol \cdot min^{-1}$ (42% of citral conversion).

Considering that reactions were performed in liquid phase under constant flow conditions, it is reasonable to assume that the main reason behind catalyst deactivation is the leaching of the active phase. In this matter, to investigate whether Ni nanoparticles were leached from the catalyst bed, post-reaction mixture was analyzed with X-ray fluorescence (XRF). The measurement of samples collected in the same time intervals as in long-term stability tests showed no traces of Ni. It is worth mentioning that Ni contributed 0.7% of the catalyst, which stands for 0.001g of Ni in

catalyst bed during each reaction. Note, however, in order to be detectable the amount of Ni leached had to be relatively high. Thus, more measurements were carried out to disprove deactivation due to metal phase leaching.
XRD investigation of spent catalyst showed no changes in catalyst morphology. In both diffraction profiles (as-prepared and spent catalyst) peaks associated with Ni were not observed. Hence, it can be assumed that nanoparticle agglomeration or Ni redepositing (Ostwald ripening)[166] caused by liquid flow did not occur or was not significant enough to affect Ni nanoparticles size and dispersion of metal active sites.

XPS analysis of both catalyst samples (as-prepared and spent) displayed no significant changes in the Ni content, once more contradicting leaching possibility. However, Ni species distribution was found modulated, namely there was an increase of the Ni^{ox}/Ni^{0} after the reaction from 6.31 to 7.09. This suggested destabilization of the metallic phase, and consequent deactivation of the catalyst.
Another possible cause for deactivation is the decrease of metallic active sites (aka active phase) by reaction components deposition (substrate, products and/or solvent). Comprehensive analysis of carbon deposits on Ni surface is limited by support thermal stability. According to literature, temperature-programmed hydrogenation (TPH) analysis of carbonaceous deposits on Ni surface was achieved at ~ 600 K (330°C).[167] According to TG analysis this temperature would lead to resin decomposition and therefore precludes the use of such method.

5.1.6. SELECTIVITY IN CITRAL HYDROGENATION

Selectivity of $NiTSNH_2$ catalyst in citral flow hydrogenation was found to be dependent on reaction conditions. As presented in Fig. 34, the reaction can be directed to produce citronellal or citronellol (C=O and conjugated C=C hydrogenation) with 100% of selectivity.

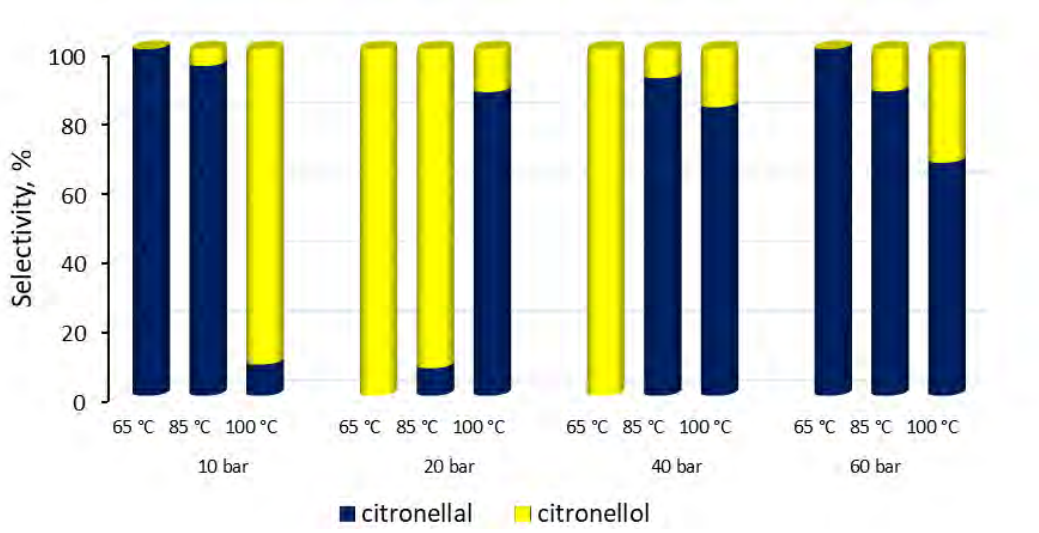

Figure 34. Dependence of reaction conditions on $NiTSNH_2$ selectivity in citral flow hydrogenation.

Chemoselectivity to conjugated C=C hydrogenation was changing with temperature and pressure. When pressure was low ($p \leq 10$ bar) selectivity to citronellal was decreasing with temperature increase, in other words, the catalyst was losing its chemoselectivity to solely reduce C=C in α position. The opposite trend was indicated when pressure was higher than 20 bar. In this case, chemoselectivity of the catalyst was rising with pressure and temperature increase. Thus, selectivity in citral flow hydrogenation over $NiTSNH_2$ can be controlled with reaction parameters but only within conjugated bonds reduction.

The main product obtained by C=C reduction, citronellal, was subjected to further hydrogenation over the same nickel catalyst. Citronellal hydrogenation was found to occur in harsher conditions: $T \geq 110°C$ and $p \geq 80$ bar. Results of selectivity studies in this reaction are shown in Fig. 35.

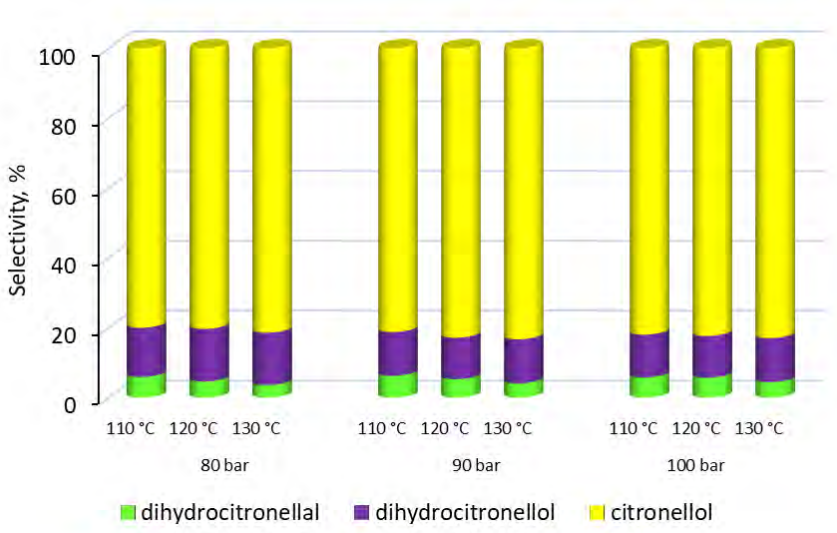

Figure 35. Dependence of reaction conditions on $NiTSNH_2$ selectivity in citronellal hydrogenation.

As expected, citronellal flow hydrogenation yielded mainly citronellol by carbonyl bond hydrogenation. This result indicates that carbonyl bond determines adsorption of α,β – unsaturated aldehyde molecule on nickel surface. Isolated alkenyl bond hydrogenation was achieved with low selectivity (~ 5%) forming dihydrocitronellal. As demonstrated, reaction conditions have no impact on selectivity in citronellal hydrogenation over $NiTSNH_2$.

5.1.7. $NiTSNH_2$ AFFINITY TO SELECTIVE ALKENYL BOND HYDROGENATION

Bond control in α,β – unsaturated aldehydes hydrogenation with nickel catalyst can result from several factors including catalyst surface morphology, reaction conditions, thermodynamic preferences or nature of the active metal.

All those aspects may impact selectivity in this reaction by influencing the adsorption of the hydrogenating molecules on Ni surface. Adsorption as a basis for catalytic surface reactions plays key role in competitive alkenyl versus carbonyl bond saturation. Hydrogenation of a specific bond can be promoted or suppressed depending on adsorption mode, which dominates on a given surface. Adsorption modes for α,β – unsaturated aldehydes on d-block metal surface are presented in Fig. 36.

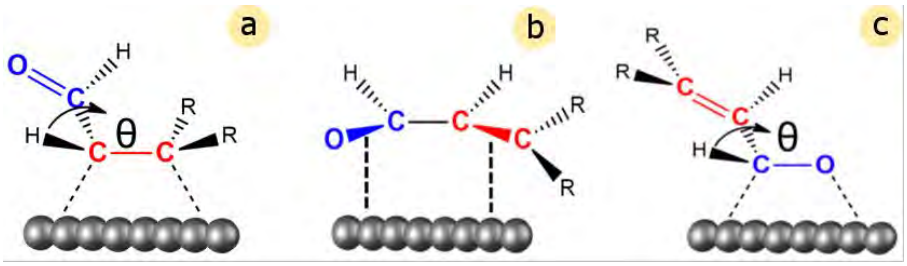

Figure 36. Modes of α,β – unsaturated aldehydes adsorption on d-block metal surface: a) di-σ_{CC} η_2; b) di-π η_2 (η_4) c) di- σ_{CO} η_2

In the Horiuti–Polyani mechanism, widely accepted for the hydrogenation of α,β-unsaturated carbonyls, at least one of adsorbed states presented in Fig. 36 is required.[168] In the case of d – σ interactions (di-σ_{CC} η_2 or di-σ_{CO} η_2), one of the unsaturated bond adsorbed on metal surface is attacked by hydrogen atoms migrating over the surface. However, when α,β-unsaturated carbonyl forms di-π η_2 (η_4) conformation, alkenyl bond hydrogenation is a thermodynamically preferred reaction, which was proved by quantum chemical calculations (Scheme 5).[17] Complex of alkenyl hydrogenation product with Ni cluster indicates lower relative energy, hence, higher stability. Therefore, C=C saturation is less energy demanding on Ni surface.

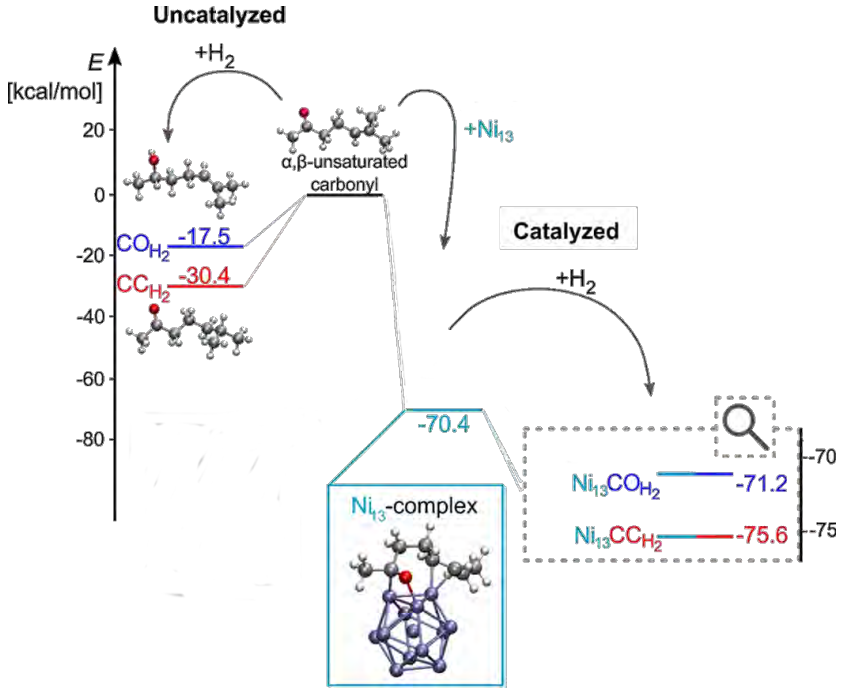

Scheme 5. Relative energies of intermediates and products in α,β-unsaturated carbonyl hydrogenation.

The adsorbed state of α,β-unsaturated carbonyl can be driven by morphological features of metal surface. As Delbecq and Sautet demonstrated[2], the adsorption mode strongly depends on the type of metal face exposed. Depending on atoms arrangement, metal face can generate stronger or weaker steric repulsion with approaching molecule (Fig. 37). Tightly packed (111) face causes increased repulsive interactions promoting di-σ η_2 form. On the other hand, (110) face indicates lower repulsive force, favoring η_4 adsorption mode which was found to support C=C hydrogenation.

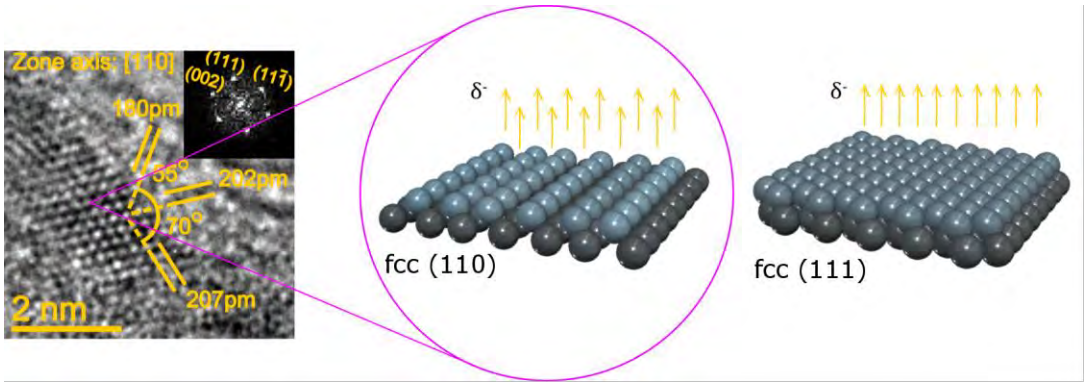

Figure 37. TEM image of Ni(110) face exposed in $NiTSNH_2$ catalyst. Ni atoms arrangement in (110) face indicates weaker stearic repulsion with approaching molecule.

Beside catalyst morphology, also electronic aspect needs to be taken into consideration. Nickel itself possesses relatively narrow d-band width. As discussed in the Chapter 1 of the dissertation, d character of metals influences their selectivity in competitive C=C vs. C=O hydrogenation. Metals which electronic structure is characterized by narrow d-band are more likely to promote C=C hydrogenation. Therefore, $NiTSNH_2$ catalyst indicates the set of morphological and electronic features which shift its selectivity to alkenyl bond hydrogenation over competitive C=O reduction.

5.2. SELECTIVE HYDROGENATION WITH MODIFIED Ni-CATALYSTS

5.2.1. *ON-THE-FLY* PARENT CATALYST ACCRETION

To study morphology-catalytic performance relation, parent $NiTSNH_2$ material was modified in terms of nickel nanoparticles size and tested in citral flow hydrogenation. Catalyst accretion protocol was developed to vary nanoparticles morphology prior to the catalytic reaction in the same high-pressure continuous flow reactor. Conducting catalyst modification and hydrogenation reaction in a sequence remarkably intensifies structure sensitivity studies for flow catalysis. Alternate modifier and reaction mixture introduction allowed monitoring changes in catalytic performance *in-situ* after modification. Thus, presented protocol offers an elegant platform for catalyst optimization in continuous flow operating.

Nanoparticles accretion was controlled by time, for which parent catalyst was subjected to saturation with Ni^{2+} ions. Using this methodology, three nickel catalysts were prepared and investigated in terms of changes in nanoparticles size. Morphology investigation was done using two techniques (XRD and TEM) to provide the most accurate estimation of Ni nanoparticles size.

Diffractograms of all prepared materials are presented in Fig. 38.

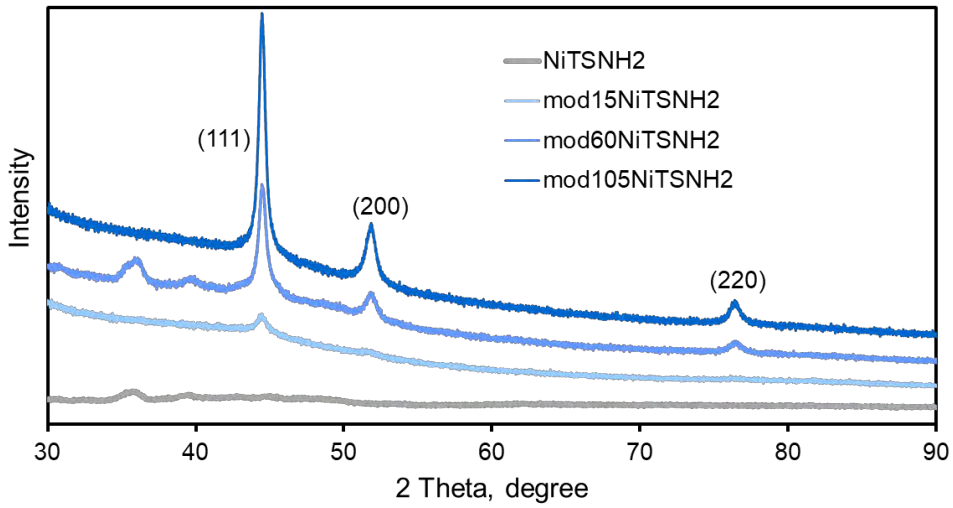

Figure 38. XRD profiles of parent catalyst before and after nanoparticles accretion.

As shown, diffraction profiles of every sample after accretion indicated peaks, which are assigned to nickel crystalline structure. The presence of those reflects suggested formation of nanoparticles bigger than 3-4 nm (parent catalyst, TEM). Additionally, samples exposed for longer accretion time displayed peaks with correspondingly

sharper linewidths, indicative direct reliance of modification time on nanoparticles size. Indeed, Ni crystallites size in samples after 15, 60 and 105 min of modification was estimated to be 5, 9 and 12 nm, respectively. TEM analysis (Fig. 39) of all modified samples led to similar conclusions, proving effectiveness of *on-the-fly* accretion method. It was revealed that during modification, nickel formed spherical nanoparticles in size of 7, 9 and 14 nm after 15, 60 and 105 min of modification, respectively.

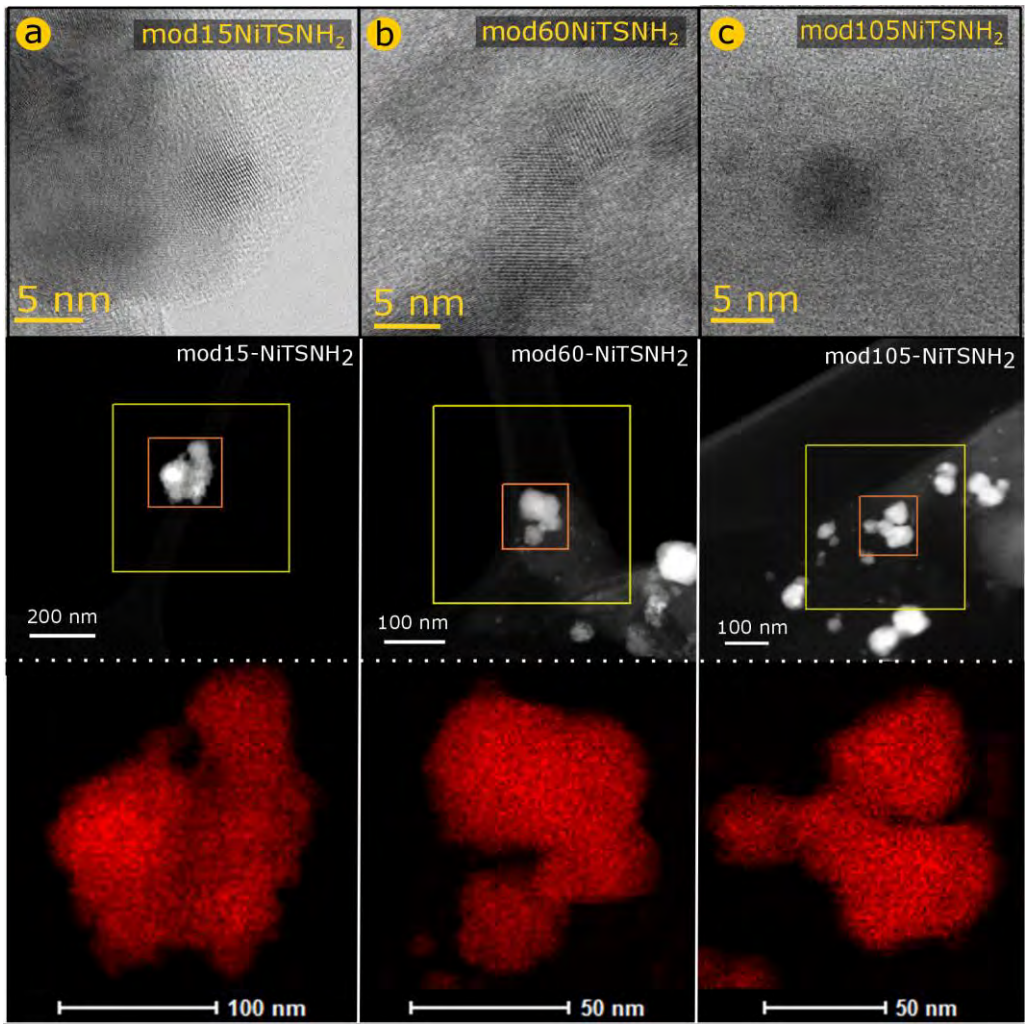

Figure 39. TEM analysis of $NiTSNH_2$ catalyst after nanoparticles modification for different time: a) 15, b) 60 and c) 105 min.

Table 2 collates results of Ni nanoparticles size estimation from both methods. Ni particles diameter length obtained from XRD analysis and TEM images show small divergences. Note that surface termination, which is always amorphous in nature, cannot be detected in X-ray diffraction technique. Therefore, XRD pertains solely to crystalline 'core' of the nanoparticles, whereas, TEM captures the whole particles.

In the case of nanoparticles accreted for 15 and 105 min, amorphous 'shell', observable in TEM images, contributed 2 nm to nanoparticles diameter. However, both techniques indicated coherency in the case of mod60NiTSNH$_2$ material, where Ni nanoparticles size were estimated to be 9 nm.

Table 2. Nickel nanoparticles size in NiTSNH$_2$ catalyst after different time of modification.

Catalyst	Modification time, min	Crystallite size (XRD), nm	NPs size (TEM), nm
NiTSNH$_2$	--	--	3-4
mod15-NiTSNH$_2$	15	5	7
mod60-NiTSNH$_2$	60	9	9
mod105-NiTSNH$_2$	105	12	14

Since modification process relied on constant delivery of Ni ions to the catalyst bed for a given time, it can be expected that besides nanoparticles size also metal loading will be increased. Taking that into consideration, samples of modified catalyst were investigated in terms of nickel content. Atomic adsorption spectrometry results showed that longer accretion time led to higher metal loading. Thus, Ni content in modified catalysts was found to reach 1.0, 3.0 and 4.9% after 15, 60 and 105 min of Ni^{2+} saturation, respectively (0.7% of parent material).

In the next step, X-ray absorption spectroscopy (XAS) was employed to determine Ni oxidation states in modified catalysts. X-ray absorption profiles were recorded near Ni K-edge (8340 eV) and presented in Fig. 40. Since XAS analysis showed that oxidized form of Ni existed only as Ni^{3+} form (Ni_2O_3) with no evidence of Ni^{2+} (NiO), the spectra were fitted using only reduced component Ni^0 and oxidized Ni^{3+} state. The presence of Ni^{3+} with no traces of Ni^{2+} on catalysts surface was also confirmed with XPS. Nevertheless, XAS analysis, done for samples in ethanol, seems to be more reliable for further discussion.

Fig. 40a shows spectral deconvolution of parent NiTSNH$_2$ catalyst. XAS analysis of unmodified material showed similar contribution of both reduced and oxidized forms of Ni. However, in this case, material sample was reduced with $NaBH_4$ prior to the measurement, which increased Ni^0 contribution. This result suggested that oxidized Ni was located only at the surface and can be easily reduced. Therefore, it can be assumed that H_2 pre-treatment at 100°C and 40 bar done before each reaction is sufficient to

reduce all superficially oxidized metal on $NiTSNH_2$ surface.

As shown in Fig. 40b, 15 min of modification caused a slight decrease in adsorption signal corresponded to Ni^{3+} component in favor of Ni^0 form. Furthermore, after 60 min of accretion (Fig. 40c), metallic Ni component decisively dominates in the sample contributing more than 90% to total nickel phase. This result indicates that 9 nm Ni nanoparticles formed after 60 min of modification were more stable and resistant to air passivation. Longer accretion (105 min, Fig. 40d) did not introduce significant changes in Ni components distribution when compared to the previous sample.

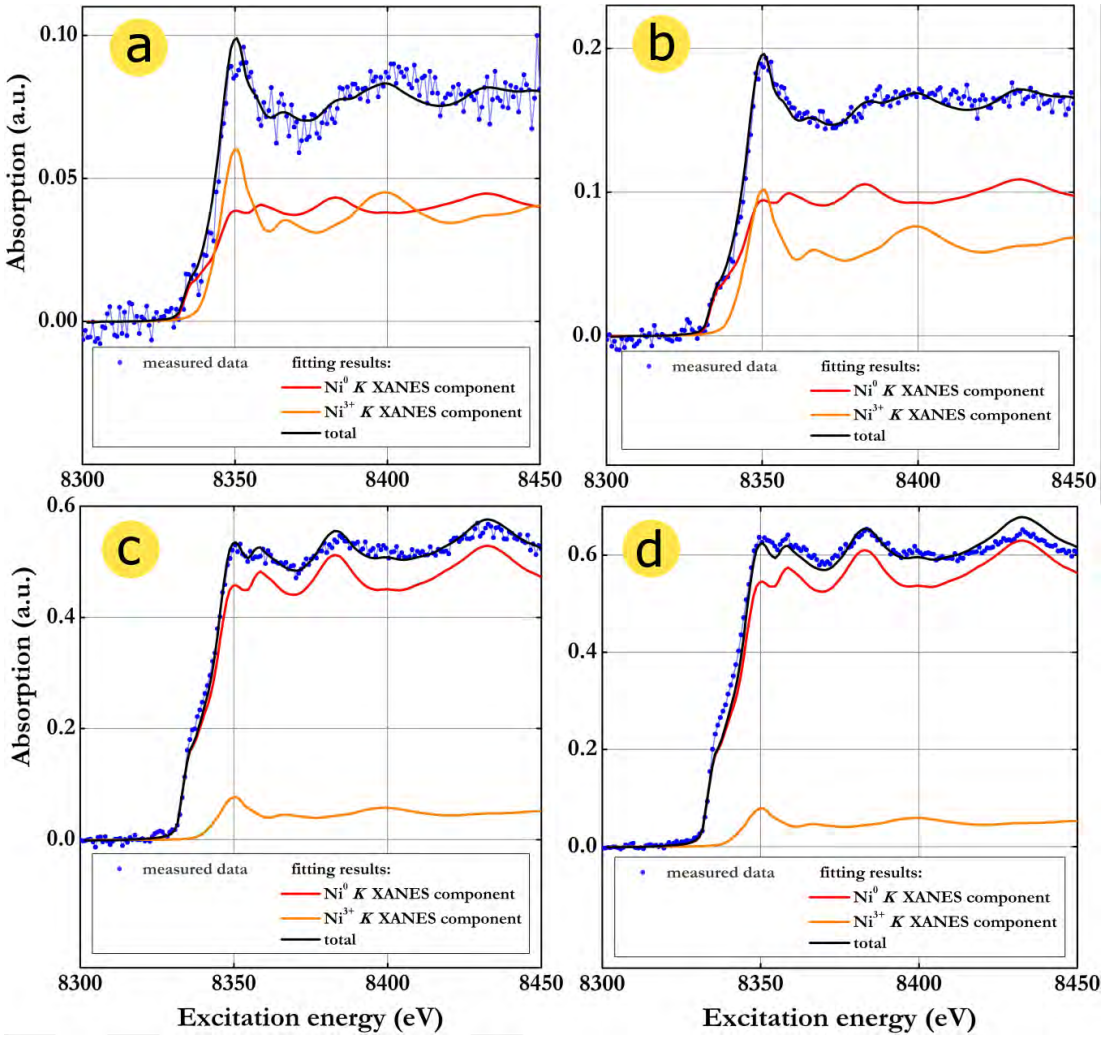

Figure 40. XAS spectra and spectral deconvolution of a) $NiTSNH_2$; b) $mod15NiTSNH_2$; c) $mod60NiTSNH_2$ and d) $mod105NiTSNH_2$.

Dependence of accretion time on Ni species contribution in modified catalyst samples is presented in Fig. 41. There is a clear trend showing increase of Ni^0 contribution with elongation of modification time. After 60 min, the catalyst indicated stability in terms of nanoparticles oxidation state.

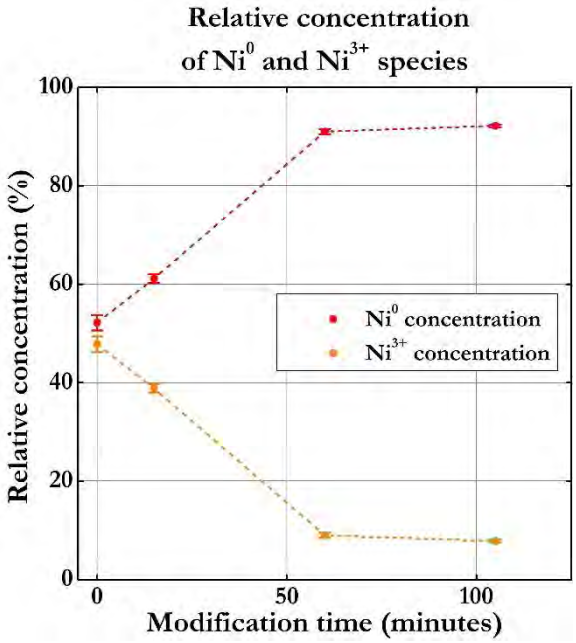

Figure 41. Relative contribution of Ni species to the XAS spectrum as a function of accretion time.

5.2.2. CITRAL HYDROGENATION WITH MODIFIED CATALYSTS

To inspect morphology-activity relation, all modified catalysts were tested in citral flow hydrogenation reaction. The structure sensitivity study was performed in convenient accretion-reaction sequential protocol. Firstly, catalytic performance of each catalyst was monitored under various reaction conditions. The activity results expressed as a conversion of citral in function of various temperature and pressure values are shown in Figures 42-44.

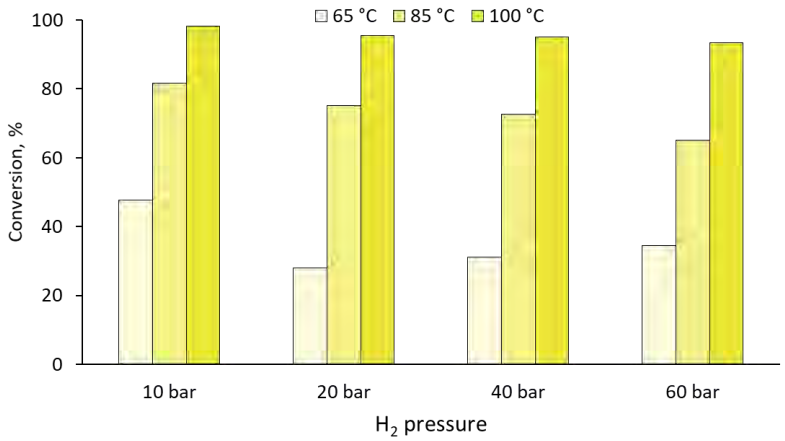

Figure 42. Temperature and pressure profile of citral hydrogenation over mod15NiTSNH$_2$.

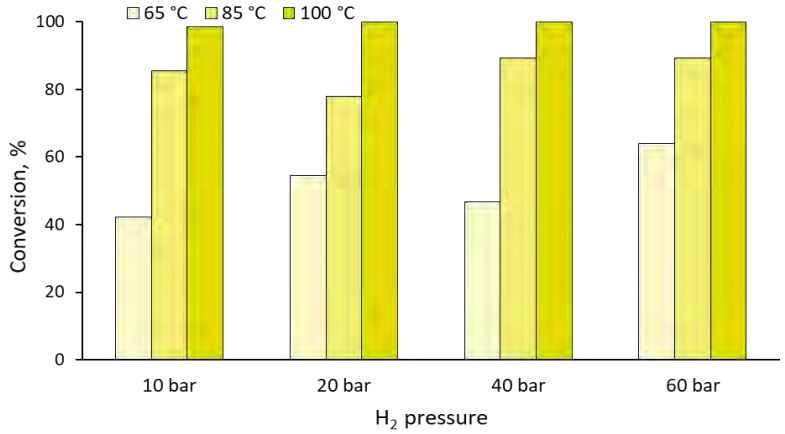

Figure 43. Temperature and pressure profile of citral hydrogenation over mod60NiTSNH$_2$.

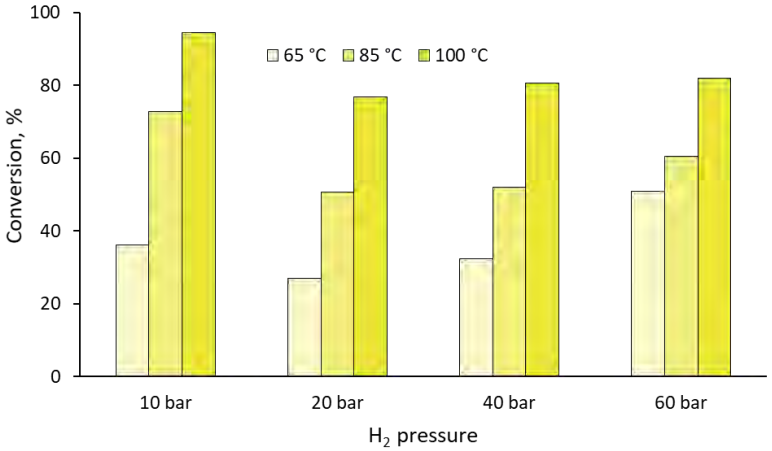

Figure 44. Temperature and pressure profile of citral hydrogenation over mod105NiTSNH$_2$.

All modified catalysts displayed similar trend of activity in citral flow hydrogenation under various reaction conditions. However, noticeable differences in catalytic

performance of each material signify structure sensitivity of the process. Catalysts with Ni nanoparticles smaller than 10 nm (mod15NiTSNH$_2$ and mod60NiTSNH$_2$) displayed 100% of citral conversion at 100°C irrespective of applied pressure. At lower temperature (<100°C), mod60NiTSNH$_2$ (9 nm) was the most active. Increase of Ni nanoparticles size to 12 nm resulted in decreased catalytic performance of mod105NiTSNH$_2$. In this case, complete conversion of citral was not achieved in any reaction conditions.

Production of desired C=C hydrogenation product (citronellal) in screening through temperature and pressure are shown in Figures 45-47.

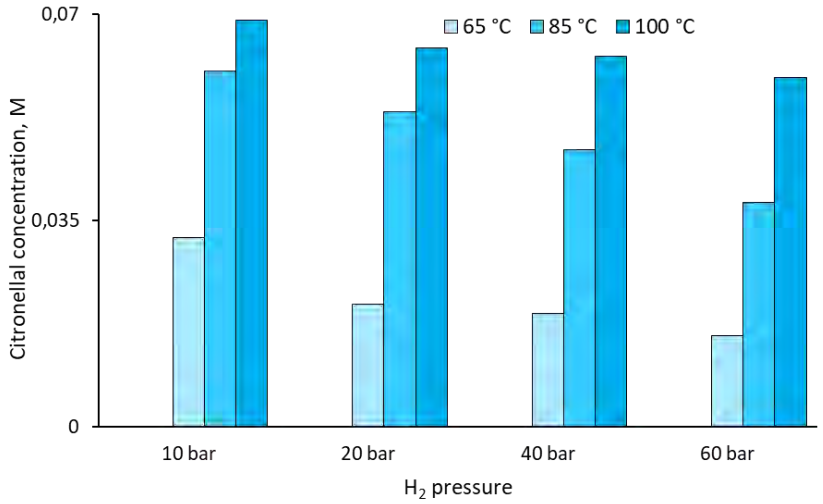

Figure 45. Citronellal production in various reaction conditions over mod15NiTSNH$_2$.

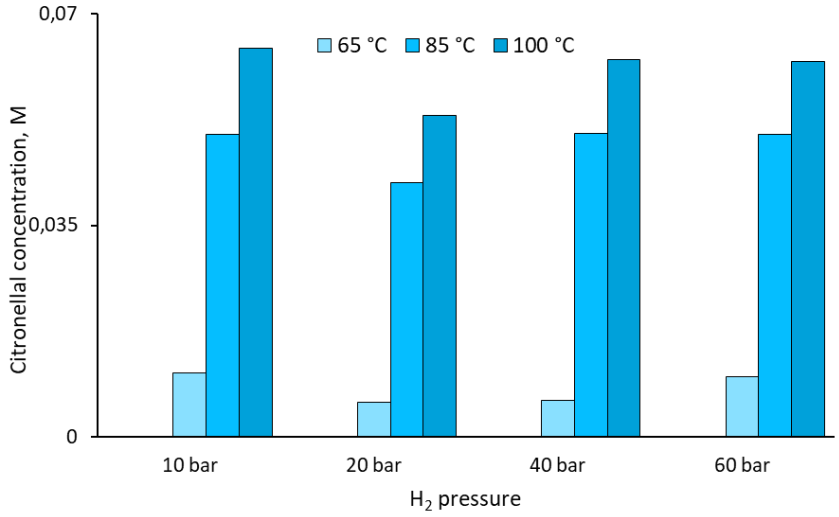

Figure 46. Citronellal production in various reaction conditions over mod60NiTSNH$_2$.

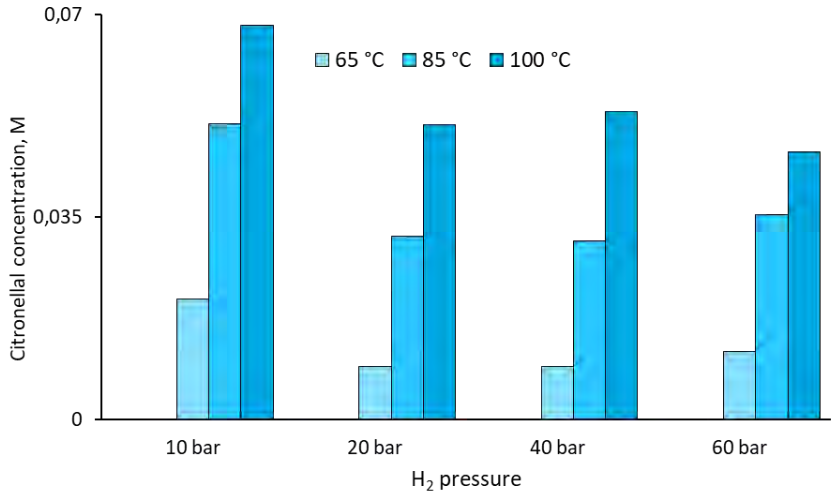

Figure 47. Citronellal production in various reaction conditions over mod105NiTSNH$_2$.

Note that results of citronellal generation in screening tests indicated similar profile as conversion outcomes. Thus, it can be stated that C=C hydrogenation was a dominant reaction irrespective of reaction conditions. Therefore, like previously, catalysts containing Ni nanoparticles smaller than 10 nm indicated the highest effectiveness in selective citral to citronellal conversion.

Selectivity of Ni catalysts after nanoparticles accretion showed significant improvement in terms of catalyst affinity to C=C reduction (Figures 49-51). Product specificity in citral flow hydrogenation over parent catalyst with small nanoparticles (3-4 nm) varied dramatically under different reaction conditions (Fig. 48). After nanoparticles size modification, the reaction was directed towards αC=C hydrogenation with great selectivity in the whole tested temperature and pressure range.

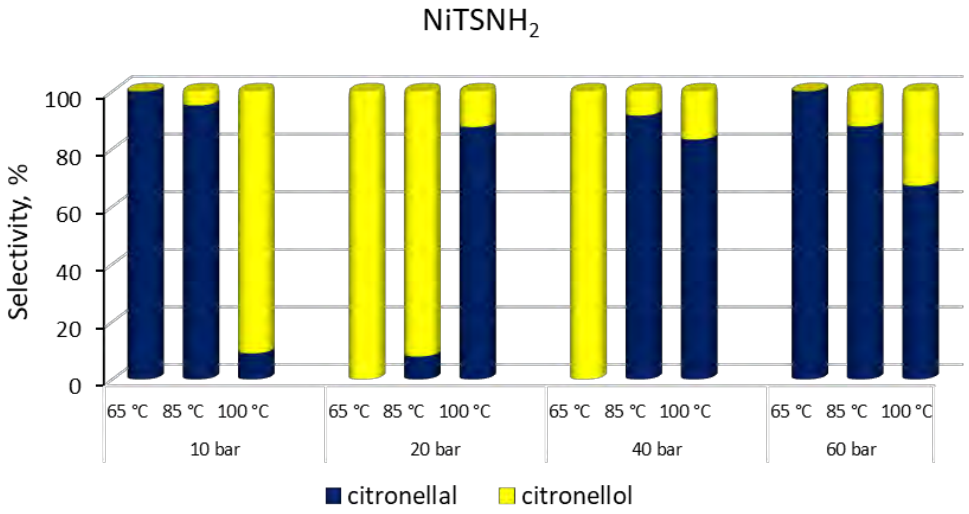

Figure 48. Dependence of reaction conditions on $NiTSNH_2$ selectivity in citral flow hydrogenation.

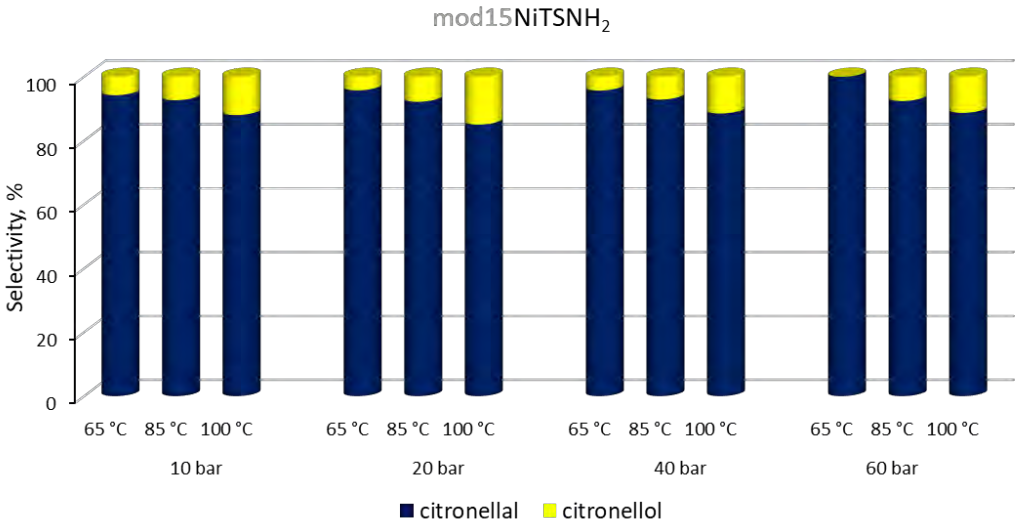

Figure 49. Dependence of reaction conditions on $mod15NiTSNH_2$ selectivity in citral flow hydrogenation.

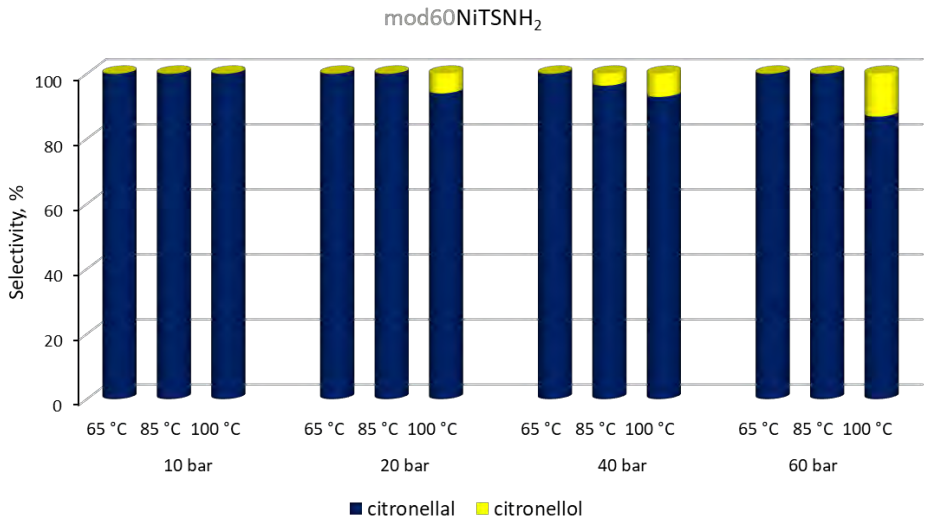

Figure 50. Dependence of reaction conditions on mod60NiTSNH$_2$ selectivity in citral flow hydrogenation.

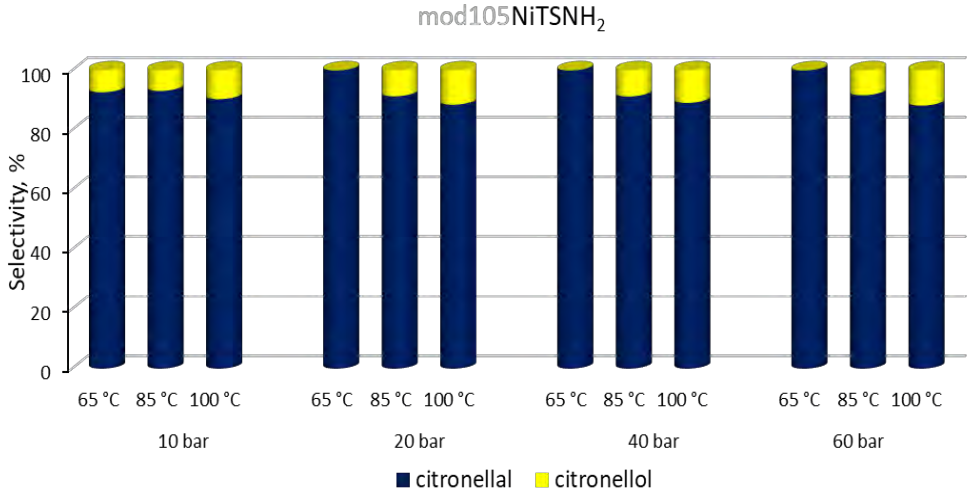

Figure 51. Dependence of reaction conditions on mod105NiTSNH$_2$ selectivity in citral flow hydrogenation.

Above-mentioned data imply that size of Ni nanoparticles is an important factor which impacts citronellal formation in flow hydrogenation of citral. It was found that reaction conditions, especially temperature, increase catalyst activity (exothermic nature of the process). Moreover, since reaction was proved to be structure sensitive, catalyst morphology modification enables process optimization leading to improved citronellal production in presented catalytic system. Fig. 52 shows yield evolution of citral to citronellal transformation over NiTSNH$_2$ catalyst with nanoparticles in different size. As shown, regardless reaction temperature, catalytic performance of tested materials

was rising with increase of Ni nanoparticles size up to 9 nm. The best result (46.5 μmol of citronellal per minute) was obtained for mod60NiTSNH$_2$ catalyst with nanoparticles in size of 9 nm. Further Ni nanoparticles accretion led to decrease in yield of citronellal production. Volcano-type plot (Fig. 52) clearly indicates the most optimal morphology of resin supported catalyst for selective αC=C hydrogenation in citral. Nanoparticles formed in 60 min of *on-the-fly* accretion seem to balance resistance to deactivation (peculiar to bigger and more energetically stable nanoparticles) and high dispersion on catalyst surface (characteristic of small particles). On that basis, it can be assumed that nanoparticles smaller than 9 nm underwent deactivation during the reaction, eventually, decreasing the number of metal active sites. On the other hand, catalyst with nanoparticles bigger than 9 nm indicated lower dispersion of Ni sites leading to the same consequence.

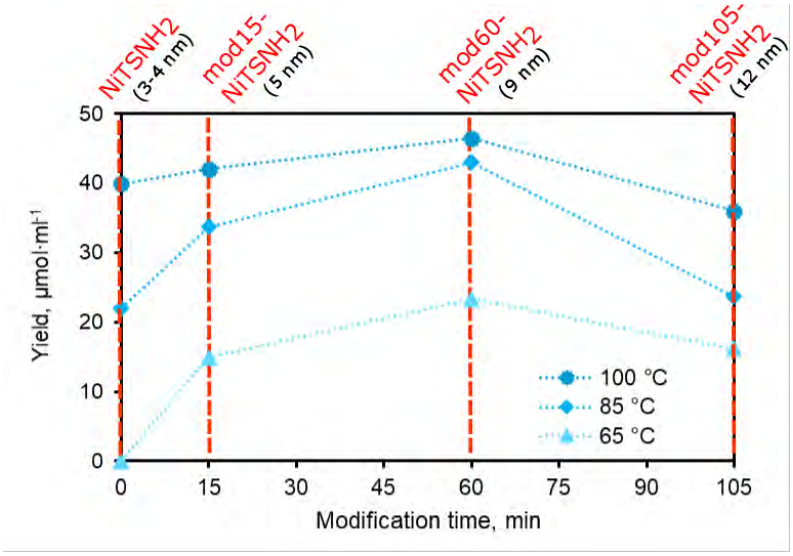

Figure 52. Yield of flow selective transformation of citral into citronellal as a function of catalyst modification time (Ni nanoparticles accretion) at different temperature values and under 40 bar.

5.2.3. LONG-TERM STABILITY TESTS

In the next stage of the studies, series of modified catalysts was subjected to stability tests. As presented in Fig. 53, all modified materials displayed similar profile of catalyst lifetime. Nevertheless, two accreted catalysts (mod15NiTSNH$_2$ and mod105NiTSNH$_2$) indicated lower stability during long-term reaction, yielding 13.3

and 19.6 μmol·min^{-1} of activity after 5 h, respectively. Only mod60NiTSNH$_2$ catalyst did not show any significant stability decrease in comparison to parent catalyst. For this material, activity value after 5 h on stream reached 23.3 μmol·min^{-1} (20.7 μmol·min^{-1} for parent catalyst). Thus, stability tests also confirmed that catalyst with 9 nm Ni nanoparticles exhibited the best performance in citral flow hydrogenation.

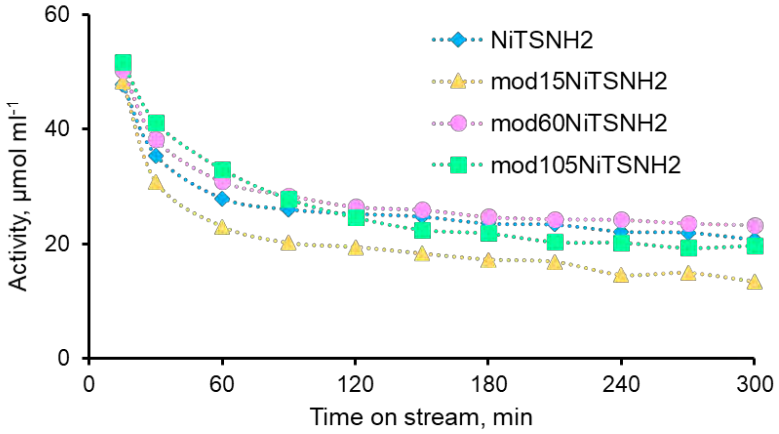

Figure 53. Long-term stability tests in citral flow hydrogenation for NiTSNH$_2$ catalyst after nanoparticles accretion.

Regarding selectivity, all modified materials showed improved affinity to αC=C hydrogenation when compared to parent NiTSNH$_2$ catalyst (Fig. 54). Citronellal was the only product after 30 min of reaction catalyzed by mod15NiTSNH$_2$ and mod60NiTSNH$_2$, hence, by catalysts with nanoparticles smaller than 10 nm.

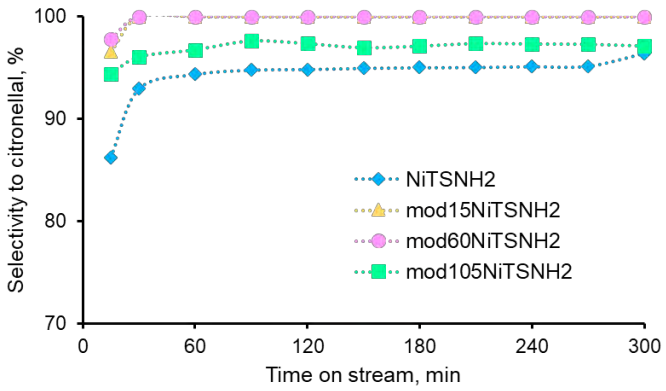

Figure 54. Selectivity to αC=C hydrogenation product in citral flow hydrogenation over modified catalysts as a function of reaction time.

To deliver accurate and comprehensive comparison of parent and modified catalyst, stability tests were conducted in the same conditions (60 bar and 85°C) for every material. However, results of optimization studies for mod60NiTSNH$_2$ catalyst showed comparably high yield in citral to citronellal flow transformation under lower pressure. Therefore, selected catalyst was subjected to long-term citral flow hydrogenation under 10 bar and at 100°C. Results are shown in Fig. 55.

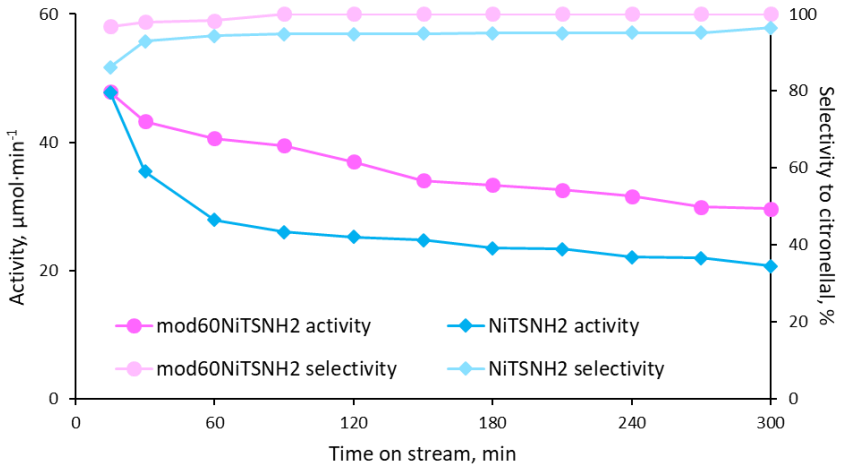

Figure 55. Long-term stability test of mod60NiTSNH$_2$ catalyst at milder conditions (10 bar, 100°C).

The reaction over mod60NiTSNH$_2$, performed under lower pressure, displayed enhanced stability for 5 h. Improvement of catalyst stability resulted in better catalytic performance of the modified catalyst leading to activity increase to 29.6 µmol·min^{-1} after 5 h on stream. This outcome was better than activity values achieved for either the same material and parent catalyst under 60 bar.

5.3. SELECTIVE HYDROGENATION WITH Pd-CATALYST

5.3.1. $PdTSNH_2$ CATALYST SPECIFICATION

Palladium is widely used in hydrogenation due to its low hydrogen activation energy and spillover properties. Nevertheless, high activities of the palladium catalysts often hinder high product specificity, especially when many competitive processes may occur in given catalytic system.

The catalysts were prepared using the same synthesis procedure (metal nanoparticles grafting on resin) adopted for the preparation of Ni nano-catalysts. Atomic absorption spectrometry measurements revealed that Pd loading was 2.2 wt.%. Since the loading is significantly higher than with the Ni catalyst (0.7% of Ni in $NiTSNH_2$), it implies that Pd nanoparticles form a much stronger covalent bond with the amino groups of the resin.

Similarly, nano-Pd catalyst was thoroughly investigated to study structural and electronic properties of the metal active phase. Firstly, $PdTSNH_2$ was subjected to XRD measurements and results are presented in Fig. 56.

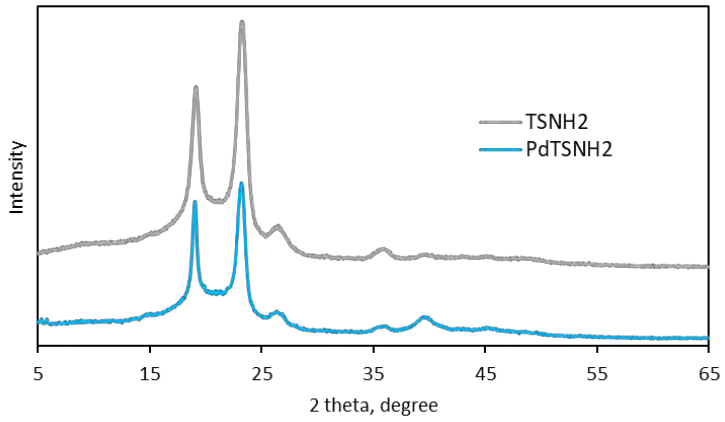

Figure 56. Powder X-ray diffraction profiles of pure resin and $PdTSNH_2$ catalyst.

XRD profiles of both samples show the representative peaks associated to resin, which were not affected by the addition of Pd nanoparticles. In the Pd containing samples, there was an extra diffraction peak at $2\theta = 40.1°$ associated to Pd(111) crystalline face.[169] The peak was used to estimate crystallite size using the line broadening method. Pd crystallite size was estimated to be ca. 4 nm.

Infrared spectra of the free resin and resin-supported catalyst indicated successful Pd

nanoparticles immobilization. The grafting of metal particles onto polymeric resin affected intensities of the vibrational bands corresponded to amino group (Fig. 57). Both N-H vibrations, bending (1647 cm^{-1}) and stretching (3470 cm^{-1})[170], were suppressed when nanoparticles were introduced to the system indicating covalent interactions between Pd and amino groups.

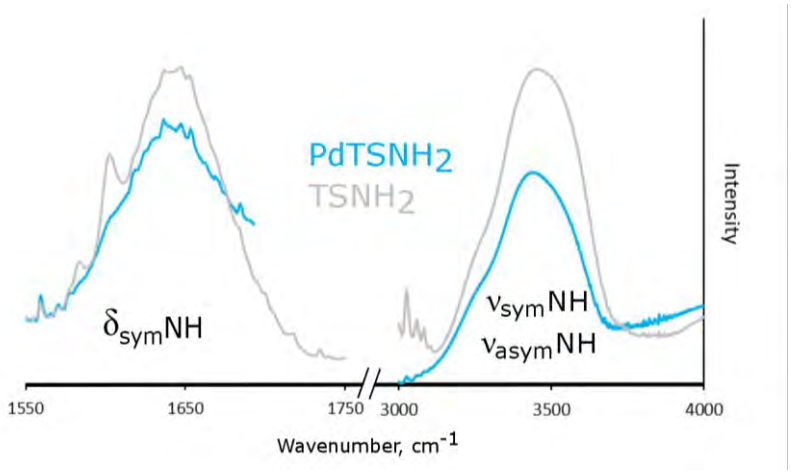

Figure 57. FT-IR bands of N-H vibrations in primary amine for $TSNH_2$ resin and catalyst after Pd nanoparticles grafting

XPS was carried out to investigate Pd oxidation state. The data fitting was successfully done with a single component vitiated by a small asymmetry constraining peak position (doublet separation 5.3 eV), area and full width half maximum. XPS spectrum of the Pd 3d region for $PdTSNH_2$ material is presented in Fig. 58. The peak at 334.8 eV corresponds to Pd $3d_{5/2}$ and represents metallic form of palladium. Additionally, small asymmetry and slight shift of the peak from reported bulk position[171] implies that reduced Pd species exist in nanoparticulated form.[172]

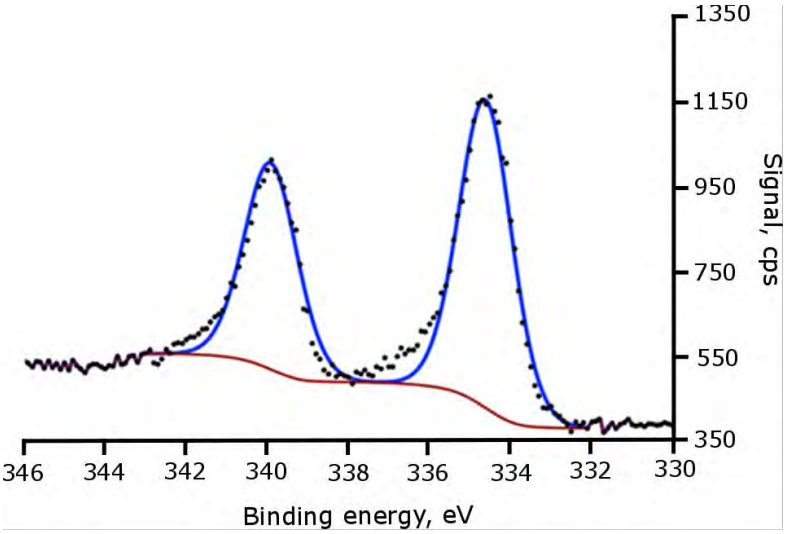

Figure 58. XPS spectrum of Pd 3d region in $PdTSNH_2$ catalyst.

5.3.2. PRENAL HYDROGENATION

To provide comprehensive comparison of both Ni and Pd nanomaterials, catalytic performance of $PdTSNH_2$ was tested with the series of α,β - unsaturated aldehydes used for parent Ni catalyst studies. Therefore, the first reaction conducted over $PdTSNH_2$ was flow hydrogenation of prenal. The influence of reaction conditions on catalytic performance of Pd catalyst in prenal hydrogenation is shown in Fig. 59 and Fig. 60.

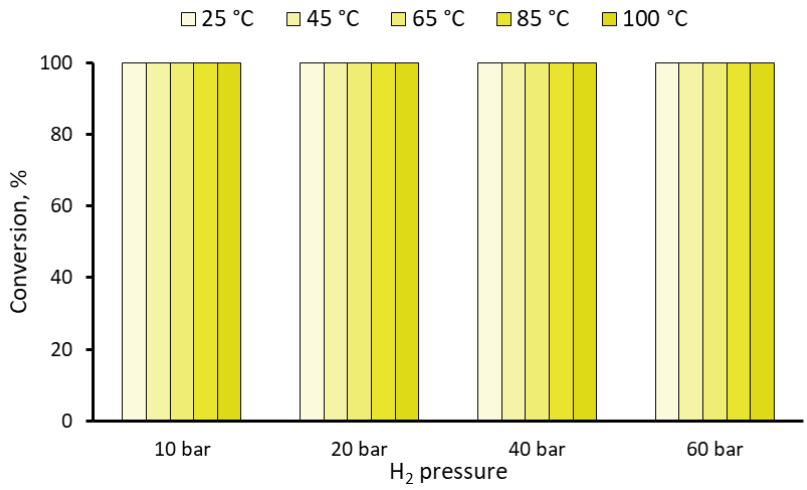

Figure 59. Temperature and pressure profile of prenal hydrogenation over $PdTSNH_2$.

As presented, palladium based catalyst displayed excellent activity in the reaction leading to complete prenal transformation irrespective of reaction temperature or pressure. Since activity test showed total conversion in all reaction conditions, process

optimization was done in accordance with C=C hydrogenation product generation (Fig. 61).

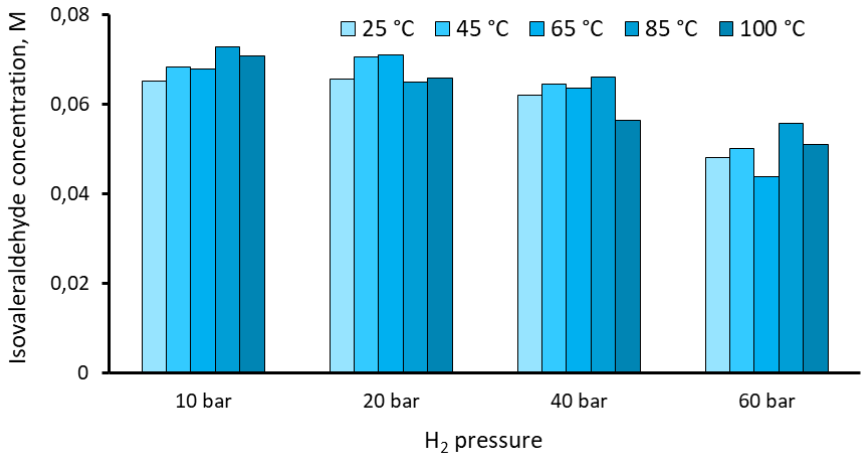

Figure 60. Isovaleraldehyde production in various reaction conditions over $PdTSNH_2$.

In this case, nano-Pd catalyst indicated similar behavior to $NiTSNH_2$. Application of both catalysts directed the reaction towards C=C hydrogenation yielding isovaleraldehyde as a main product. However, the reaction catalyzed by nano-Pd indicated better effectiveness in isovaleraldehyde production under lower pressure. It was found that the highest amount of C=C hydrogenation product was generated at 85°C and 10 bar, hence, those parameters were selected for stability tests (Fig. 62).

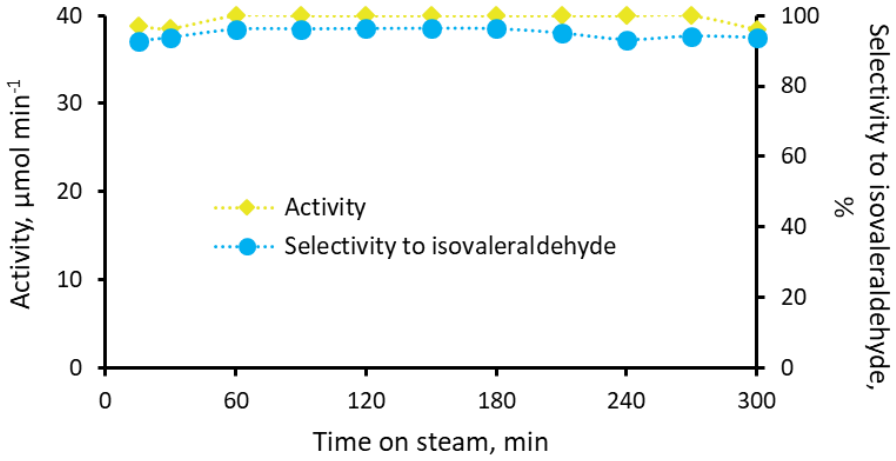

Figure 61. Long-term stability test of $PdTSNH_2$ in prenal hydrogenation at 85°C and 10 bar.

As presented, continuous flow prenal to isovaleradehyde transformation over $PdTSNH_2$ occurred with excellent efficiency and high stability during 5 h test. The complete prenal conversion (39.9 µmol·min^{-1}) slightly dropped for sample collected after 5 h on stream and reached 96% (38.4 µmol·min^{-1}). The great stability was also

preserved in terms of catalyst selectivity towards C=C hydrogenation. Presented catalytic system indicated high and undisturbed product specificity for 5 h, yielding ~94% of isovaleraldehyde during stability test.

5.3.3. CINNAMALDEHYDE HYDROGENATION

High activity of palladium nano-catalyst in flow hydrogenation process was confirmed with second α,β-unsaturated aldehyde under investigation – cinnamaldehyde. In this case, the reaction catalyzed by $PdTSNH_2$ also led to complete aldehyde conversion in the whole array of tested reaction conditions (Fig. 62).

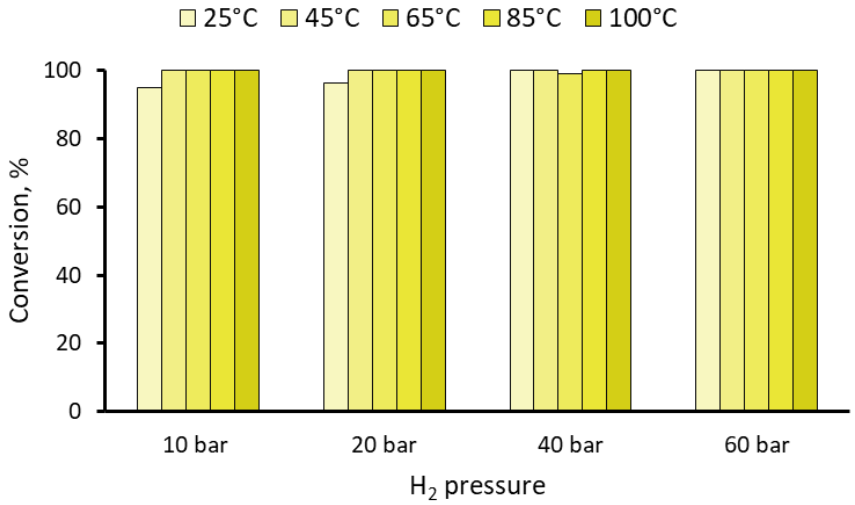

Figure 62. Temperature and pressure profile of cinnamaldehyde hydrogenation over $PdTSNH_2$.

Nevertheless, the high ability of palladium nanoparticles to catalyze flow hydrogenation led to low product specificity in this reaction. Application of Pd catalyst in α,β-unsaturated aldehydes hydrogenation activated both unsaturated bonds forming hydrocinnamyl alcohol as a main product. Semi-saturated compound of chemoselective C=C hydrogenation was generated with remarkably lower yield in comparison to adequate reaction conducted over Ni-based catalyst. Hydrocinnamaldehyde production (desired product) as a function of reaction conditions is shown in Fig. 63.

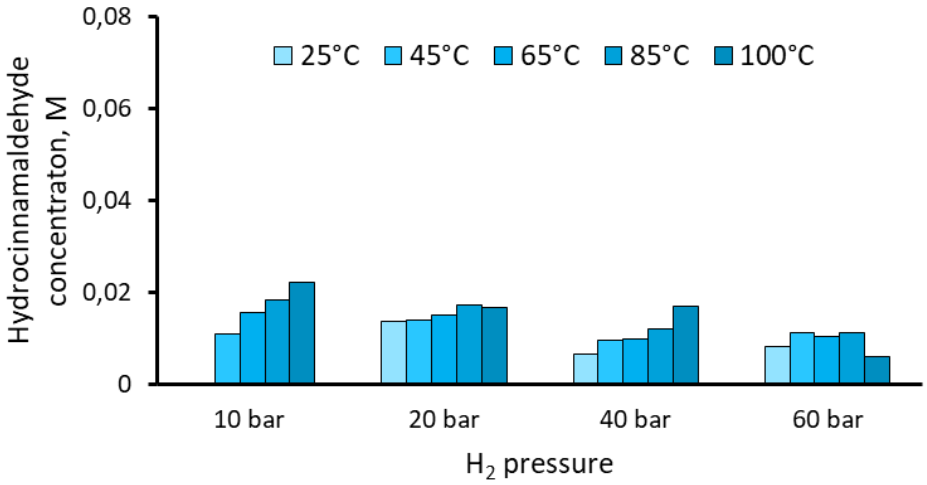

Figure 63. Hydroinnamaldehyde production in various reaction conditions over $PdTSNH_2$.

According to those outcomes, the highest amount (0.022 M) of desired product was obtained at 100°C and under 10 bar of pressure. It is worth noticing that application of Pd as a catalyst in flow hydrogenation reactions shifts the peak of catalyst effectiveness in C=C reduction towards lower pressure.

As the most optimal reaction parameters were revealed, the $PdTSNH_2$ catalyst was subjected to stability test in continuous flow cinnamaldehyde production (Fig. 64).

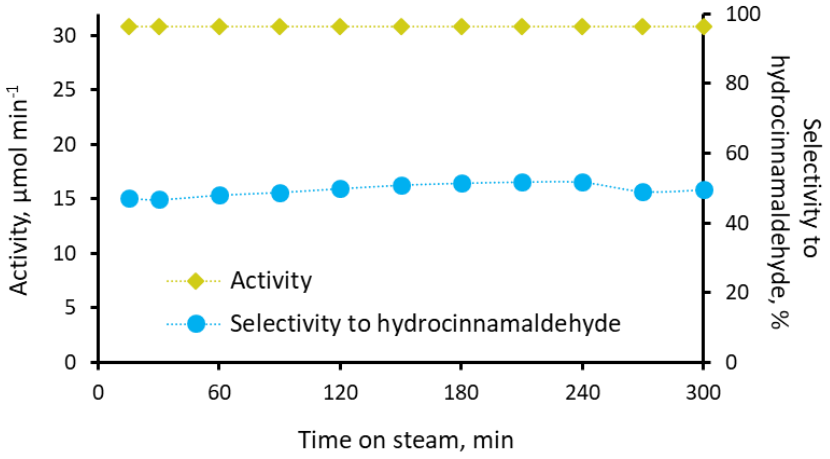

Figure 64. Long-term stability test of $PdTSNH_2$ in cinnamaldehyde hydrogenation at 100°C and 10 bar.

As shown, the catalyst did not display any symptoms of deactivation, transforming all cinnamaldehyde flown through the catalyst bed for 5 h. The selectivity to C=C hydrogenation was also maintained on a stable level of ~50% during the whole experiment. Therefore, since the initial cinnamaldehyde delivery to the catalyst bed

was 30.8 μmol·min^{-1}, presented catalytic system was able to produce ~15 μmol of hydrocinnamaldehyde per minute.

5.3.4. CITRAL HYDROGENATION

Finally, $PdTSNH_2$ catalyst was applied to citral flow hydrogenation. Citral, as an α,β-unsaturated aldehyde with an additional alkenyl bond in isolated position, serves more variants of hydrogenation pathways than both previous compounds. Therefore, high product specificity as a result of bond control in citral hydrogenation is more challenging to achieve.

As could be expected, utilization of palladium based nanomaterial led to complete conversion of citral delivered to the catalyst bed irrespective of temperature and pressure of the reaction (Fig. 65).

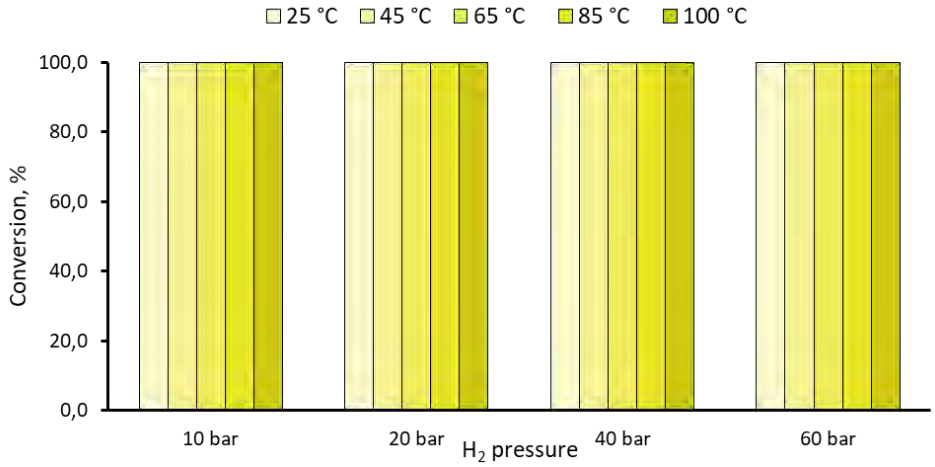

Figure 65. Temperature and pressure profile of citral hydrogenation over $PdTSNH_2$.

While the high activity of the Pd catalyst could be expected, the temperature profile of desired product formation displayed unforeseen trend. As presented in Fig. 66, the amount of αC=C hydrogenation product generated during the reaction lowered with temperature increase. Thus, unlike previous examples, selective flow transformation of citral into citronellal over $PdTSNH_2$ was the most effective at room temperature and under pressure of 20 bar.

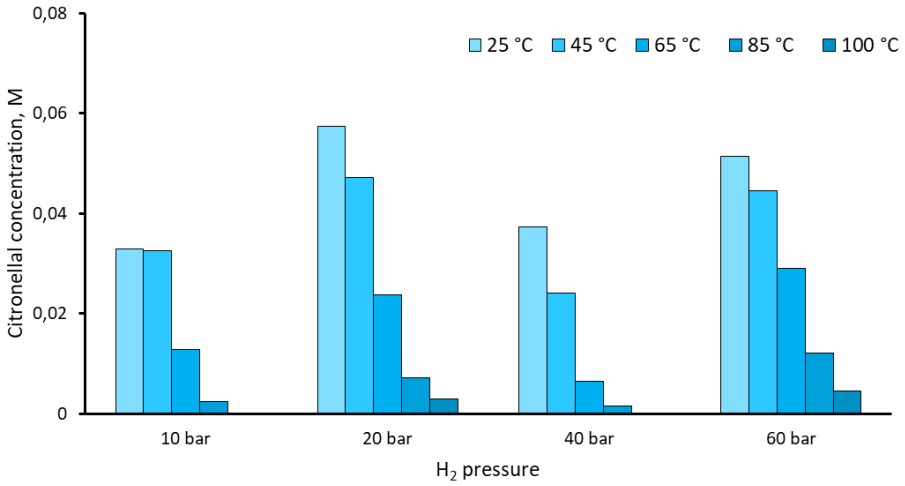

Figure 66. Citronellal production in various reaction conditions over $PdTSNH_2$.

The temperature dependence of catalytic performance in presented system clearly showed that another competitive reactions occurred in presence of the palladium catalyst. The combination of very active noble metal and higher temperature increased affinity of the catalyst to promote more energy-demanding hydrogenation of isolated C=C and C=O bonds. The selectivity results of flow citral hydrogenation over Pd based nanocatalyst are shown in Fig. 67.

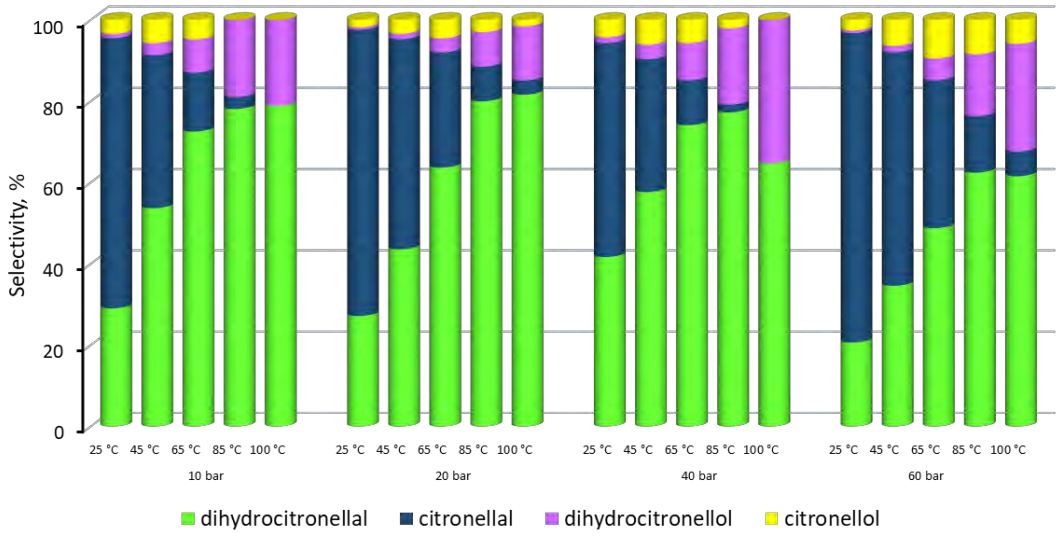

Figure 67. Dependence of reaction conditions on $PdTSNH_2$ selectivity in citral flow hydrogenation.

Those results evidence that at higher temperature Pd nanoparticles directed the reaction towards hydrogenation of isolated C=C bond (dihydrocitronellal - DHC) and further to C=O bond reduction (dihydrocitronellol). In other words, the presented

catalytic system loses its chemoselectivity when the reaction temperature is raised. It should be highlighted that in every parameters of temperature and pressure, the reaction over Pd catalyst yielded four different products. This abundant and diverse product composition remarkably decreases product specificity of the system.

At temperature higher than 25°C, dihydrocitronellal was a dominant product of both conjugated and isolated carbonyl bonds saturation. In the light of industrial meaning, catalytic flow DHC production is also an interesting chemical transformation. In this case, DHC amount produced during flow hydrogenation of citral over $PdTSNH_2$ elevated with temperature increase (Fig. 68). Moreover, DHC formation was the most effective under relatively low pressure (10 bar). Thus, the highest amount of DHC (0.07 M; ~80% of selectivity) was obtained at 100°C and 10 bar.

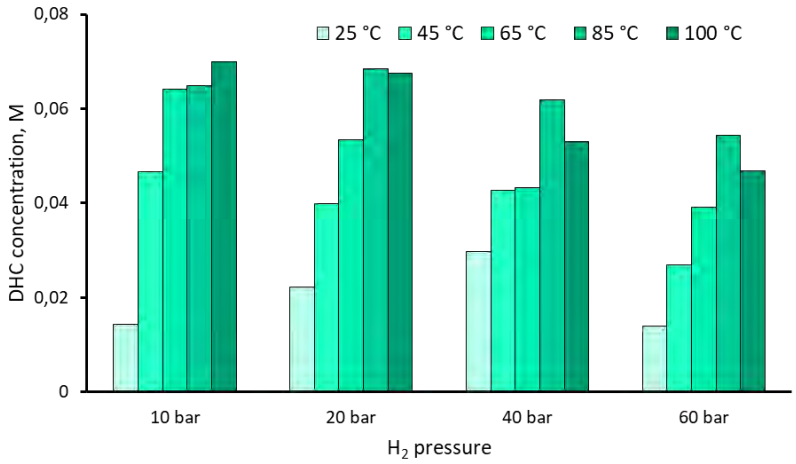

Figure 68. Dihydrocitronellal production in various reaction conditions over $PdTSNH_2$.

Nonetheless, stability test was carried out under conditions optimal for selective αC=C hydrogenation and results are presented in Fig. 69 and Fig. 70. The catalyst maintained great activity with no signs of deactivation in constant flow reaction for 5 h. Similarly, presented catalytic system exhibited high stability in terms of product distribution, continuously yielding citronellal with 66% of selectivity during the whole experiment.

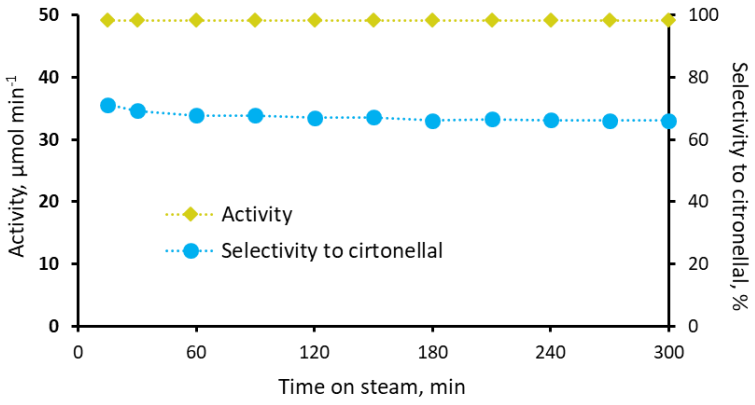

Figure 69. Long-term stability test of $PdTSNH_2$ in citral hydrogenation at 25°C and 20 bar.

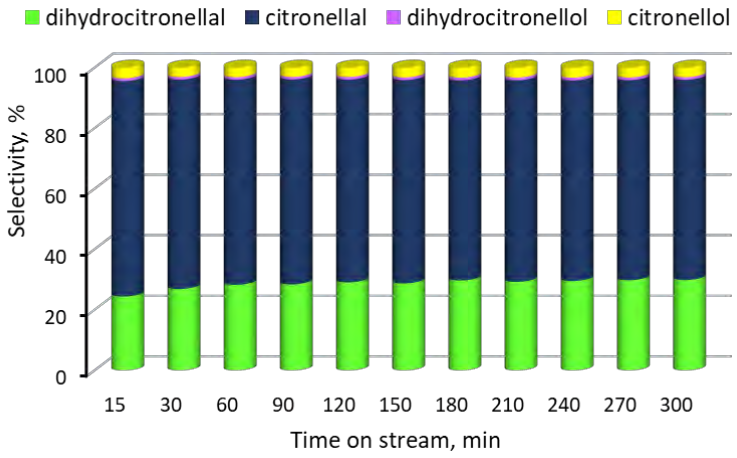

Figure 70. Products composition in long-term citral flow hydrogenation over $PdTSNH_2$.

5.3.5. CITRAL HYDROGENATION OVER COMMERCIAL 10%Pd/C

In addition, citral flow hydrogenation was performed with commercially available catalyst 10% Pd/C MicroCatCart (ThalesNano)[173]. Carbon supported palladium can be treated as an accurate representative of common and conventional catalysts used currently in hydrogenation transformations. Therefore, comparison of those two catalytic materials (2.2% $PdTSNH_2$ vs. 10% Pd/C) can bring essential characterization data on the resin-supported catalyst especially in the light of industrial usability. Note that since the distributor did not provide any specification of 10% Pd/C catalyst morphology, the comparison pertains only catalytic performance of the materials.

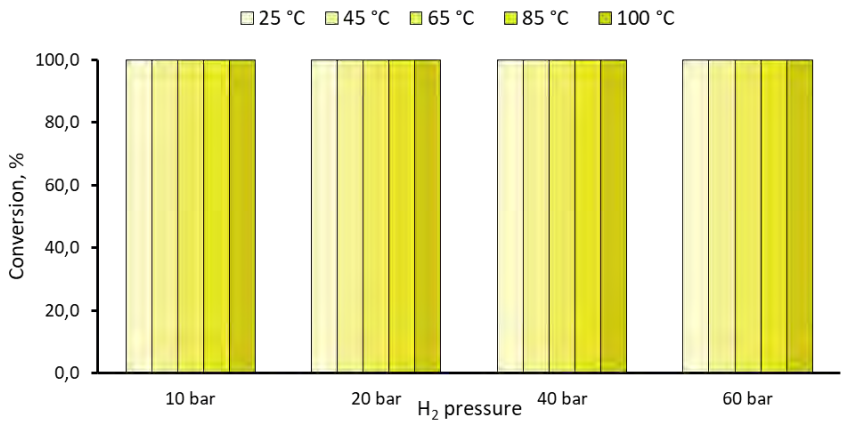

Figure 71. Temperature and pressure profile of citral hydrogenation over 10%Pd/C.

As can be seen in Fig. 71, irrespective of reaction conditions, all citral flown through catalyst bed packed with Pd/C underwent hydrogenation. In this matter, there were no differences between catalysts since both materials indicated great activity in the process. However, product compositions and selectivity profiles of both Pd based materials displayed significant dissimilarities.

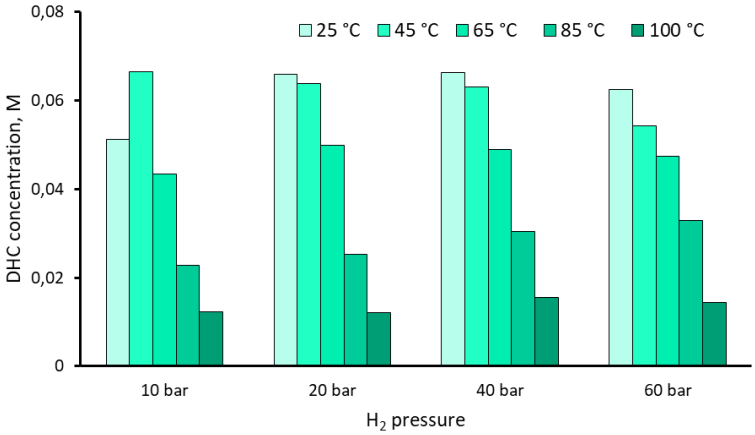

Figure 72. Dihydrocitronellal production in various reaction conditions over 10%Pd/C.

Fig. 72 shows amount of DHC formed during flow citral hydrogenation over commercial material at various reaction conditions. In this case hydrogenation of both olefin bonds was a main and dominant process at temperature below 65°C. Further temperature increase lowered DHC generation exhibiting directly opposite temperature profile when compared to $PdTSNH_2$. Additionally, as shown in Fig. 73, at higher temperature hydrogenation process was not a main transformation in this catalytic system. Above temperature of 85°C investigated aldehyde formed acetals with ethanol molecules which was used as a solvent. Citronellal as a product of selective hydrogenation of αC=C bond was found in traces. Considering those

outcomes, it can be stated that commercial 10%Pd/C displayed lower chemoselectivity than 2.2% $PdTSNH_2$. Moreover, in the case of carbon supported catalyst the reaction was directed towards unwanted side processes of acetals formation.

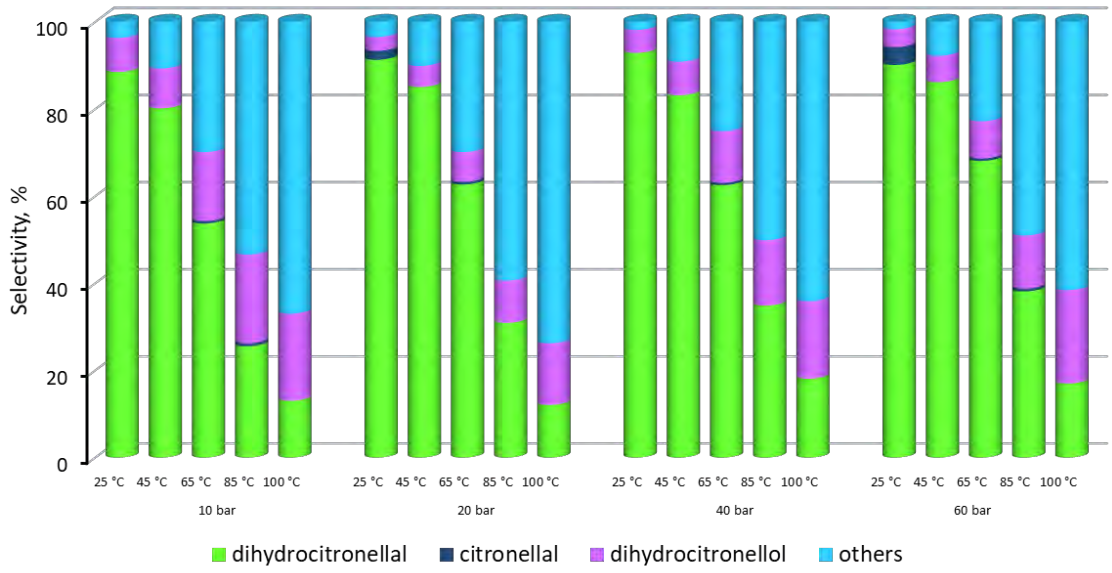

Figure 73. Dependence of reaction conditions on Pd/C selectivity in citral flow hydrogenation.

5.4. DISSCUSION

Due to numerous advantages, flow catalysis and continuous processing are considered as the future of chemical manufacturing. Dynamic growth of this technology is being referred as a flow revolution towards safer and more effective chemical protocols.[174,175] Process intensification driven by flow operating is undoubtedly a milestone for more compact yet highly efficient strategies in chemical production.

Presented studies collate coherent and innovative catalytic systems for enhanced and optimized production of selected pharmaceuticals and fragrances. To summarize the research, the most essential outcomes and their impact on flow catalysis development are highlighted in the subsequent paragraphs of this section.

5.4.1. METAL-RESIN CATALYST SYNTHESIS

The heart of every catalytic system is a catalyst. In presented studies the catalyst and its preparation procedure were specifically designed for its final destination. Thus, the combination of pre-prepared metal nanoparticles and functionalized resin succesfully achieved in two-step, 'green' synthesis suits demending liquid phase flow conditions.

Scheme 6. Functionalized resin supported metal nanoparticles.

The procedure of Ni nanoparticles preparation was inspired by Hou et al.[176] report. However, originally Ni nanoparticles were prepared at relatively high temperature (180°C) with *o*-dichlorobenzene as a solvent, hence, the method was not in line with green chemistry principals. In presented approach, it was shown that Ni nanoparticles can be successfully synthesized in ethanol at room temperature. Moreover, in this system the growth of Ni nanoparticles can be controlled with only one capping agent (trioctylphosphine oxide), whereas, the original protocol involved hexadecylamine as

an additional stabilizer. Therefore, by lowering the temperature of the process, reducing the reagent and equipment (dry ice/methanol cooler) and replacing Cl-containing solvent with ethanol, a new and green method for Ni NPs formation was demonstrated and successfully applied in catalyst synthesis.

Since catalyst preparation protocol follows two separate steps: nanoparticles formation and their subsequent grafting on resin, this methodology can be implemented to synthesis of various resin supported nanomaterials. The first step enables attaining desired morphology of any nanoparticles destined to be immobilized on the support. Thus, presented methodologhy was used to graft Pd and Cu_2O nanoparticles[177] on functionalized polymeric resin. Nevertheless, the metal content in synthesized materials was hardly controlled and depend on type of the metal. In the case of Pd, all nanoparticles were anchored on the support, whereas, Ni nanopartcles were immobilized partially leading to > 1% of metal contribution. However, it was shown that Ni loading can be precisely increased with *on-the-fly* modyfication performed in the continous flow microreactor.

Metal decorated polymer appears to be ideal for quick surface reactions since it indicates well exposed and easly accessible metal phase. In comprison to catalysts supported by traditional materials such as silica or activated carbon, the resin supported catalyst has moderatly developed surface propeties. This feature can be beneficial in flow applications since it may lower the residential time assuring consistency of flow processing. Additionally, it was found that porosity of metal-resin system can be tuned by polarity of a solvent in accordance to swelling properties of a given resin-solvent configuration. Therefore, it is possible to introduce subtle changes in the flow-through network by proper solvent selection, which in consequence may influence a residential time of the system.

5.4.2. CATALYTIC FLOW HYDROGENATION OVER $NiTSNH_2$

Nickel based catalyst, $NiTSNH_2$, was found very effective, active and highly selective in competitive flow hydrogenation of C=C vs. C=O bond in α,β – unsaturated aldehydes. Reactions conducted for 5 h yielded corresponded αC=C saturation product with selectivities on the level of 95% with all tested compounds.

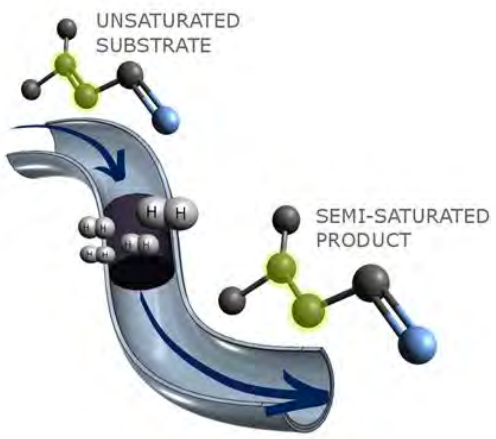

Scheme 7. Continuous-flow hydrogenation for production of value-added chemicals.

Moreover, application of continuous flow enables circulation of flowing substrate, making catalyst activity a secondary aspect of the process. Note, that $NiTSNH_2$ catalyst contained very low metal loading – 0.7%, hence, such small Ni contribution additionally increases overall effectiveness of the material. Taking all those factors into consideration, presented catalyst is a ready-to-use product, which can be employed in selective flow hydrogenation processes relevant for industry especially pharma and cosmetics.

Despite the fact that the selectivity of $NiTSNH_2$ is not a suprising outcome in the light of the current state-of-the-art findings on Ni selectivity, the presented flow system offers remarkable improvements to modern studies on catalytic processes. Primarily, flow catalysis introduces significant benefits in terms of time savings. In flow micro-reactor, the optimization studies can be conducted over single catalyst bed. Thus, investigating the influence of rection temperature, pressure, flow rate (residential time), solvent, pH etc. can be conducted in a sequence over single sample of the catalyst. In the case of stationary conditions each optimization study requires arrangement of a new batch. Therefore, besides time, application of flow catalysis decreases use of expenditures such as chemicals and energy. Consequently, flow operating allows obtaining immediate response after each change of reaction parameters. As it was shown, optimization protocol employed in the studies facilitates preparation of temperature and pressure profiles for studied reaction with short times and low usege of reagents (Fig. 74). In result, flow optimization can be treated as a intesified characterization protocol applied for catalyst activity investigation in a given catalytic system.

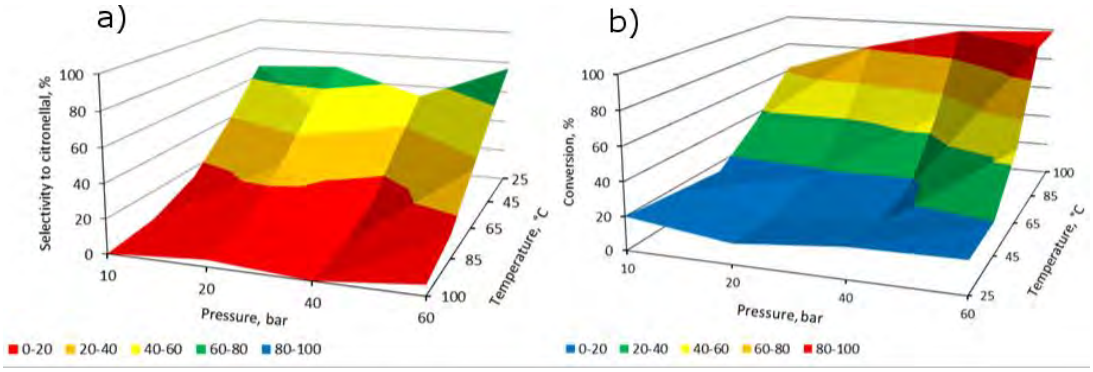

Figure 74. Temperature and pressure profiles of citral flow hydrogenation: a) selectivity to citronellal over $PdTSNH_2$ and b) citral conversion over $NiTSNH_2$

In flow micro-reactor setup, catalyst is packed in a replaceable cartridge installed as a coherent part of the reactor. This configuration makes catalyst a part of the device rather than a solid phase dispersed in reaction mixture. In this light, flow catalysis brings additional profits when compared to stationary batch conditions. Packed-bed system does not require further procedures for catalyst separation since cartridge can be easily replaced and catalyst recovered. Therefore, it can be beneficial for material investigation after the reaction (deactivation studies). Moreover, the catalyst separation is necessary to perform its regeneration usually conducted outside catalytic reactor. In this case flow processing guaranties constant operating since cartridge with deactivated catalyst can be replaced with new one while used material undergoes regeneration.

Catalyst, as a separate phase of the catalytic system was found very convenient and advantageous during long-term stability tests. Since flow catalysis with micro-reactor ensures high surface area-to-volume ratio the mass transfer in such system is highly efficient. Therefore, all compound subjected to hydrogenation was flown directly through catalyst bed undergoing the actual surface reaction. In other words, high atom efficiency assures that product samples collected in given time intervals more accurately represent time evolution of reaction progress. The fact that reaction products continuously leave the catalytic system can be also profitable when reaction products can poison catalyst. In such case, constant flow may inhibit poisoning and elongate catalyst lifetime.

As shown previously, flow catalysis can be employed for leaching investigation. In contrary to batch conditions, post-reaction mixture does not contain catalyst; hence, any traces of metal present in product samples are leached from the catalyst. Therefore,

leaching can be easily monitored by product samples analysis in terms of metal content (e.g. with X-ray fluorescence). High surface area-to-volume ratio also leads to great heat transfer in flow micro-reactors. In this matter, strict temperature control in flow processing does not only improve safety but also can be used to govern the selectivity of the process. Herein, it was demonstrated that citral flow hydrogenation over $NiTSNH_2$ can be aimed towards citronellal or citronellol by changing the reaction conditions (Fig. 34). Therefore, parameter resetting in flow catalysis enables directing the ongoing reaction towards different product. In that case, various products can be collected to separate containers. In batch operations, selectivity change of ongoing reaction would only affect product composition decreasing product-specificity of the process.

5.4.3. ON-THE-FLY CATALYST MODYFICATION

Within the research, novel, convenient and elegant protocol for structure sensitivity studies in flow micro-reactor was developed. It was shown that *on-the-fly* accretion of Ni nanoparticles could be successfully carried out in sequence with catalytic reaction.

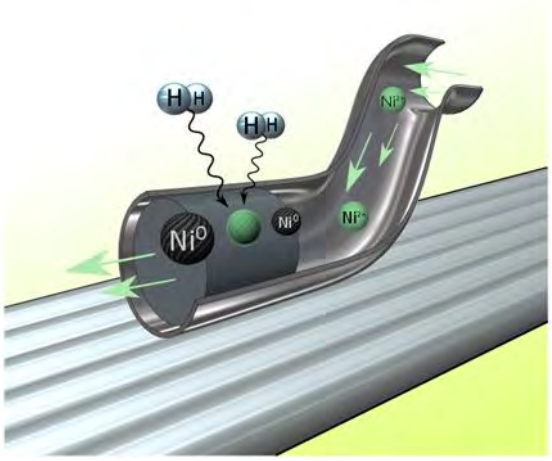

Scheme 8. On-the-fly catalyst accretion in continuous-flow micro-reactor.

This multistep strategy intensifies investigation of morphology-activity interaction in flow systems, enabling catalyst modification in catalytic reactor. Using this methodology, it was revealed that Ni nanoparticles in size of 9 nm were the best in citral flow hydrogenation. Catalyst optimization improved its catalytic behavior in terms of activity, selectivity (100% of αC=C saturation product) and lowered reaction

parameters optimal for the process. Presented approach relies on sequential introduction of modifier and reaction mixture; hence, both catalyst modification and catalytic reaction are done over the same catalyst bed. It is a great improvement in comparison to conventional methodologies for structure sensitivity studies, where catalyst samples with varied morphology are done in separate synthesis as isolated batches. Therefore, catalyst modification performed in flow reactor with H_2 source appears as a highly intensified protocol for *in-situ* catalyst modification, which leads to significant savings in reagent, energy and time consumption.

Additionally, improvement in resources management is empowered by the fact that reaction is carried out as a consecutive step to the catalyst accretion. Performing multiple operations on the same catalyst bed (modification → reaction → modification → …) offers a convenient procedure which drops expenditures intake.

Herein, *on-the-fly* alternate modification-reaction protocol was used to accrete Ni nanoparticles immobilized on resin support. For that, the pre-prepared catalyst was saturated with modifier containing Ni ions, which were subsequently reduced with hydrogen. Nevertheless, this technique offers much wider array of applications concerning catalyst properties alteration. This procedure can be successfully applied for *e.g.* introduction of second metal such as Sn.[17] Thus, it is possible to monitor the influence of second metal on selectivity and activity in given catalytic system. Moreover, since the reaction is performed as a consecutive step, it is possible to obtain immediate information on how presence and amount of second metal affects performance of the catalyst.

This flow modification method can be also employed in research on selective poisoning. By flowing the specific modifiers through catalyst bed it is possible to adsorb surface additives, which selectively block given surface defects. For instance, it was proved that thiol group can selectively decorate platinum surface and consequently tune its selectivity.[178] Thus, flow operating brings new perspectives for quick, compact and convenient investigation of catalyst surface modification.

5.4.4. MULTIFUNCTIONALITY OF FLOW CATALYSIS

Comparison of Ni-based catalyst with similar $PdTSNH_2$ showed that in citral flow hydrogenation Ni indicates superior product specificity to Pd in this metal-support configuration. As shown in Tab. 3, $NiTSNH_2$ (9 nm) yielded 100% of desired product (66% for $PdTSNH_2$). Despite lower activity, Ni catalyst seems to be a reasonable and attractive alternative for noble metals especially in flow operating when moderate activity can be increased by flow circulation.

Table 3. Summary of α,β – unsaturated aldehydes flow hydrogenation over resin supported Ni and Pd catalysts.

Catalyst	Metal Loading, %	Nanoaprticles size (TEM), nm	Unsaturated carbonyl	Activity*, μmol·min^{-1}	Conversion* %	C=C selectivity* %	T, °C	p, bar	f, ml·min^{-1}
$NiTSNH_2$	0.7	3-4	prenal	11.7	37	95	85	60	0.5
			cinnamaldehyde	22.5	87	92	100	40	0.5
			citral	20.7	42	96	85	60	0.5
mod15 $NiTSNH_2$	1.0	7 / 5*	citral	13.3	25	100	85	60	0.5
mod60 $NiTSNH_2$	3.0	9 / 9*	citral	29.6	55	100	100	10	0.5
mod105 $NiTSNH_2$	4.9	14 / 12*	citral	19.6	36	97	85	60	0.5
$PdTSNH_2$	2.2	4*	citral	49.2	100	66	25	20	0.5
			cinnamaldehyde	30.8	100	49	100	10	0.5
			prenal	38.4	100	94	85	10	0.5

** nanopartciles size estiamted with XRD; * values correspond to results after 5h on stream*

Application of $PdTSNH_2$ in citral flow hydrogenation promoted simultaneous saturation of both olefin bonds, yielding DHC (dihydrocitronellal). Additionally, resin supported catalyst showed better product specificity in comparison to commercial Pd/C commonly used in citral hydrogenation.[179] The difference in product distribution over those two Pd-based materials may result from different metal loadings. It can be stated that in the case of commercial catalyst, 10% of palladium guarantees dense dispersion of Pd active sites promoting hydrogenation of all unsaturated bonds and further formation of unwanted acetals. On the other hand, resin supported catalyst, which contained approximately 5 times lower metal contribution, shifted process selectivity towards αC=C saturation and further to hydrogenation of both alkenyl bonds.

5.5. SUMMARY

In this work I have demonstrated that with resin supported Ni and Pd nano-catalysts, citral flow hydrogenation can be directed towards three different semi-saturated products (Scheme 9). In other words, presented catalytic system indicates high bond control, which is of great importance to those branches of industry in which high product specificity is the most important factor.

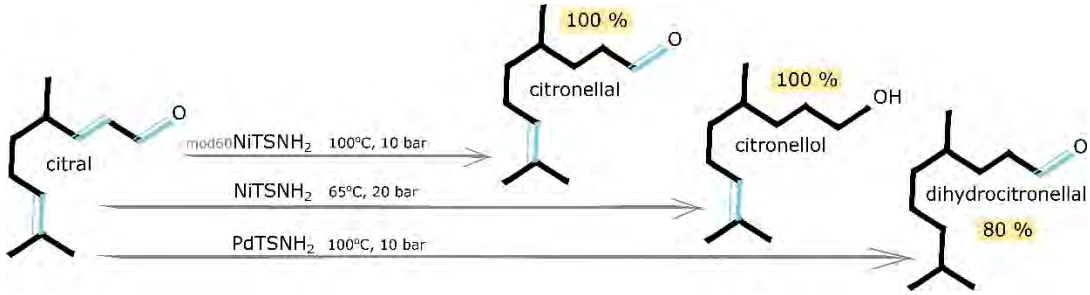

Scheme 9. Possible pathways of citral flow hydrogenation over resin supported catalysts.

With continuous flow micro-reactor technology, packed-bed catalyst can be easily replaced. Therefore, citral flow hydrogenation can be directed towards various products with high selectivity by simple cartridge replacement without the need for assembling a new catalytic system.

In this matter, flow catalysis is a great platform for multi-step operations. Presented catalytic flow system can be extended with additional elements such as heaters, coolers, filters, membranes or extra catalysts beds. Therefore, sequential processes usually conducted in separate stages can be intensified to one compact system. Thus, flow microfluidic device can be coupled with analyzing device such as liquid chromatograph, which would introduce additional improvements in terms of process intensification.

Finally, flow catalysis with micro-reactor technology is a multifunctional tool, which offers a plethora of benefits for academia and industry. As demonstrated in the dissertation, flow processing can be applied in numerous protocols, such as catalytic reaction, reaction parameter optimization and catalyst modification. Besides safety and economical profits, flow chemistry is a perfect technique for process intensification listed as a one of the most important prospects for new generation chemical manufacturing.

6. List of scientific publications

Cover Feature:
On-the-fly catalyst accretion and screening in chemoselective flow hydrogenation
D. Giziński , W. Błachucki, A. Śrębowata, M. Zienkiewicz-Machnik, I. Goszewska, , A. Kubas, D. Lisovytskiy, M. Pisarek, J. Szlachetko, J. Sá, *ChemCatChem* (2018)

Tuning nano-nickel selectivity with tin in flow hydrogenation of 6-methyl-5-hepten-2-one by surface organometallic chemistry modification
M. Zienkiewicz-Machnik, I. Goszewska, A. Śrębowata, A. Kubas, **D. Giziński**, G. Słowik, K. Matus, D. Lisovytskiy, M. Pisarek, J. Sá, *Cat. Today* (2017)

Chemoselective flow hydrogenation of α,β-unsaturated aldehyde over nano-nickel
D. Giziński, I. Goszewska, M. Zieliński, D. Lisovytskiy, K. Nikiforov, J. Masternak, M. Zienkiewicz-Machnik, A. Śrębowata, J. Sá, *Cat. Comm.* 98 (2017) 17-21

p-Nitrophenol flow hydrogenation with nano-Cu_2O grafted on polymeric resin
C. Paun, **D. Giziński**, M. Zienkiewicz-Machnik, D. Banaś, A. Kubala-Kukuś, J. Sá *Cat. Comm.* 92 (2017) 61-64

A novel nano-palladium catalyst for contiuous-flow chemoselective hydrogenation reactions
I. Goszewska, **D. Giziński**, M. Zienkiewicz-Machnik, D. Lisovytskiy, K. Nikiforov, J. Masterniak, A. Śrębowata, J. Sá, *Cat. Comm.* 94 (2017) 64-68

Remarkable effect of soft-templating synthesis procedure on catalytic properties of mesoporous carbon supported Ni in hydrodechlorination of trichloroethylene in liquid phase A. Śrębowata, I.I. Kamińska, **D. Giziński**, D. Wideł, J. Oszczudłowski, Cat. Today 251 (2015) 60-65

Book chapter

"Hydrogenation with low-cost transition metals" 2015 CRC Press
Chapter III: *"Hydrogenation by copper catalysts"* **D. Giziński**, J. Sá

7. List of scientific presentations

Oral presentations

14th Pannonian International Symposium on Catalysis
03-07.09.2018 Starý Smokovec, High Tatras, Slovak Republic
Bond control in citral hydrogenation over resin supported catalysts
D. Giziński , W. Błachucki, A. Śrębowata, A. Kubas, K. Matus, D. Lisovytskiy, M. Pisarek, J. Sá,
Catalytic hydrogenation for environmental protection and formation of value added products A. Śrębowata, I. Goszewska, M. Zienkiewicz-Machnik, **D. Giziński**, E. Kowalewski, A. Kubas, W. Błachucki, S. Dzwigaj, G. Słowik, M. Pisarek, K. Matus, J. Sá (keynote lecture)

International Conference on Catalysis and Surface Chemistry/50th Polish Annual Conference on Catalysis
18-23.03.2018 Cracow, Poland
Flow catalysis: a multifunctional tool for chemoselective hydrogenation
D. Giziński, M. Zienkiewicz-Machnik, I. Goszewska, A. Kubas, A. Śrębowata, J. Sá

2nd International Conference on Catalysis and Chemical Engineering
19-21.02.2018 Paris, France
Switchable flow hydrogenation chemoselectivity by simple Sn modification of Ni nano-catalyst
D. Giziński, I. Goszewska, M. Zienkiewicz-Machnik, A. Śrębowata, J. Sá

49th Polish Annual Conference on Catalysis, 15-17.03.2017 Cracow, Poland
Chemoselective flow hydrogenation of α,β-unsaturated aldehydes over nano-nickel
D. Giziński, I. Goszewska, M. Zienkiewicz-Machnik, M. Zieliński, D. Lisovytskiy, A. Śrębowata, J. Sá

Poster presentations

International Conference on Catalysis and Surface Chemistry/50th Polish Annual Conference on Catalysis
18-23.03.2018 Cracow, Poland
Development of Ni and Ni-Sn catalysts for continuous flow chemoselective hydrogenation of 6-methyl-5-hepten-2-one
M. Zienkiewicz-Machnik, I. Goszewska, A. Śrębowata, A. Kubas, **D. Giziński**, G. Słowik, K. Matus, D. Lisovytskiy, M. Pisarek, J. Sá

EuropaCat
27-31.08.2017 Florence, Italy
Flow catalysis for selective hydrogenation over transition metal nanoparticles grafted

on resin **D. Giziński**, I. Goszewska, M. Zienkiewicz-Machnik, M. Zieliński, D. Lisovytskiy, K. Nikiforov, J. Masternak, A. Śrębowata, J. Sá

Highly efficient, selective and low-temperature catalytic hydrodechlorination of tetrachloromethane with silica-supported Ir and Ir-M (M=Pt, Pd, Au) catalysts
M. Bonarowska, M. Zieliński, J. Sá, G. Słowik, **D. Giziński**

ChemSession'17
09.06.2017 Warsaw, Poland
Chemoselective flow hydrogenation of unsaturated aldehydes over nano-nickel
D. Giziński, I. Goszewska, M. Zienkiewicz-Machnik, A. Śrębowata, J. Sá

49th Polish Annual Conference on Catalysis
15-17.03.2017 Cracow, Poland
Comparison studies between palladium and nickel nano-catalysts employed in continuous-flow selective hydrogenation
I. Goszewska, **D. Giziński**, M. Zienkiewicz-Machnik, A. Śrębowata, J. Sá

13th Pannonian International Symposium on Catalysis,
19-23.09.2016, Siofok, Hungary
Synthesis of polymeric resin supported transition metals for hydrogenation of α,β-unsaturated aldehydes
D. Giziński, I. Goszewska, G. Słowik, A. Śrębowata, J. Sá

48th Polish Annual Conference on Catalysis,
16-18.03.2016 Cracow, Poland
Synthesis of polymeric resin supported transition metals catalysts for hydrogenation processes **D. Giziński**, I. Goszewska, D. Lisovytskiy, G. Słowik, A. Śrębowata, J. Sá

46th Polish Annual Conference on Catalysis, 19-21.03.2014 Cracow, Poland
Turbostratic carbon supported Pd-Ni alloys in catalytic purification of water
A. Śrębowata, **D. Giziński**, W. Raróg-Pilecka, D. Lisovytskiy

8. Bibliography

[1]J.K. Nørskov, F. Abild-Pedersen, *Nature*, 461 (2009) 1223-1225

[2] C.W. Bamforth, *Chemistry of Brewing,* (2003), Elsevier Science Ltd., p.446

[3] A. Muller, J. Bowers, WO Patent WO 99/08 (February 25, 1999) to First Chemical Corporation

[4] I. Kroschwitz (Ed.) Kirk-Othmer, *En. Of Chem. Tech.,* vol. 6, 4th ed., Wiley, New York (1992) p. 349

[5] https://www.femaflavor.org/flavor-library/26-dimethyloctanal, accessed 10.12.2018

[6] D. Kalemba, A. Kunicka, *Curr. Med. Chem.,* 10 (2003) 813-829

[7] https://www3.epa.gov/pesticides/chem_search/reg_actions/registration/fs_PC-167004_22-Apr-04.pdf, accessed 10.12.2018

[8] U.K.Singh, M.A. Vannice, *J. Catal.,* 199 (2001) 73

[9] F. Delbecq, P. Sautet, *J. Catal.*, 152 (1995) 217

[10] D.V. Sokolskii, A.M. Pak, M.A. Ginzburg, V.F. Vozdvizhenskii, *React. Kinet. Catal. Lett.,* 33 (1987) 399

[11] A. Giroir-Fendler, D. Richard, P. Gallezot, "*Heterogeneous Catalysis and Fine Chemicals. Studies in Surface Science and Catalysis."* Elsevier: Amsterdam, Netherlands, 1988

[12] K.R. Kahsar, D.K. Schwartz, J.W. Medlin, *J. Mol. Catal. A: Chem,* 396 (2015) 188

[13] K.R. Kahsar, D.K. Schwartz, J.W. Medlin, *J. Am. Chem. Soc.,* 136 (2014) 520

[14] M. Makosch, W.Lin, V. Bumbálek, J. Sá, J.W. Medlin, K. Hungerbühler, J.A. van Bokhoven, *ACS Catal.*, 2 (2012) 2079

[15] Z. Weng, F. Zaera, *J. Phys. Chem. C.,* 118 (2014) 3672

[16] A.R. Rautio P.Mäki-Arvela, A. Aho, K. Eränen, K. Kordas, *Cat. Today,* 241 (2015) 170-178

[17] M. Zienkiewicz-Machnik, I. Goszewska, A. Śrębowata, A. Kubas, D. Giziński, G. Słowik, K. Matus, D. Lisovytskiy, M. Pisarek, J. Sá, *Cat. Today,* 308 (2018) 38-44

[18] M. Bidaoui, C. Especel, S. Sabour, L. Benatallah, N. Saib-Bouchenafa, S. Royer, O. Mohammedi, *J. Mol. Catal. A: Chem.,* 399 (2015) 97-105

[19] J.P.Stassi, P.D. Zgolicz, V.I. Rodriguez, S.R. Miguel, O.A. Scelza, *Appl. Catal.A: General,* 497 (2015) 58-71

[20] P.-F. Qu, J.-G. Chen, Y.-H. Song, Z.-T. Liu, Y. Li, J. Lu, J. Jiang, *Cat. Comm.*, 68 (2015) 105-109

[21] H. Pan, J. Li, J. Lu, G. Wang, W. Xie, P. Wu, X. Li, *J.Catal.,* 354 (2017) 24-36

[22] Y. Dai, X. Gao, X. Chu, C. Jiang, Y. Yao, Z. Guo, C. Zhou, C. Wang, H. Wang, Y. Yang, *J. Catal.,* 364 (2018) 192-203

[23] S. Galvagno, A. Donato, G. Neri, R. Pietropaolo, *J. Mol. Catal.,* 49 (1989) 223-232

[24] I. Ro, I.B. Aragao, Z.J. Brentzel, Y. Liu, K.R. Rivera-Dones, M.R. Ball, D. Zanchet, G.W. Huber, J.A. Dumestic, *Appl. Catal. B: Enviromental,* 231 (2018) 182-190

[25] D. Richards, P. Fouilloux, P. Gallezot, *Proceeding of the 9th International Congress on Catalysis,* Elsevier, Calgary, Canada, 1988, p. 1074

[26] P. Gallezot, D. Richards, G. Bergeret, *Novel Materials in Heterogeneous Catalysis,* ACS Symposium Series Vol. 437, ACS, Washington, DC, 1990, p. 150

[27] M. Steffan, F. Klasovsky, J. Arras, C. Roth, J. Radnik, H. Hofmeister, P. Claus, *Adv. Synth. Catal.,* 350 (2008) 1337-1348

[28] S. Wei, Y. Zhao, G. Fan, L. Yang, F. Li, *Chem. Eng. J.,* 322 (2017) 234-245

[29] R. Malathi, R.P. Viswanath, *App. Catal. A. General,* 208 (2001) 323-327

[30] T. Ekou, C. Especel, S. Royer, *Catal. Today,* 173 (2011) 44-52

[31] E. Bailón-Grcia, F. Carrasco-Martin, A.F. Perez-Cadenas, F.J. Maldonado-Hódar, *J. Catal.,* 244 (2016) 701-711

[32] M. Steffan, M. Lucas, A. Brandner, M. Wollny, N. Oldenburg, P. Claus, *Chem. Eng. Technol.,* 30 (2007) 481-486; M. Steffan, M. Lucas, A. Brandner, M. Wollny, N. Oldenburg, P. Claus, *Chem. Eng. Technol.,* 78 (2006) 923-929

[33] V. Satagopan, S.B. Chandalia, *J. Chem. Technol. Biotechnol.,* 59 (1994) 257-263

[34] J. Zhu, M. Lu, M. Li, J. Zhu, Y. Shan, *Mater. Chem. Phys.,* 132 (2012) 316-323

[35] Z. Wang, R. Liu, F. Zhao, X. Liu, M. Lu, J. Meng, *Langumir,* 26 (2010) 10135-10140

[36] K.R. Kahsar, S. Johnson, D.K. Schwartz, J.W. Medlin, *Top. Catal.,* 57 (2014) 1505-1511

[37] M.A. Aramendia, V. Borau, C. Jimenez, J.M. Marinas, A. Porras, F.J. Urbano, *J. Catal.,* 172 (1997) 46-54

[38] S.-F. Fujita, H. Mitani, C. Zhang, K. Li, F. Zhao, M. Arai, *Mol. Catal.,* 441 (2017) 12-29

[39] T. Szumełda, A. Drelinkiewicz, R. Kosydar, J. Gurgul, *Appl. Catal. A: General,* 487 (2014) 1-15

[40] R. Li, W. Yao, Y. Jin, W. Jia, X. Chen, J. Chen, J. Zheng, Y. Hu, D. Han, J. Zhao, *Chem. Eng. J.,* 351 (2018) 995-1005

[41] A.S. Nagpure, L. Gurrala, P. Gogoi, S.V. Chilukuri, *RSC. Adv.,* 6 (2016) 44333-44340

[42] J.Y. Liu, *ChemCatChem,* 3 (2011) 934-948E.

[43] B. Zhang, D.S. Su, *ChemCatChem,* 7 (2015) 3639-3645

[44] T.-Y. Chung, C.-S. Tsao, H.-P. Tseng, C.-H. Chen, M.-S. Yu, J. Coll. Interf. Sci., 441 (2015) 98

[45] Castillejos, A.M. Garcia-Minguillán, B. Bachiller-Baeza, I. Rodrigez-Ramos, A. Guerrero-Ruiz, *Catal. Today,* 301 (2018) 248-257

[46] D. Divakar, M. Manikandan, T. SIvakumar, *J. Chem. Technol. Biotechnol.,* 83 (2008) 1472-1478

[47] J. Khandei, R.C. Hoffmann, J. Engstler, J.J. Schneider, J. Arras, P. Claus, G. Cherkashinin, *Chem.-Eur. J.,* 16 (2010) 2300-2308

[48] K.-J. You, C.-T. Chang, B.-J. Liaw, C.-T. Huang, Y.Z. Chen, *Appl. Catal. A: General,* 361 (2009) 65-71

[49] L. Liu, B. Qiao, Y. Ma, J. Zhang, Y. Deng, *Dalton Trans.,* (2008) 2542-2548

[50] P.G.N. Martens, P. Vanderzande, X. Ye, H. Poelman, I.F.J. Vankelecom, D.E. De Vos, *Appl. Catal. A: General,* 335 (2009) 176-183

[51] F. Klasovsky, M. Steffan, J. Arras, J. Radnik, P. Claus, *Open Phys. Chem. J.,* 1 (2007) 1-4

[52] L. Luza, C.P. Rambor, A. Gual, J. A. Fernandes, D. Eberhardt, J. Dupont, *ACS Catal.,* 7 (2017) 2791-2799

[53] M. Butt, X. Feng, Y. Yamamoto, A.I. Almansour, N. Arumugam, R.S. Kumar, M. Bao, *Asian J. Org. Chem.,* 6 (2017) 867-872

[54] P. Reyes, H. Rojas, G. Pecchi, J.L.G. Fierro, *J. Mol. Catal.,* 179 (2002) 293

[55] H. Rojas, G. Borda, P. Reyes, J.J. Martinez, J. Valencia, J.L.G. Fierro, *Catal. Today,* 133-135 (2008) 699-705

[56] M. Tamura, K. Tokonami, Y. Nakagawa, K. Tomishige, *ACS Sustainable Chem. Eng.,* 5 (2017) 3685-3697

[57] M. Tamura, K. Tokonami, Y. Nakagawa, K. Tomishige, *ACS Catal.,* 6 (2017) 3600-3609

[58] J.-F. Yuan, C.-Q. Luo, Q.-Y. Yu, A.-P. Jia, G.-S. Hu, J.-Q. Lu, M.-F. Luo, *Catal. Sci. Technol.*, 6 (2016) 4294-4305

[59] P. Mäki-Arvela, L.-P. Tiainen, R. Gil, T. Salmi, *Stud. Surf. Sci. Catal.,* 108 (1997) 273-280; T. Salmi, P. Mäki-Arvela, J. Wärnå, K. Eränen, A. Denecheau, K. Alho, D.Y. Murzin, *Ind. Eng. Chem. Res.,* 46 (2007) 3912-3921

[60] P. Mäki-Arvela, L.-P. Tiainen, M. Lindbland, K. Demirkan, N. Kumar, R. Sjöholm, T. Ollonqvist, J. Väyrynen, T. Salmi, D.Y. Murzin, *Appl. Catal. A: General,* 241 (2003) 271-288

[61] N. Neelakandeswari, G. Sangami, P. Emayavaramban, S. Ganesh Babu, R. Karvembu, N. Dharmaraj, *J. Mol. Cata. A: Chem.,* 365 (2012) 90-99

[62] M.G. Prakash, R. Mahalakshmy, K.R. Krishnamurthy, B. Viswanathan, *Catal. Sci. Technol.,* 5 (2015) 3313-3321

[63] W. Lin, H. Cheng, L. He, Y. Yu, F. Zhao, *J. Catal.,* 303 (2013) 110-116

[64] A. Ungureanu, B. Dragoi, A. Chirieac, C. Ciotonea, S. Royer, D. Duprez, A.S. Mamede, E. Dumitriu, *ACS Appl. Mater. Interfaces,* 5 (2013) 3010-3025

[65] S. Gryglewicz, A. Śliwak, J. Ćwikła, G. Gryglewicz, *Catal. Lett.,* 144 (2014) 62-69

[66] H. Wang, Y. Shu, M. Zheng, T. Zhang, *Catal. Lett.,* 124 (2008) 219-225

[67] Y. Tang, D. Yang, F. Qin, J. Hu, C. Wang, H. Xu, *J. Solid State Chem.,* 182 (2009) 2279-2284

[68] M. Cerron-Alarcón, B. Bachiller-Baeza, A. Guerrero-Ruiz, I. Rodriguez-Ramos, *J. Mol. Catal. A: Chem.,* 258 (2006) 221-230

[69] N. Mahata, A.F. Cunha, J.J.M. Órfão, J.L. Figueiredo, *Chem. Eng. J.,* 188 (2012) 155-159

[70] F. Yang, Z. Jiang, G. Fan, F. Li, *Catal. Sci. Technol.,* 4 (2014) 1123-1131

[71] S. Bhogeswararao, V. Pavan Kumar, K.V.R. Chary, D. Srinivas, *Catal. Lett.,* 143 (2013) 1266-1276

[72] B.-J. Liaw, S-J. Chiang, S.-W. Chen, Y.-Z. Chen, *Appl. Catal. A: General,* 346 (2008) 179-188

[73] N. Kalyon, K. Hofmann, J. Malter, M. Lucas, P. Claus, B. Albert, *J. Catal.,* 352 (2017) 436-441

[74] C. Rudolf, B. Dragoi, A. Ungureanu, A. Chirieac, S. Royer, A. Nastro, E. Dumitriu, *Catal. Sci. Technol.,* 4 (2014) 179-189

[75] X. Xu, L. Li, W. Han, J. Luo, D. Zhang, Y. Wang, G. Li, *Catal. Comm.,* 109 (2018) 50-54

[76] J.-J. Shi, H.-J. Feng, C.-L. Qv, D. Zhao, S.-G. Hong, N. Zhang, *Appl. Catal. A: General,* 561 (2018) 127-136

[77] J. Liu, L. Chen, H. Cui, J. Zhang, C.Y. Su, *Chem. Soc. Rev.,* 43 (2014) 6011-6061

[78] Z. Chen, J. Chen, Y. Li, *Chinese J. Catal.,* 38 (2017) 1108-1126

[79] L. Zhang, X. Chen, Z. Peng, C. Liang, *Mol. Catal.,* 449 (2018) 14-24

[80] K. Kouachi, G. Lafaye, C. Especel, O. Cherifi, P. Marécot, *J. Mol. Catal. A: General*, 280 (2008) 52-60

[81] J. Lee, S.P. Burt, C.A. Carrero, A.C. Alba-Rubio, I. Ro, B.J. O'Neill, H.J. Kim, D.H.K. Jackson, T.F. Kuech, I. Hermans, J.A. Dumesic, G.W. Huber, *J. Catal.,* 330 (2015) 19-27

[82] M. Audemar, C. Ciotonea, K.D.O. Vigier, S. Royer, A. Ungureanu, B. Dragoi, E. Dumitriu, F. Jérôme, *ChemSusChem,* 8 (2015) 1885-1891

[83] X. Chen, X. Li, S. Liu, Z. Li, *Ind. Eng. Chem. Res.,* 54 (2015) 4756-4762

[84] P. Jiang, X. Li, W. Gao, X. Wang, Y. Tang, K. Lan, B. Wang, R. Li, *Catal. Comm.,* 111 (2018) 6-9

[85] L.J. Malobela, J. Heveling, W.G. Augustyn, L.M. Cele, *Ind. Eng. Chem. Res.,* 53 (2014) 13910-13919

[86] M.G. Prakash, R. Mahalakshmy, K.R. Krishnamurthy, B. Viswanathan, *Catal. Today,* 263 (2016) 105-111

[87] S. Rana, S.B. Jonnalagadda, *RSC Adv.,* 7 (2017) 2869-2879

[88] J. Alvarez-Rodriguez, M. Cerro-Arćon, A. Guerrero-Ruiz, I. Rodriguez-Ramos, *Appl. Catal. A: General,* 348 (2008) 241-250

[89] J. Court, J. Jablonski, S. Hamar-Thibault, *Stud. Surf. Sci. Catal.,* 78 (1993) 155-162

[90] C. Ramshaw, *The Incentive for Process Intensification, Proceedings, 1st Intl. Conf. Proc. Intensif. for Chem. Ind.* BHR Group, London, (1995) 1

[91] A.I. Stankiewicz, J.A. Moulijn, *Chem. Eng. Prog.,* (2000) 22-34

[92] A. Renken, L. Kiwi-Minsken, *Adv. Catal.,* 53 (2010) 47-122

[93] V. Hessel, C. Knobloch, H. Löwe, *Chem. Eng.,* 1 (2008) 1-16

[94] C.N. Satterfield, *Mass Transfer in Heterogeneous Catalysis,* M.I.T. Press, (1970)

[95] R. Munirathinam, J. Huskens, W. Verboom, *Adv. Syn. Catal.,* 357 (2015) 1093-1123

[96] C. Yungus, *'Heat transfer: A practical approach'* (2nd edition), Boston: McGraw-Hill, (2003)

[97] C. Wiles, P. Watts, *Green Chem.,* 16 (2014) 55-62

[98] A. Pohar, I. Plazl, *Ind. Eng. Chem. Res.,* 47 (2008) 7447-7455

[99] V. Hessel, D. Kralish, N. Kockmann, *'Novel Process Window: Innovative Gates to Intensified and Sustainable Chemical Processes'* Wiley VCh, Weinheim, (2014)

[100] T.J. Ober, D. Foresti, J.A. Lewis, *Proc. Nati. Acad. Sci.,* 112 (2015) 12293-12298

[101] J. Weisman, '*Handbook of Fluids in Motion'*, *Chapter 15. Two-phase flows patterns,* N.P. Cheremisinoff, R. Gupta Ann Arbor Science Publishers, (1983)

[102] A. Salić, A. Tusek, B. Zelić, *J. Appl. Biomed.,* 10 (2012) 137-153

[103] J. Yue, E.V. Rebrov, J.C. Shouten, *Lab Chip.,* 14 (2014) 1632-1649

[104] J. Chen, W. Song, D. Xu, *Front. Heat Mass Transf.,* 8 (2017) 1-10

[105] S. Odiba, M. Olea, S. Hodgson, A. Adgar, P. Russell, *J. Chem. Eng. Process Technol.,* 7 (2016) 297

[106] I. Rossetti, *Cat. Today,* 308 (2018) 20-31

[107] A. Bogdan, N. Sach, *Adv. Synth. Catal.,* 351 (2009) 849-854

[108] O. Wörz, K. Jäckel, T. Richter, A. Wolf, *Chem. Eng. Technol.,* 24 (2001) 138-142

[109] G. Shore, S. Morin, M.G. Organ, *Angew. Chem. Int. Ed.,* 45 (2006) 2761-2766

[110] J. Ganley, K. Riechmann, E. Seebauer, R. Massel, *J. Catal.,* 227 (2004) 26-32

[111] R. Javaid, S.-I. Kawasaki, A. Suzuki, T.M. Suzuki, *Beilstein J. Org. Chem.,* 9 (2013) 1156-1163

[112] K. Haas-Santo, M. Fichtner, K. Schubert, *Appl. Catal. A:Gen.,* 220 (2001) 79-92

[113] J. Kobayashi, Y. Mori, K. Okomoto, R. Akiyama, M. Ueno, T. Kitamori, S. Kobayashi, *Science* 304 (2004) 1305-1308

[114] E.V. Rebrov, E.A. Klinger, A. Berenguer-Murcia, E.M. Sulman, J.C. Schouten, *Org. Process Res. Dev.,* 13 (2009) 991-998

[115] Z. Zeng, W. Qiu, Z. Huang, *Anal. Chem.,* 73 (2001) 2429-2436

[116] A. Stefanescu, A.C. van Veen, C. Mirodatos, J.C. Beziat, E. Duval-Brunel, *Catal. Today,* 125 (2007) 16-23

[117] a) T. Conant, A. Karim, A.K. Datye, *Catal. Today,* 125 (2007) 11-15; b) O. de la Iglesia, V. Sebastián, R. Mallada, G. Nikolaidis, J. Coronas, G. Kolb, R. Zapf, V. Hessel, J.

Santamaria, *Catal. Today*, 125 (2007) 2-10; c) A. Kundu, J.M. Park, J.E. Ahn, S.S. Park, Y.G. Shul, H.S. Han, *Fuel* 86 (2007) 1331-1336

[118] K. Nakanishi, N. Soga, *J. Am. Ceram. Soc.,* 74 (1991) 2518-2530

[119] M.T. Alotaibi, M.J. Taylor, D. Liu, S.K. Beaumont, G. Keriakou, *Surf. Sci.,* 646 (2016) 179-185

[120] A. Koreniuk, K. Maresz, K. Odrozek, J. Mrowiec-Bialon, *Microporous Mesoporous Mater.,* 229 (2016) 98-105

[121] E.B. Anderson, M.R. Buchmeiser, *ChemCatChem,* 4 (2012) 30-44

[122] S. Xie, F. Svec, J.M.J. Frechet, *Biotechnol. Bioeng.,* 62 (1999) 30-35

[123] M.R. Buchmeiser, *Polymer,* 48 (2007) 2187-2198

[124] M. Mayr, B. Mayr, M.R. Buchmeiser, *Agew. Chem. Int. Ed.,* 40 (2001) 3839-3842

[125] M.J. Beier, W. Knolle, A. Prager-Duschke, M.R. Buchmeiser, *Macromol. Rapid Comm.,* 29 (2008) 904-909

[126] K.F. Bolton, A.J. Cantry, J.A. Deverell, R.M. Guijt, E.F. Hilder, T. Rodemann, J.A. Smith, *Tetrehedron Lett.,* 47 (2006) 9321-9324

[127] R. Bandari, A. Prager, T. Höche, M.R. Buchmeiser, *Arkivoc,* 4 (2011) 54-70

[128] L.J. Durndell, K. Wilson, A.F. Lee, *RSC Adv.,* 5 (2015) 80022-80026

[129] X. Liu, B.Unal, K.F. Jensen, *Catal. Sci. Technol.,* 2 (2012) 2134-2138

[130] I. Denčić, S. de Vaan, T. Noël, J. Meuldijk, M. de Croon, V. Hessel, *Ind. Eng. Chem. Res.,* 52 (2013) 10951-10960

[131] C. Moreno-Marrodan, P. Barbaro, M. Catalano, A. Taurino, *Dalton Trans.,* 41 (2012) 12666-12673

[132] F. Ligouri, P. Barbaro, *J. Catal.,* 311 (2014) 212-220

[133] S. Kobayashi, M. Okumura, Y. Akatsuka, H. Miyamura, M. Ueno, H. Oyamada, *ChemCatChem,* 7 (2015) 4025-4029

[134] Y. Saito, H. Ishitani, M. Ueno, S. Kobayashi, *ChemistryOpen.,* 6 (2017) 211-215

[135] M. Ueno, Y. Morii, K. Uramoto, H. Oyamada, Y. Mori, S. Kobayashi, *J. Flow Chem.,* 4 (2014) 160-163

[136] Y. Saito, H. Ishitani, S. Kobayashi, *Asian J. Org. Chem.,* 5 (2016) 1124-1127

[137] D. Gericke, D. Ott, V.G. Matveera, *RSC Adv.,* 5 (2015) 15898-15908

[138] T. Osako, K. Torii, A. Tazawa, Y. Uozomi, *RSC Adv.,* 5 (2015) 45760-45766

[139] R. Hudson, G. Hamasaka, T. Osako, Y.M.A. Yamada, C.-J. Li, Y. Uozumi, A. Moores, *Green Chem.,* 15 (2013) 2141-2148

[140] P. Stephenson, P. Licence, S.K. Ross, M. Poliakoff, *Green Chem.,* 6 (2004) 521-523

[141] U. Hintermair, T. Höfener, T. Pullmann, G. Franció, W. Leitner, *ChemCatChem,* 2 (2010) 150-154

[142] I.M. Mándity, S.B. Ötwös, G. Szölösi, F. Fülöp, *Chem. Rec.,* 16 (2016) 1018-1033

[143] F. Derikvand, F. Bigi, R. Maggi, C.G. Piscopo, G. Sartori, *J. Catal.,* 271 (2010) 99-103

[144] N. Zotova, K. Hellgardt, G.H. Kelsall, A.S. Jessiman, K.K. Hii, *Green Chem.,* 12 (2010) 2157-2163

[145] V. Pascanu, A. Bermejo-Gómez, C. Ayats, *ACS Catal.,* 5 (2015) 472-479

[146] S. Doherty, J.G. Knight, M.A. Carroll, *RSC Adv.,* 6 (2016) 73118-73131

[147] K.C. Basavaraju, S. Sharma, R.A. Maurya, D.-P. Kim, *Angew. Chem. Int. Ed.,* 52 (2013) 6735-6738

[148] N. Elizarov, M. Pucheault, S. Antoniotti, *ChemistrySelect.,* 1 (2016) 3219-3222

[149] A. Nanoyama, N. Kumagai, M. Shibasaki, *Tetrahedron,* 7 (2017) 1517-1521

[150] S. Seghers, L. Protasova, S. Mullens, J.W. Thybaut, C.V. Stevens, *Green Chem.,* 19 (2017) 237-248

[151] A. Furuta, T. Fukuyama, I. Ryu, *Bull. Chem. Soc. Jpn.,* 90 (2017) 607-612

[152] Y. Matsushita, N. Ohba, S. Kumada, K. Sakeda, T. Suzuki, T. Ichimura, *Chem. Eng. J.* 135 (2008) 303-308

[153] T.H. Rehm, S. Gros, P. Löb, A. Renken, *React. Chem. Eng.,* 1 (2016) 636-648

[154] I.R. Baxendale, J. Deeley, C.Cm. Griffiths-Johns, S.V. Ley, S. Saaby, G.K. Tranmer, *Chem. Comm.,* (2006) 2566-2568

[155] X. Fan, M. Gonzalez Manchon, K. Wilson, S. Tennison, A. Kozynchenko, A.A. Lapkin, P.K. Plucinski, *J. Catal.,* 267 (2009) 114-120

[156] J. Wu, J.A. Kozak, F. Simeon, T.A. Hatton, T.F. Jamison, *Chem. Sci.,* 5 (2014) 1227-1231

[157] http://www.rapp-polymere.com/#index.php?id=98&currency=eur, accessed 27.11.2018

[159] R. Santini, M.C. Griffith, M. Qi, *Tetrahedron Lett.*, 39 (1998) 8951-8954

[160] M. Králik, A. Biffis, *J. Mol. Catal. A: Chem.,* 177 (2001) 113-138

[161] S.T. Marshall, M. O'Brien, B. Oetter, A. Corpuz, R.M. Richards, D.K. Schwartz, J.W. Medlin, *Nat. Mater.,* 9 (2010) 853-858

[162] A.A. Dabbawala, D.K. Mishra, J.-S. Hwang, *Cat. Today,* 265 (2016) 163-173

[163] B.P. Loechel, H.H. Strehblow, *J. Electrochem. Soc.*, 131 (1984) 713; J.C. Klein, D.M. Hercules, *J. Catal.,* 82 (1983) 424

[164] S.O. Grim, L.J. Matienzo, W.E. Swartz Jr, *J. Am. Chem. Soc.,* 94 (1972) 5116-5117

[165] H. Zhang, Q. Fu, Y. Yao, Z. Zhang, T. Ma, D. Tan, X. Bao, *Langumir,* 24 (2008) 10874-10878; C. Paun, G. Słowik, E. Lewin, J. Sá, *RSC Adv.,* 90 (2016) 87564-87568

[166] R. Narayanan, M.A. El-Sayed, *J. Am. Chem. Soc.,* 125 (2003) 8340-8347

[167] A. Śrębowata, I.I.Kamińska, D. Giziński, D. Wideł, J. Oszczudłowski, *Cat. Today,* 251 (2015) 60-65

[168] M. Polanyi, J. Horiuti, *Trans. Faraday Soc.,* 30 (1937) 1164; *e.g.* M. Neurock, R.A. van Santen, *J. Phys. Chem. B,* 104 (2000) 11127-11145

[169] H. Yoshida, T. Zama, S.Fujita, J. Panpranot, M. Arai, *RSC Adv.,* 4 (2014) 24922-24928

[170] T. Ramanathan, F.T. Fisher, R.S. Ruoff, L.C. Brinson, *Chem. Mater.* 17 (2005) 1290–1295

[171] M. Brun, A. Berthet, J.C. Bertolini, *J. Electron Spectrosc. Relat. Phenom.* 104 (1999) 55–60

[172] C. Paun, G. Słowik, E. Lewin, J. Sá, *RSC Adv.* 6 (2016) 87564–87568; E.H. Voogt, A.J.M. Mens, O.L.J. Gijzeman, J.W. Geus, *Surf. Sci.* 350 (1996) 21–31

[173] http://webshop.thalesnano.com/10-pdc-microcatcart-4120

[174] A. Mehta, *'The flow revolution'* (2017) https://www.chemistryworld.com/features/the-flow-revolution/2500496.article?fbclid=IwAR2k-nDfrazKnQSlzjKuVYPf4iHYjKaClHKXer7Fdq8iWYY-mnLsEyQwhe0 , accessed 06.12.2018

[175] Chemjobber, *'Beyond buckets and batches'* (2017) https://www.chemistryworld.com/opinion/beyond-buckets-and-batches/3008314.article , accessed 06.12.2018

[176] Y. Hou, H. Kondoh, T. Ohta, S.Gao, *Appl. Surf. Sci.,* 241 (2005) 218-222

[177] C. Paun, D. Giziński, M. Zienkiewicz-Machnik, D. Banaś, A. Kubala-Kukuś, J. Sá, *Cat. Comm.,* 92 (2017) 61-64

[178] M. Makosch, W.-I. Lin, V. Bumbálek, J. Sá, J.W. Medlin, K. Hungerbuhler, J.A. van Bokhoven, *ASC Catal.,* 2 (2012) 2079-2081; Z. Weng, F.Zaera, *J. Phys. Chem. C,* 118 (2014) 3672-3679

[179] C. Kohlpaintner, M. Schulte, J. Falbe, P. Lappe, J. Weber, G.D. Frey, "Ullmann's Encyclopedia of Industrial Chemistry", Wiley-VCH Verlag GmbH & Co. KGaA, Weinheim, 2013